SEMI-ANNUAL STATUS REPORT #5

TO THE NATIONAL AERONAUTICS AND SPACE ADMINISTRATION

GODDARD GRANT IN-46-CR 199951 918.

CRUSTAL DYNAMICS PROJECT

NASA GRANT NAG 5-814

"The Interpretation of Crustal Dynamics Data in Terms of Plate Motions and Regional Deformation Near Plate Boundaries"

for the period

22 September 1988 - 21 March 1989

Principal Investigator: Prof. Sean C. Solomon
Department of Earth, Atmospheric, and Planetary Sciences
Massachusetts Institute of Technology
Cambridge, MA 02139

6 April 1989

TABLE OF CONTENTS

This is a Semi-annual Status Report on research conducted between 22 September 1988 and 21 March 1989 under NASA Grant NAG 5-814, entitled "The Interpretation of Crustal Dynamics Data in Terms of Plate Motions and Regional Deformation near Plate Boundaries." This grant supports the research of two Investigators (S. C. Solomon and M. N. Toksöz), two Research Staff (E. A. Bergman and R. Reilinger), and two Ph.D. students (J. M. Sauber and A. Sheehan) on behalf of the NASA Geodynamics and Crustal Dynamics Programs. With the completion of her Ph.D. in November 1988, Jeanne Sauber left our group to take a staff position at the NASA Goddard Space Flight Center.

The focus of the research has been in two broad areas during the most recent 6-month period: (1) the nature and dynamics of time-dependent deformation and stress along major seismic zones, and (2) the nature of the lithospheric strain field in intraplate regions. The principal findings of our research to date are described in the accompanying appendices. The first two are a reprint of a recently published paper and a preprint of a paper now in press. The third is the abstract of J. Sauber's Ph.D. thesis. The final three appendices are two abstracts of papers submitted to the 1989 Spring AGU Meeting and a report of recent field work supported by this project in the Imperial Valley and Salton Trough, California.

APPENDIX 1

The Earthquake Deformation Cycle: Examples from South America and the Western United States

Robert Reilinger

From *Proceedings of China-United States Symposium on Crustal Deformation and Earthquakes*, pp. 76-89, Seismological Press, Beijing, 1988.

PROCEEDINGS
OF
CHINA-UNITED STATES SYMPOSIUM
ON

CRUSTAL DEFORMATION AND EARTHQUAKES

Edited by

Institute of Seismology

State Seismological Bureau

SEISMOLOGICAL PRESS

BEIJING

1988

THE EARTHQUAKE DEFORMATION CYCLE: EXAMPLES FROM SOUTH AMERICA AND THE WESTERN UNITED STATES

Robert Reilinger
Department of Earth, Atmospheric and Planetary Sciences
Earth Resources Laboratory
Massachusetts Institute of Technology
Cambridge, Massachusetts 02139 USA

ABSTRACT. A particularly detailed set of releveling observations in the vicinity of an intraplate, thrust earthquake (M 7.4) in Argentina, indicate a cyclic pattern of deformation very similar to that reported previously for interplate earthquakes. This deformation cycle, which may be characteristic of many seismically active areas, consists of: 1) steady strain accumulation, possibly punctuated by strain reversals, 2) coseismic strain release, 3) a period of continued strain release due to after-slip (persisting for perhaps a year or so), 4) rapid postseismic strain accumulation which decreases exponentially and grades into steady strain accumulation. Deformation associated with three earthquakes in the U.S. (1940, M7.1 Imperial Valley California; 1964, M8.4 Alaska; 1959, M7.5 Hebgen Lake, Montana) are interpreted in light of this general earthquake cycle and are used to investigate the mechanics of strain release for these events. These examples indicate that large postseismic movements can occur for strike-slip, thrust, and normal fault events, and both viscoelastic relaxation and postseismic after-slip must be incorporated in models of earthquake related deformation. The mechanics of the strain release process revealed by these examples has implications for estimating earthquake repeat times from geodetic observations near active faults.

INTRODUCTION

Observations of crustal movements (geodetic and geologic), primarily in the vicinity of large earthquakes along active plate margins, have revealed a cyclic pattern of deformation (e.g. Thatcher, 1984) associated with these events. Recent analyses of geodetic measurements in the U.S. and abroad suggest that this deformation cycle (perhaps with some modifications) may apply to intraplate as well as plate boundary earthquakes. This paper briefly reviews the observed earthquake deformation cycle (primarily vertical movements) placing particular emphasis on recent interpretations of deformation associated with a 1977 earthquake in Argentina. Examples are presented for deformation associated with three major earthquakes in North America. These earthquakes are characterized by three very different modes of

deformation; a strike-slip event along the Pacific-North American plate boundary in S. California (M7.1, 1940 Imperial Valley), a major interplate thrust event in S. Alaska (M8.4, 1964 Alaska), and an intraplate normal fault event along the Intermountain Seismic Belt in southwestern Montana (M7.5, 1959 Hebgen Lake). The observations and interpretations presented here have direct implications for the mechanics of strain accumulation and release and provide a physical basis for estimating earthquake recurrence times in the areas considered.

THE EARTHQUAKE DEFORMATION CYCLE

Figure 1A shows the idealized earthquake deformation cycle as recently summarized by Thatcher (1984) primarily on the basis of observations at convergent plate boundaries. The idealized cycle consists of interseismic strain accumulation leading to failure (coseismic). The essentially instantaneous coseismic deformation is followed by rapid postseismic recovery (i.e. opposite coseismic movements) which grades into steady state interseismic strain accumulation. Permanent deformation results when the postseismic and interseismic strain do not exactly balance the coseismic deformation. For the case shown in Figure 1A, permanent deformation is in the same sense as the coseismic deformation. The absence of a preseismic phase of deformation in the idealized cycle may reflect the lack of appropriate observations rather than evidence that anomalous (in relation to interseismic strain) preseismic movements do not occur.

A particularly detailed example of the earthquake deformation cycle, which is generally consistent with the idealized cycle shown in Figure 1A, exists for the 1977 Caucete, Argentina earthquake. This event is unique in that multiple precise leveling surveys were conducted in the immediate epicentral area prior to the earthquake (Volponi et al., 1983). These pre-earthquake surveys, together with post-earthquake surveys conducted specifically to monitor earthquake deformation, provide information on vertical movements which occurred prior to, during and after the event (Volponi et al., 1983; Kadinsky-Cade et al., 1985; Reilinger and Kadinsky-Cade, 1985).

Figure 1B shows the time behavior of movements in the vicinity of the 1977 Caucete, Argentina earthquake (solid circles). This time behavior, together with the spatial pattern of each phase of deformation, provides a basis for understanding fault behavior in this area. One possible interpretation, which is generally consistent with the idealized earthquake cycle, consists of the following sequence of events (Reilinger and Kadinsky-Cade, 1985). Deformation during the first preseismic period (1938 to 1967) results from slip on the eventual coseismic fault in the same sense as the 1977 coseismic slip. This slip may have been induced

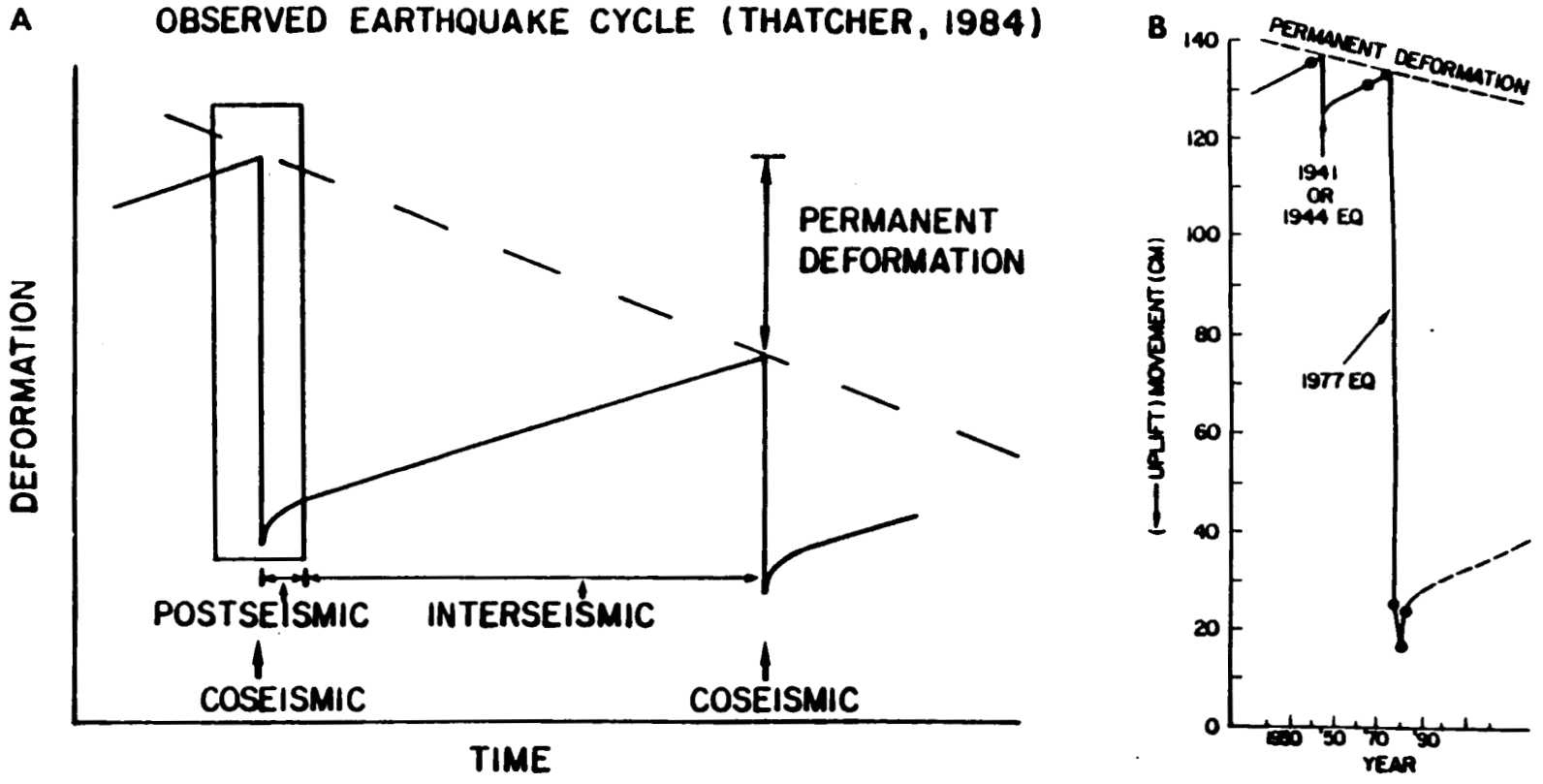

Figure 1: A) Idealized earthquake deformation cycle. Rectangle shows portion of cycle covered by observations in Figure 1B.

B) Relative movement versus time for benchmark near the epicenter of the 1977, Caucete, Argentina earthquake (from Reilinger and Kadinsky-Cade, 1985)

by the 1944 San Juan earthquake (M7.5) which occurred well west of the 1977 epicenter or may represent coseismic slip for a M6.5 earthquake in 1941 which occurred near the 1977 event. Deformation during the second preseismic period (1967 to 1976) is due to interseismic strain accumulation leading up to the large coseismic (1976 to 1978) fault slip. During the first postseismic period (1978 to 1980) movements result from after-slip (same direction as coseismic slip) on the coseismic fault, and movements for the second period (1980 to 1981) reflect the phase of rapid post-seismic recovery, possibly due to viscoelastic relaxation in the asthenosphere. The permanent deformation (uplift ~ 1mm/yr) is determined independently from geological observations; namely 4 - 5 km of relief developed over 4 - 5 MY. This interpretation, while generally consistent with the earthquake deformation cycle shown in Figure 1A, suggests two possible modifications in this cycle. First, at least for this particular event, there is evidence for long term precursory deformation (between 40 years and 10 years before event), although no unusual deformation was detected during the 10 years immediately preceeding the event. Second, continued slip apparently occurred on the earthquake fault for at least one year following the earthquake. It is not known to what extent either of these modifications apply more generally, although significant after-slip has been suggested for a number of other events, for example the 1940 and 1979 Imperial Valley earthquakes (Reilinger, 1984; Sharp et al., 1982).

1940 IMPERIAL VALLEY EARTHQUAKE

The Imperial Valley of Southern California is a complex transition zone between crustal spreading in the Gulf of California to the south and right lateral transform motion along the San Andreas system to the north. Historically the Imperial Valley has been one of the most seismically active areas in the U.S. It is characterized by predominantly right stepping, right lateral en echelon faults presumably linked by zones of crustal spreading. The Imperial and Brawley faults, major elements of the system of faults that transect the Valley, experienced a significant earthquake (located on the Imperial fault) and associated surface faulting in 1940 (M7.1). Figure 2A (upper right) shows a schematic view of the Imperial and Brawley faults and the location of two leveling routes surveyed by first order leveling by the National Geodetic Survey (NGS) in 1931, 1941, and 1972 (more recent surveys have been conducted but are not presented here). Profiles of relative elevation change along these two routes for the coseismic period (1931 to 1941) and the post-seismic period (1941 to 1972) are compared with two possible models for fault-related deformation in Figures 2A and 2B respectively (Reilinger, 1984). In both cases the models represent deformation of an elastic half-space due to a finite length, horizontal dislocation (pure strike-slip) on a vertical, rectang-

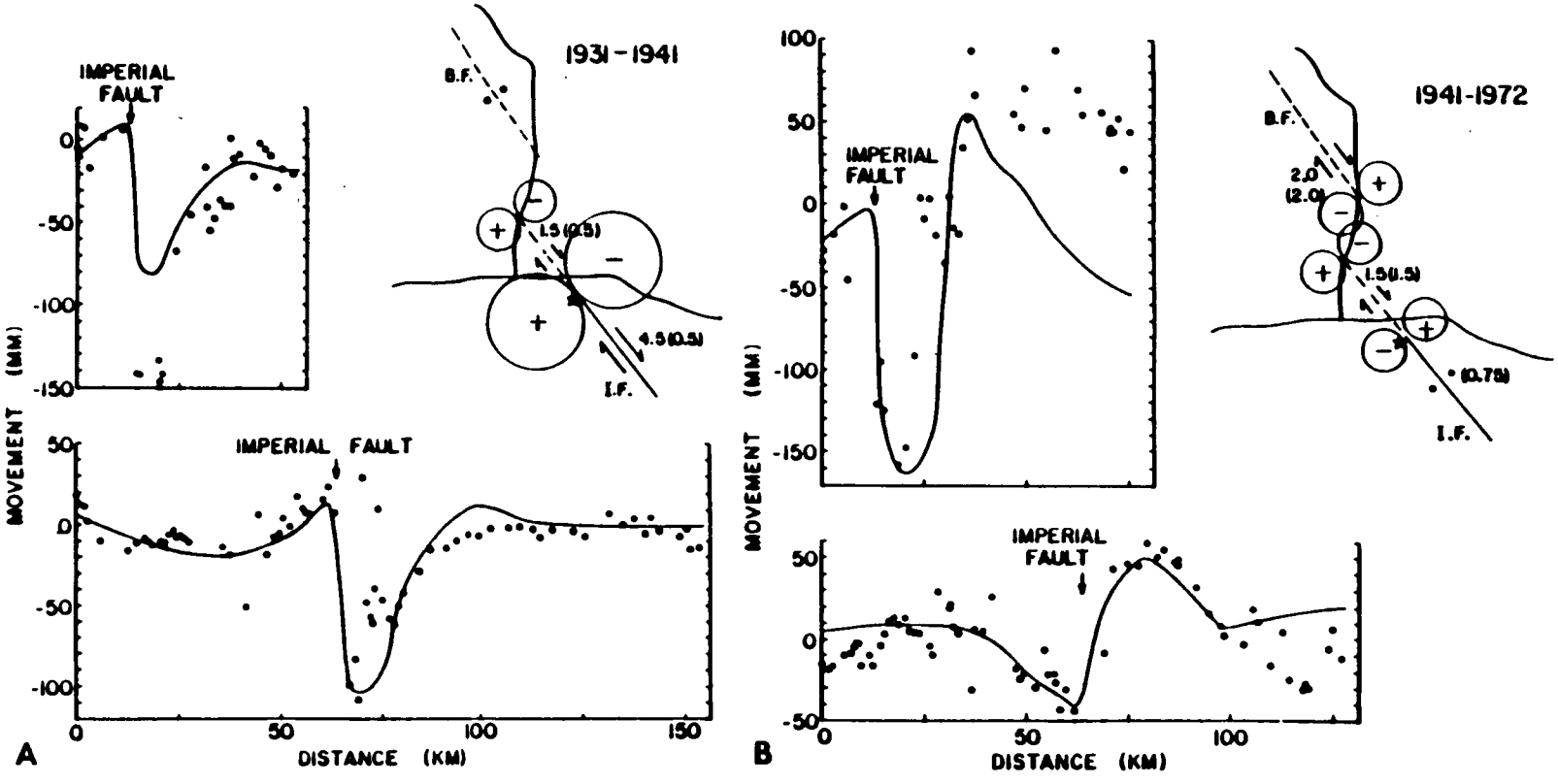

Figure 2: A) Map view showing leveling routes and model of fault offsets for coseismic (1931 to 1941) vertical movements in Imperial Valley. Star indicates 1940 epicenter. Numbers indicate shallow (0 - 13km) slip; numbers in brackets slip at depth (13 - 100km). Comparison between observed (points) and theoretical vertical movements along north-south route (top left) and east-west route (bottom). I.F. - Imperial fault, B.F. - Brawley fault. (Reilinger, 1984).

B) Model of fault offsets for postseismic (1941 to 1972) vertical movements. Format as in Figure 2A

ular fault. The major features of the coseismic model (Figure 2A) are large, shallow slip on the southern part of the Imperial fault (4.5m), lesser shallow slip on the northern part of the Imperial fault (1.5 m), and no slip on the Brawley fault. A somewhat improved fit is obtained by allowing a small amount of slip (0.5m) at depth along the entire length of the fault (presumably aseismic slip below the seismogenic zone). The primary features of the postseismic model (Figure 2B) are relatively large slip extending from near the surface to great depth (100 km) on the northern Imperial fault and the Brawley fault, no shallow slip on the southern Imperial fault, and lesser deep slip on the southern Imperial fault. Although these models appear somewhat complex, they suggest a rather simple scenario for coseismic and postseismic fault behavior. The earthquake caused large coseismic slip on the southern Imperial fault which transferred stress to the northern section of the Imperial fault and the Brawley fault. These stresses were subsequently released by aseismic slip to shallow depths on these fault segments during the postseismic period. This scenario is qualitatively consistent with observed coseismic offsets at the surface (Trifunac and Brune, 1970), geodetic estimates of horizontal deformation (Thatcher, 1979, Snay et al., 1982), and geophysical observations (fault creep, seismicity, surface faulting) of fault behavior (Reilinger, 1984).

Examination of Figures 2A and B indicate that the overall shallow slip (coseismic plus postseismic) was less on the northern Imperial and Brawley faults than on the southern Imperial fault. This difference in shallow slip may have contributed to surface faulting associated with the 1979, M6.6 Imperial Valley earthquake. This event caused surface faulting on the northern part of the Imperial fault and Brawley fault but not on the southern part of the Imperial fault even though the earthquake apparently initiated on the southern Imperial fault (Sharp et al., 1982).

Sauber et al. (1984) have investigated the contribution of viscoelastic relaxation to postseismic deformation for the 1940 Imperial Valley earthquake. They note that the reversal of the sense of movement during the postseismic period relative to the coseismic period along the east-west leveling route (Figures 2A, B) is qualitatively consistent with movements predicted by models of viscoelastic relaxation (e.g. Yang and Toksoz, 1981). Sauber et al. (1984) suggest that, while viscoelastic relaxation may account for some of the postseismic deformation, additional mechanisms such as fault creep are required to match the observations.

1964 ALASKA EARTHQUAKE

The 1964 (M8.4) Alaska earthquake occurred where the oceanic Pacific plate is being thrust under the North American plate at a rate of about 5 cm/yr. Surface displacements caused by the earthquake were well documented, affecting an area of at least

140,000 km^2 (e.g. Plafker, 1969). An interpreted profile (perpendicular to trench) of the observed coseismic deformation is shown in Figure 3A (Brown et al., 1977). This deformation was shown to be generally consistent with low-angle thrusting (12 m) on a fault approximately 600-800 km long, 200 km wide and dipping about 10° (Figure 3A). Analysis of the coseismic deformation associated with this event was instrumental in defining the subduction process and solidifying the plate tectonics hypothesis (e.g. Savage and Hastie, 1966, Hastie and Savage, 1970).

Following the 1964 earthquake the NGS conducted multiple leveling surveys (1964, 1965, 1968, 1975) specifically to monitor postseismic deformation along a route located in the zone of major coseismic subsidence. The elevation change profile derived from the 1964 and 1975 surveys is shown in Figure 3A and the time behavior of deformation in Figure 3B (Brown et al., 1977). These leveling data, in conjunction with tide gauge observations indicated exponentially decreasing uplift during the postseismic period in a region which had subsided 2 m during the earthquake. This uplift exceeded 0.5 m during the 10 years following the event.

Brown et al. (1977) interpreted the postseismic uplift as resulting from after-slip down-dip of the coseismic fault (Figure 3A, bottom). More recently Wahr and Wyss (1980) suggested that the observed postseismic deformation following the Alaska event resulted from viscoelastic relaxation in the asthenosphere (a possibility also considered by Brown et al., 1977). Both of these mechanisms are generally consistent with the temporal and spatial character of the deformation.

1959 HEBGEN LAKE EARTHQUAKE

The 1959, M7.5 Hebgen Lake earthquake occurred near the intersection of the Intermountain Seismic Belt and the Idaho Seismic Zone in southwestern Montana, USA. The Intermountain Seismic Belt, a major zone of seismicity that extends from southern Utah northward through Montana, is characterized by east-west tensional stress and is generally coincident with a north trending zone of normal faults which have apparently been active since mid-Tertiary (Smith and Sbar, 1974). A sub-belt of the Intermountain Seismic Belt, the Idaho Seismic Zone, crosscuts the Intermountain Seismic Belt, extending approximately east-west from the Yellowstone area through central Idaho. The Idaho Seismic Zone is dominated by north-south tension (Trimble and Smith, 1975).

Myers and Hamilton (1964) and Savage and Hastie (1966) reported and interpreted coseismic deformation (geodetic and field observations) for the 1959 event. The observed deformation and seismic observations indicated that the earthquake was a normal fault event on a northwest-southeast striking, south dipping (~ 55°) fault. Coseismic subsidence reached a maximum

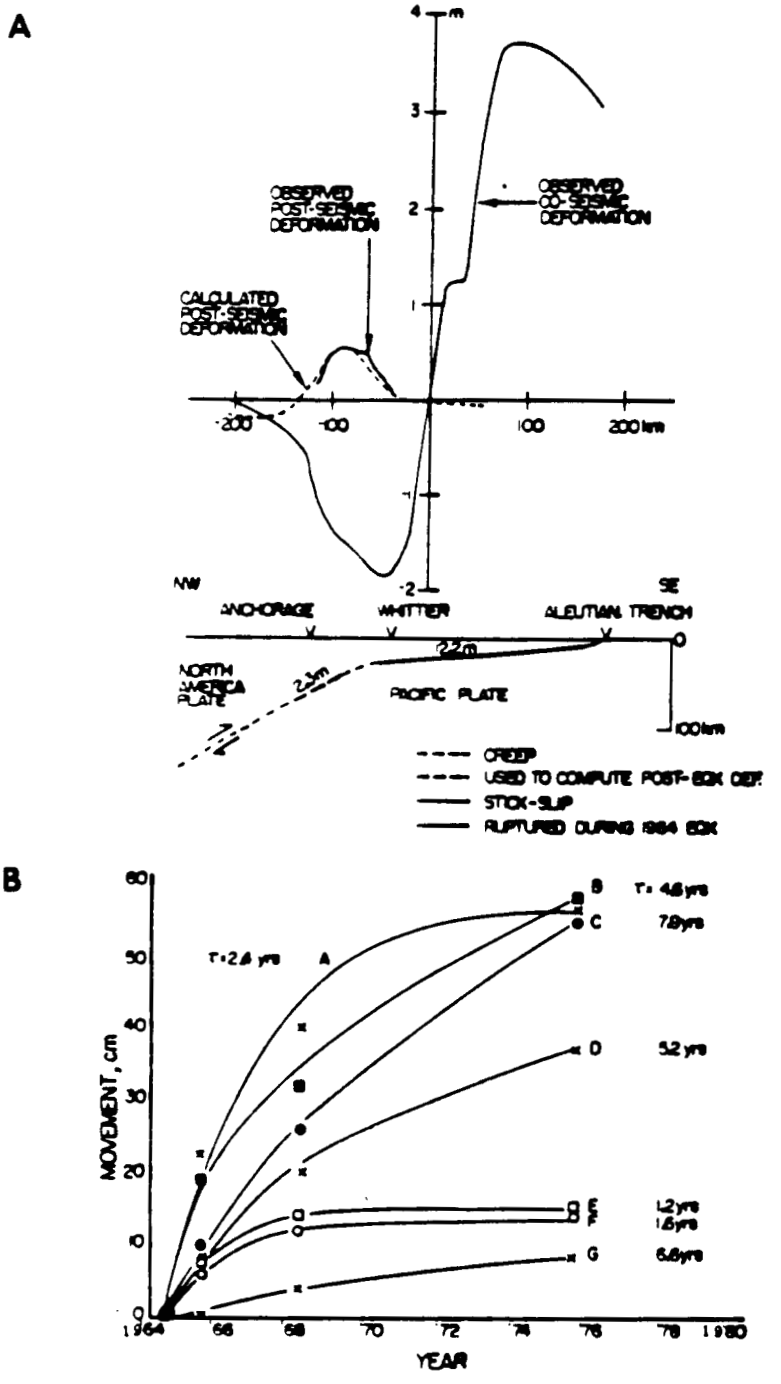

Figure 3: A) Buried creep model for the observed postseismic deformation following the 1964, Alaska earthquake (from Brown et al., 1977).

B) Time behavior of observed postseismic uplift following 1964, Alaska earthquake. The fitted exponential functions, of form $Y=A(1-e^{-t/\tau})$ where Y is uplift, t is time, and A is a constant, are shown by solid lines (from Brown et al., 1977).

of about 6.7 m just south of the major surface break, requiring about 10 m of slip on the fault. In 1983 the NGS releveled a 440 km long route which tranversed the Hebgen Lake region, approximately normal to the earthquake fault, and which passed within about 25 km of the 1959 epicenter (Reilinger, 1985). This route was previously leveled in 1923 and 1960. Short segments of this route were surveyed in 1967 and 1975. The elevation change profile derived from the 1960 and 1983 surveys is shown along with two models of postseismic deformation in Figure 4A. All of the elevation change observations (including profiles derived from the 1923, 1960, 1967 and 1975 surveys) are consistent with a pattern of deformation consisting of uplift centered on the eastward projection of the coseismic fault and subsidence south of the fault (Reilinger et al., 1977; Reilinger, 1985). Relative movements for the postseismic period 1960 to 1983 reach 30 $\pm$ 2 cm and extend over a distance of at least 150 km.

Some indication of the time behavior of this deformation can be obtained by examining elevation changes between two benchmarks located about 40 km south of the earthquake epicenter. This is the only section of the route where sufficient information is available for this purpose (surveyed in 1923, 1960, 1967 and 1983). A plot of the movement between these marks versus time is shown in Figure 4B. The rate of vertical deformation appears to be decreasing exponentially with a characteristic decay time of about ten years.

The USGS has been conducting trilateration measurements to monitor horizontal strain in the Hebgen Lake region since 1973. Their observations indicate uniaxial extension normal to the Hebgen Lake fault at a rate of 0.28 $\pm$ .02 μstrain/yr (Savage, 1983). This is the largest strain rate observed anywhere in the conterminous U.S. outside of California and is comparable in magnitude to strains observed along the San Andreas fault.

One interpretation of the observed vertical movements for the period 1960 to 1983 is illustrated in Figure 4A. The models show the expected viscoelastic deformation following normal faulting of an elastic layer overlying a viscoelastic half-space (model modified from Thatcher et al., 1980). The thickness of the elastic layer (~ 30-40 km) and viscosity of the asthenosphere (~ 10^{20} Poise) are roughly consistent with estimates determined from isostatic rebound of Lake Bonneville which was located about 300 km south of the Hebgen Lake region. Postseismic viscoelastic relaxation may also account for the large horizontal strain rate. A particularly important aspect of the observed postseismic deformation in the Hebgen Lake area is that it is virtually impossible to fit with models of after-slip on the coseismic fault and/or down dip of the coseismic fault.

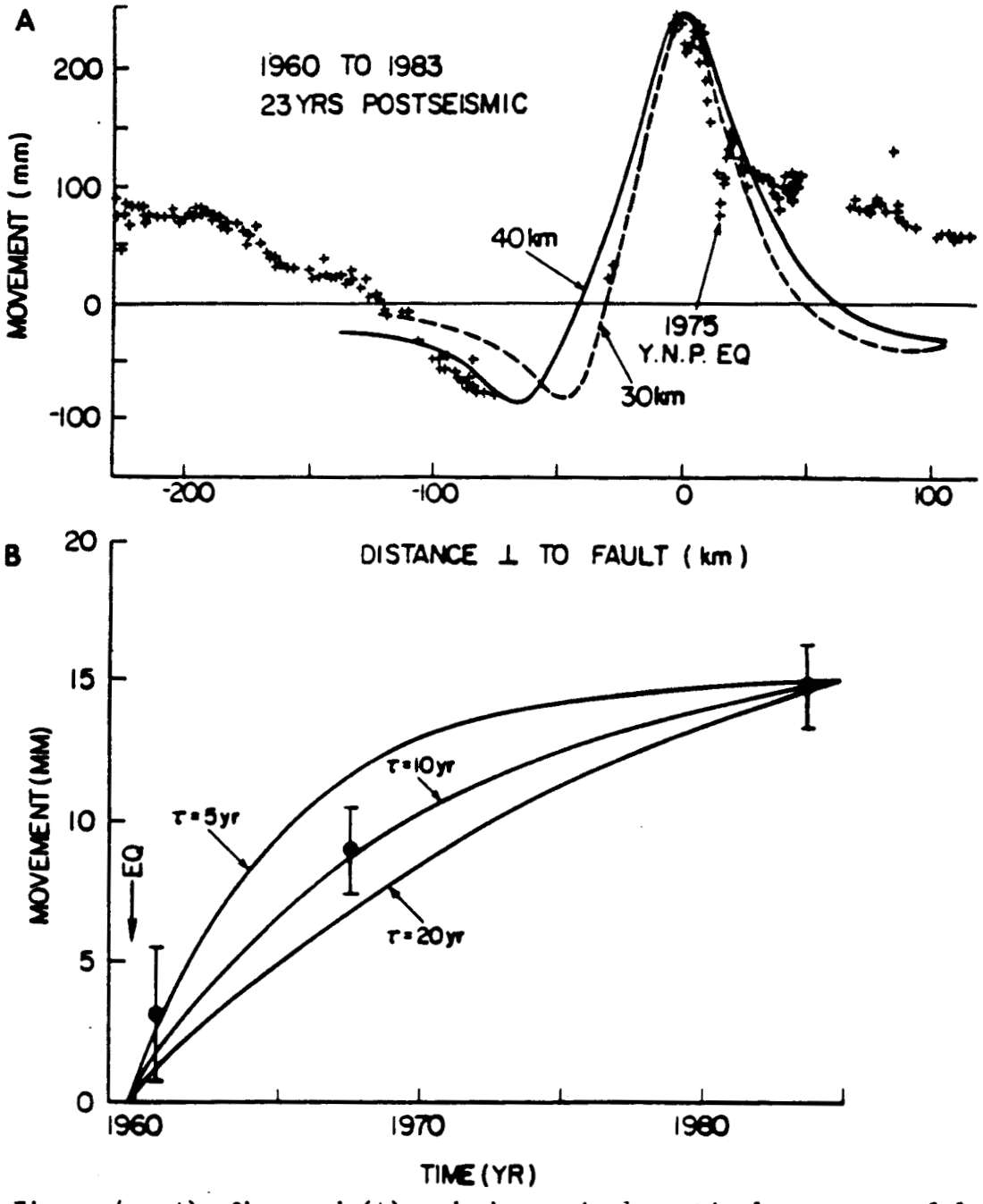

Figure 4: A) Observed (+) and theoretical vertical movements following 1959 Hebgen Lake earthquake. 1975 Y.N.P. EQ shows vertical movements due to 1975 Yellowstone earthquake. Models represent postseismic viscoelastic relaxation for faulting of an elastic layer (thickness of 30 km, 40 km) overlying a viscoelastic half-space. Models modified from Thatcher et al., 1980.

B) Time behavior of deformation following the Hebgen Lake earthquake. Model curves as in Figure 3B.

IMPLICATIONS FOR EARTHQUAKE PREDICTION

The interpretation of the observed deformation in the vicinity of the 1977 Argentina earthquake provides a basis for estimating recurrence times for earthquakes on the fault responsible for this event. Examination of Figure 1B indicates that the 1977 earthquake occurred when strain had accumulated (since the previous slip event in 1941 or 1944) to the level defined by the observed permanent deformation as determined by independent geological observations. This behavior is consistent with that expected from the time predictable model of earthquake occurrence (Shimazaki and Nakata, 1980). According to this model, the interval between two earthquakes on the same fault should be the quotient of the elastic strain drop accompanying the first earthquake and the average rate of elastic strain accumulation during the interval between earthquakes (i.e. total strain accumulation minus permanent, anelastic strain: Sykes and Quittmeyer, 1981; Thatcher, 1984). To the extent that the time predictable model is appropriate for the longer term fault behavior in this area, it is possible to estimate the time to the next earthquake from the observed deformation leading up to the 1977 event (assuming this represents the average interseismic strain rate), the deformation that accompanied the 1977 earthquake, and permanent deformation as given by geological observations. This procedure yields an estimate of 200 to 600 years for the time to the next earthquake on the fault responsible for the 1977 event (Reilinger and Kadinsky-Cade, 1985).

Deformations following each of the earthquakes described here clearly indicate that rapid postseismic movements occur for both interplate and intraplate events. The observed vertical movements following the Imperial Valley and Alaska earthquakes illustrate the inherent ambiquity in the interpretation of such postseismic deformation. Because of the large dimensions and shallow dips of the coseismic faults associated with subduction related earthquakes, it is very difficult to distinguish between creep mechanisms and viscoelastic relaxation (both have similar wavelengths). This ambiguity has been discussed in detail by Thatcher and Rundle (1984). This same ambiguity exists for strike-slip events such as the 1940 Imperial Valley earthquake (Sauber et al., 1984). On the other hand, the Hebgen Lake event clearly indicates that models of earthquake related deformation must include postseismic viscoelastic relaxation. Thatcher (1984), on the basis of observations in Japan, suggests that postseismic deformation may be characterized by two timescales. The first, of about a year or less, apparently results from after-slip, and the second (which persists for 10's of years) reflects viscoelastic relaxation. This interpretation appears to be supported by the observations presented here.

Understanding the nature of postseismic deformation has important implications for estimating earthquake recurrence times from the time predictable model. In essence, postseismic deformation represents a period of rapid strain accumulation. This rapid strain accumulation will tend to reduce the time interval between earthquakes (Figure 1A). On the other hand, rates of strain accumulation determined from geodetic observations during periods following major earthquakes will be larger than average interseismic strain rates. Extrapolating these large rates will tend to give recurrence times which are too short. The Hebgen Lake region is a case in point. As mentioned earlier, the USGS has been measuring horizontal strain in the Hebgen Lake region since about 1973. These measurements indicate uniaxial extension perpendicular to the Hebgen Lake fault at a surprizingly rapid average rate (0.25 strain/yr; Savage, 1983). Savage (1983) points out that if these measurements reflect steady state strain accumulation, the next earthquake on the Hebgen Lake fault should occur in 100 to 200 years. However, if these large strain rates reflect postseismic viscoelastic relaxation, then recurrence times would be considerably larger.

While our understanding of the earthquake cycle is clearly incomplete, the observations and interpretations summarized here may help provide a basis for understanding the mechanics of strain accumulation and release and thereby aid in earthquake prediction.

Acknowledgements. Supported in part by the SCEEE/Air Force Geophysics Scholar Program, USGS Contract 14-08-0001-21998, NASA Grant NAS5-27339 and NSF Grant 8410366-EAR.

References

Brown, L.D., R.E. Reilinger, S.R. Holdahl, and E.I. Balazs, 1977: Postseismic crustal uplift near Anchorage, Alaska, J. Geophys. Res., 82, 3369-3378.

Hastie, L.M., and J.C. Savage, 1970: A dislocation model for the Alaska earthquake, Bull. Seismol. Soc. Amer., 60, 1389-1392.

Kadinsky-Cade, K., R. Reilinger, and B. Isacks, 1985: Surface deformation associated with the November 23, 1977 San Juan, Argentina earthquake sequence, J. Geophys. Res., in press.

Myers, W.F., and W. Hamilton, 1964: Deformation accompanying the Hebgen Lake earthquake of August 17, 1959, U.S. Geol. Surv. Pap. 435, 55-98.

Plafker, G., 1969: Tectonics of the March 27, 1964, Alaska earthquake, U.S. Geol. Surv. Prof. Pap., 543-I, 1-74.

Reilinger, R., 1984: Coseismic and postseismic vertical movements associated with the 1940 M7.1 Imperial Valley, California, earthquake, J. Geophys. Res., 89, 4531-4537.

Reilinger, R., 1985: Vertical movements associated with the 1959, M7.1 Hebgen Lake, Montana earthquake, U.S. Geol. Surv. Open-File Rep. 85-290, 519-530.

Reilinger, R.E., G.P. Citron, and L.D. Brown, 1977: Recent vertical crustal movements from precise leveling data in southwestern Montana, western Yellowstone Park, and the Snake River plain, J. Geophys. Res., 82, 5349-5359.

Reilinger, R., and K. Kadinsky-Cade, 1985: The earthquake deformation cycle in the Andean back-arc, western Argentina, J. Geophys. Res., in press.

Sauber, J., R. Reilinger and M.N. Toksoz, 1984: Postseismic viscoelastic relaxation associated with the 1940 Imperial Valley earthquake, EOS, Trans. Am. Geophys. Union, 65, 190. 190.

Savage, J.C., 1983: Strain accumulation in the western United States, Ann. Rev. Earth Planet. Sci., 11, 11-43.

Savage, J.C., and L.M. Hastie, 1966: Surface deformation associated with dipslip faulting, J. Geophys. Res., 71, 4897-4904.

Sharp, R.V., et al, 1982: Surface faulting in the central Imperial Valley, U.S. Geol. Survey Prof. Pap., 1254, 119-143.

Shimazaki, K., and T. Nakata, 1980: Time-predictable recurrence model for large earthquakes, Geophys. Res. Lett., 7, 279-282.

Smith, R.B., and M.L. Sbar, 1974: Contemporary tectonics and seismicity of the western United States with emphasis on the Intermountain Seismic Belt, Geol. Soc. Amer. Bull., 85, 1205-1218.

Snay, R.A., M.W. Cline, and E.L. Timmerman, 1982: Horizontal deformation in the Imperial Valley, California, between 1934 and 1980, J. Geophys. Res., 87, 3959-3968.

Sykes, L.R., and R.C. Quittmeyer, 1981: Repeat times of great earthquakes along simple plate boundaries, in Earthquake Prediction: An International Review, Maurice Ewing Series, vol. 4, ed. D.W. Simpson and P.G. Richards, 217-247.

Thatcher, W., 1979: Horizontal crustal deformation from historic geodetic measurements in Southern California, J. Geophys. Res., 84, 2351-2370.

Thatcher, W., 1984: The earthquake deformation cycle, recurrence, and the time predictable model, J. Geophys. Res., 89, 5674-5680.

Thatcher, W., T. Matsuda, T. Kato, and J. Rundle, 1980: Lithospheric loading by the 1896 Riku-u earthquake, northern Japan: Implications for plate flexure and asthenospheric rheology, J. Geophys. Res., 85, 6429-6435.

Thatcher, W., and J.B. Rundle, 1984: A viscoelastic coupling model for the cyclic deformation due to periodically repeated earthquakes at subduction zones, J. Geophys. Res., 89, 7631-7640.

Trifunac, M.D., and J.N. Brune, 1970: Complexity of energy release during the Imperial Valley, California, earthquake of 1940, Bull. Seismol. Soc. Amer., 60, 137-160

Trimble, A.B. and R.B. Smith, 1975: Seismicity and contemporary tectonics of the Hebgen Lake - Yellowstone Park region, J. Geophys. Res., 80, 773-741.

Volponi, F., A. Robles, and J. Sisterna, 1983: Gravity variations in the epicentral zone of the Caucete earthquake, November 23rd, 1977, Universidat Nacional de San Juan, Instituto Sismologico Zonda, 12 pp.

Wahr, J., and M. Wyss, 1980: Interpretation of postseismic deformation with a viscoelastic relaxation model, J. Geophys. Res., 85, 6471-6477.

Yang, M., and M.N. Toksoz, 1981: Time-dependent deformation and stress relaxation after strike-slip earthquakes, J. Geophys. Res., 86, 2889-2901.

APPENDIX 2

Geodetic Measurement of Deformation East of the San Andreas Fault in Central California

Jeanne Sauber, Michael Lisowski, and Sean C. Solomon

To appear in *Slow Deformation and Transmission of Stress in the Earth*, edited by S. Cohen and P. Vanicek, Geophys. Mon. Ser., Amer. Geophys. Un., Washington, D.C., 1989.

GEODETIC MEASUREMENT OF DEFORMATION EAST OF THE SAN ANDREAS FAULT IN CENTRAL CALIFORNIA

Jeanne Sauber

Department of Earth, Atmospheric, and Planetary Sciences, Massachusetts Institute of Technology, Cambridge, MA 02139

Michael Lisowski

U.S. Geological Survey, Menlo Park, CA 94025

Sean C. Solomon

Department of Earth, Atmospheric, and Planetary Sciences, Massachusetts Institute of Technology, Cambridge, MA 02139

Abstract. Triangulation and trilateration data from two geodetic networks located between the San Andreas fault and the Great Valley have been used to calculate shear strain rates in the Diablo Range and to estimate the slip rate along the Calaveras and Paicines faults in central California. The shear strain rates, $\dot{\gamma}_1$ and $\dot{\gamma}_2$, were estimated independently from angle changes using Prescott's method and from the simultaneous reduction for station position and strain parameters using the DYNAP method with corrections to reduce the triangulation and trilateration data to a common reference surface. On the basis of Prescott's method, the average shear strain rate across the Diablo Range for the time period between 1962 and 1982 is 0.15 ± 0.08 μrad/yr, with the orientation of the most compressive strain (β) at N16°E ± 14°. Utilizing corrections for the deflection of the vertical and the geoid - reference ellipsoid separation computed on the basis of local gravity observations, $\dot{\gamma} = 0.19 \pm 0.09$ μrad/yr and β = N16°E ± 13°. Although $\dot{\gamma}$ is not significantly greater than zero, at the 95% confidence level the orientation of β is similar to the direction of maximum compressive strain indicated by the orientation of major fold structures in the region (N25°E). We infer that the measured strain is due to compression across the folds of this area; the average shear straining corresponds to a relative shortening rate of 5.7 ± 2.7 mm/yr. In contrast to the situation throughout most of the Coast Ranges where fold axes have orientations approximately parallel to the San Andreas fault, within the Diablo Range between Hollister and Coalinga the trends of the fold axes are different and are thought to be controlled by reactivation of older structures. From trilateration measurements made between 1972 and 1987 on lines that are within 10 km of the San Andreas fault, a slip rate of 10-12 mm/yr was calculated for the Calaveras-Paicines fault south of Hollister. The slip rate on the Paicines fault decreases to 4 mm/yr near Bitter. To distinguish between different models that describe the distribution of strike-slip and compressive displacements within the southern Coast Ranges we compared the findings of regional geologic and geodetic studies with predictions from kinematic plate models. Such comparisons support the view that the fault-parallel component of the San Andreas "discrepancy vector" may be accommodated by strike-slip

motion on the Rinconada as well as the San Gregorio fault. Geological and seismicity data, as well as our geodetic results, suggest that northeast-southwest compression in the Coast Ranges of central California may be localized to two regions, the 30-km-wide zone spanned by the triangulation and trilateration network of this study and a second zone to the west of the Rinconada fault. The inferred shortening to the east of the San Andreas fault may represent a significant component of the fault-normal compression predicted by the discrepancy vector.

Introduction

Although most of the relative motion between the Pacific and North American plates in central California is accommodated by slip along the San Andreas fault, distributed compressive and right-lateral strike-slip motion also occurs on faults with surface traces subparallel to the San Andreas fault located between the continental escarpment and the Great Valley [*Gawthrop*, 1977; *Page*, 1981; *Crouch et al.*, 1984; *Eaton*, 1984; *Minster and Jordan*, 1984, 1987; *Namson and Davis*, 1988]. The axis of greatest compression across this region, the southern Coast Ranges subprovince [*Page*, 1981], is thought to be oriented nearly perpendicular to the trend of the San Andreas fault, a result attributed to a combination of slightly convergent relative motion between the Pacific and North American plates and low shear strength along the fault zone [*Mount and Suppe*, 1987; *Zoback et al.*, 1987]. While most recent earthquakes in central California are located on the San Andreas fault (Figure 1), scattered diffuse activity also occurs between the San Andreas fault and the Great Valley. The May 1983 Coalinga earthquake (M_L=6.7), which involved slip on a thrust or reverse fault beneath a young surface fold [*Stein and King*, 1984; *Stein*, 1985], has focused attention on the importance of understanding the state of stress and the rates of deformation to the east of the San Andreas fault in this region and their relation to the overall deformation in the Coast Ranges. In this paper we determine rates of crustal strain in the Diablo Range north of Coalinga from a triangulation and trilateration network and from line-length changes determined by means of trilateration measurements within 10 km of the San Andreas fault. These geodetic results are then compared with other geological and geophysical data to characterize the nature of deformation across the southern Coast Ranges.

Tectonic Setting

The principal strike-slip faults in central California have been well characterized by geologic and geodetic studies. The branched system of subparallel faults near Hollister coalesces southward into a single shear zone, the San Andreas fault, south of Hepsedam (Figure 2). The Calaveras fault is the primary active fault to the northeast of the San Andreas fault near Hollister, while to the southeast of Hollister several faults comprise the southern end of the Calaveras fault zone, among which the Paicines fault is most prominent. Horizontal deformation across the San Andreas and Calaveras-Paicines faults in central California has been measured with near-fault alinement arrays, creepmeters, and trilateration at short and intermediate distances [*Savage and Burford*, 1973; *Thatcher*, 1979a; *Burford and Harsh*, 1980; *Lisowski and Prescott*, 1981]. Between Hollister and Hepsedam (Figure 2), the rate of steady surface slip

(creep) across the San Andreas fault increases from ~ 13 to 32 mm/yr and surface slip on the Calaveras-Paicines fault decreases from ~17 to 0 mm/yr. Between Hepsedam and the latitude of Coalinga (Figure 2) near-fault and intermediate-scale geodetic measurements of right-lateral slip are in good agreement and indicate creep at a rate of approximately 32 mm/yr. The rate of slip on this segment of the San Andreas fault estimated from Holocene geological data is 34 ± 3 mm/yr [*Sieh and Jahns*, 1984] at an azimuth of N41°W ± 2° [*Minster and Jordan*, 1984; *Mount and Suppe*, 1987]. Southward of the latitude of Coalinga shallow slip on the San Andreas fault decreases and the width of the zone of deformation increases over the transition to a locked segment of the San Andreas fault in the Carrizo Plain (the southern aseismic portion of the San Andreas in Figure 1).

The major structural features in the region of this study are shown in Figures 2 and 3. Within 5-10 km to the east of the San Andreas fault the primary geologic structures are related to dextral shear on the San Andreas and Calaveras-Paicines faults (Figure 2). The Diablo Range to the east of this region is a broad antiform which trends approximately N65°W [*Page*, 1985] and encompasses subsidiary fold structures such as the Vallecitos syncline (Figure 3). North of Coalinga the range is pierced by the New Idria diapir (Figure 3) of serpentine and Franciscan rocks. Along the northeast boundary of the study area is the Ortigalita fault (Figure 2), a high-angle fault along or near the contact of Franciscan rocks and the Great Valley sequence to the east [*Raymond*, 1973]. Trenching of the Ortigalita fault zone shows exposed offsets of late Pleistocene and Holocene soils, with possibly as much as 5 km of Quaternary right-slip displacement [*Hart et al.*, 1986].

Multiple phases of deformation in the Diablo Range have been documented by structural analysis [*Namson and Davis*, 1988]. *Harding* [1976] pointed out that there are folds of middle to late Miocene age which are synchronous with the initiation of displacement on the San Andreas fault. The most recent uplift of the Diablo Range began in Pliocene time and most likely accelerated in the Pleistocene [*Page*, 1981; *Page and Engebretson*, 1984]. The Quaternary (< 2.2 Ma) folding is more widely distributed and of much greater structural relief than the Miocene folds [*Namson and Davis*, 1988].

Focal mechanisms of earthquakes in the Diablo Range [*Eaton*, 1985] show a mixture of thrust, reverse, and strike-slip faulting. The locations of three of the larger earthquakes with well-determined focal mechanisms, the October 1982 Idria event (M_L=5.5), the May 1983 Coalinga event (M_L=6.7), and the August 1985 North Kettleman Hills event (M_L=5.5), are given in Figure 1. The focal mechanism determined for the Idria earthquake indicates thrust faulting on a plane oriented N72°E or reverse slip on a plane oriented N64°W [*Eaton*, 1985]. The Coalinga and Kettleman Hills events have similar focal mechanisms with slip occurring on fault planes oriented at about N53°W as either thrusting on a plane dipping shallowly to the southwest or reverse slip on a plane steeply dipping to the northeast [*Eaton*, 1985; J.P. Eaton, personal communication, 1987]. A preliminary focal mechanism determined for an earthquake which occurred on the Ortigalita fault on January 6, 1988 (M_L=3.7), indicates right-lateral slip on a fault plane oriented ~N25°W or left-lateral slip on a plane oriented N65°E (P.A. Reasenberg, personal communication, 1988). The earthquake focal mechanisms and geological structures in the area suggest two primary modes of deformation to the

northeast of the San Andreas fault: compression normal to the major fold structures of the region and right-lateral strike-slip motion on faults such as the Calaveras-Paicines and the Ortigalita.

By way of comparison, in the Coast Ranges to the west of the San Andreas fault focal mechanisms [*Gawthrop*, 1977; *Eaton*, 1984; *Dehlinger and Bolt*, 1987] and extensive geological mapping [summarized in *Crouch et al.*, 1984; *Slemmons*, 1987] suggest variable modes of deformation. Between the San Andreas and the Rinconada faults (Figure 1) is the seismically quiescent Salinian block. The upper crust is composed of high-strength granite which is only weakly folded and sparsely faulted [*Dehlinger and Bolt*, 1987; *Slemmons*, 1987]. Focal mechanisms from the Rinconada fault show a mixture of right-lateral strike-slip faulting on northwest striking planes, oblique slip, and reverse faulting [*Gawthrop*, 1977; *Dehlinger and Bolt*, 1987]. From field mapping of recent offsets, D.B. Slemmons (personal communication, 1987) and E.W. Hart (personal communication, 1988) suggest that right-lateral strike-slip faulting dominates the displacement along the Rinconada fault. Between the Rinconada and the San Gregorio-Hosgri faults (Figure 1) the upper crust consists of the very heterogeneous Franciscan complex. Focal mechanisms from this region indicate dominantly oblique reverse faulting along northwest-trending, northeast dipping planes, with P axes oriented N20°-50°E or S20°-50°W [*Dehlinger and Bolt*, 1987]. Significant late-Quaternary right-lateral strike-slip offsets have been measured on the San Gregorio fault [*Clark et al.*, 1984]. South of Monterey Bay this fault branches into several splays, with some branches showing primarily right-lateral strike-slip displacement and others showing east-up reverse faulting [*Hamilton*, 1987]. Focal mechanisms from the San Gregorio-Hosgri fault also indicate right-lateral strike-slip faulting and oblique reverse faulting with a right-lateral component on a northeast dipping plane [*Gawthrop*, 1977; *Eaton*, 1984; *Dehlinger and Bolt*, 1987].

Geodetic Strain Rates

We make use of two geodetic networks to estimate current rates of deformation to the east of the San Andreas fault in central California. The San Benito triangulation and trilateration network spans the Paicines fault zone just east of the San Andreas fault, extends eastward to the western margin of the Great Valley, and is 50 km in extent in the southeast-northwest direction across the Diablo Range (Figure 3). To examine more localized deformation within the zone 10 km to the east of the San Andreas fault, short- and intermediate-range lines from the U.S. Geological Survey (USGS) Coalinga trilateration network were utilized. The geodetic results derived from the Coalinga trilateration data provide an update to the slip rates estimated for the Calaveras and Paicines faults by *Lisowski and Prescott* [1981].

To distinguish between engineering and tensor shear strain, we denote the former by γ and give in units of μrad, whereas the latter is denoted by ε and is given in units of μstrain [*Savage*, 1983]. Uncertainties, where not otherwise stated, are one standard deviation (σ).

San Benito Network

A triangulation survey of the San Benito network was conducted in 1962 by the National Geodetic Survey, and in 1982 a trilateration survey of the San Benito network was performed by the USGS. For interstation visibility, triangulation and trilateration stations are situated on the highest points in a region; thus, many of the stations in the San Benito network are located near anticlinal peaks (Figure 2). To determine the rates of deformation from the San Benito data the observations were processed utilizing two independent procedures: an extended version of Frank's method [*Prescott*, 1976] and the DYNAP method [*Snay*, 1986; *Drew and Snay*, 1988]. In the Appendix we discuss the accuracy of the triangulation and trilateration measurements utilized in this study, the assumptions made in our estimation of the horizontal shear parameters, the considerations involved in combining triangulation and trilateration data to determine the rate of shear strain utilizing the Prescott and DYNAP methods, the corrections applied to reduce the triangulation and trilateration observations to a common reference system, and the methods used to estimate the deflection of the vertical components and the geoid - reference ellipsoid separation needed to make the reduction corrections.

Utilizing both methods we calculate the horizontal shear strain rate components $\dot{\gamma}_1$ and $\dot{\gamma}_2$. In terms of elements ε_{ij} of the strain tensor, $\gamma_1 = \varepsilon_{11} - \varepsilon_{22}$ and $\gamma_2 = \varepsilon_{12} + \varepsilon_{21}$, where the strain tensor is referred to a geographic coordinate system in which the 1-axis is directed east and the the 2-axis is directed north. The strain component γ_2 is equal to the decrease induced by strain in the right angle between northward- and eastward-directed lines, whereas γ_1 is equal to the increase in the angle between lines directed northwest and northeast. Results are generally given in terms of the maximum shear strain rate $\dot{\gamma}$, where $\dot{\gamma}^2 = \dot{\gamma}_1^2 + \dot{\gamma}_2^2$, and the orientation ψ of the vertical plane with maximum rate of right-lateral shear [*Frank*, 1966; *Prescott*, 1976]. For comparison with the trends of fold structures of the Diablo Range, the orientation β of the maximum rate of compressive strain is sometimes given instead of the orientation of maximum rate of right-lateral shear.

Results with Prescott's method. The observations used to estimate $\dot{\gamma}_1$ and $\dot{\gamma}_2$ in the extended version of Frank's method [*Prescott*, 1976] are changes in angles. In this study we determined angle changes from two different data types, reflecting the different types of surveys made in 1962 and 1982. Further, we compared angles measured on the Earth's surface to angles determined from a network adjustment on a reference ellipsoid. In using data derived from different measurement techniques it is preferable to reduce the data to a common reference surface. The required reduction corrections are discussed in the Appendix. In employing Prescott's procedure to determine the strain parameters we did not make these corrections. In our use of the alternative DYNAP method these corrections are performed, and we compare the results from the two techniques to illustrate in part the utility of making these corrections.

The angle changes associated with the stations Bitter, Hepsedam, and Panoche were significantly larger than angle changes from other portions of the network and were, therefore, examined separately. Bitter and Hepsedam are located near the Paicines fault zone. Using only the 11 angle measurements that include one of the stations Bitter or Hepsedam gives $\dot{\gamma} = 0.56 \pm 0.16$ μrad/yr and $\Psi = \text{N}28^\circ\text{W} \pm 11^\circ$ The shear strain rate across the approximately 10-km-wide zone to the northeast of stations

Bitter and Hepsedam, assuming right-lateral motion on the Paicines fault, implies a rate of slip of 5 ± 2 mm/yr. Additional geodetic data from the Coalinga trilateration network relating to deformation across the San Andreas and Calaveras-Paicines faults are discussed in the next section.

The relatively large angle changes around station Panoche are not so easily explained. Using only the seven angle changes that include Panoche gives $\dot{\gamma}$ = 0.76 ± 0.27 μrad/yr and ψ = N58°W ± 9°, or β = N13°W ± 9°. These results are not consistent with either shear strain across the Ortigalita fault zone or contraction across the major fold structures of the region.

The strain rate parameters estimated on the basis of 25 angle changes in the central portion of the San Benito network, excluding angles to Bitter, Hepsedam, or Panoche, were $\dot{\gamma}$ = 0.15 ± 0.08 μrad/yr and β = N16°E ± 14°, or ψ = N29°W ± 14°. The standard deviations reflect both misfit and data uncertainties due to measurement imprecision.

To search for significant strain inhomogeneity, the shear strain parameters were estimated from spatial subsets of these data, again excluding the Bitter, Hepsedam, and Panoche stations (Table 1). There is a trade-off between improving the precision of the strain estimate by using a larger number of angles and averaging spatial variations as the size of the sampled region is increased. The data were first broken into two distinct groups, one set closer to the Great Valley ("east") and one set closer to the San Andreas fault ("west"). If the measured rates of shear strain were due to strain accumulation on the adjacent San Andreas fault, the rate of shear strain would be higher in the western subnet. Alternatively, if the rate of compressive strain was higher across the folds near the Great Valley, the eastern subnet might show a higher shear strain rate. There is no suggestion of a significant rate difference, however, between the strain rates determined from the eastern and western data subgroups. The set of 25 angles were also divided into "north" and "south" sets to look for any change which might be associated with along-strike variations on the San Andreas and Calaveras-Paicines faults. Although the strain rate results differ in the subnets, particularly in the orientation of maximum rate of compression, the magnitudes and orientations of strain rate in the various subregions are not significantly different from the average values determined from the complete set of 25 angles.

Results with the DYNAP method. In a second approach, the directions observed in 1962 and the distances measured in 1982 were employed to solve simultaneously for crustal motion parameters and the horizontal positional coordinates of the geodetic stations using the DYNAP method [*Snay*, 1986; *Drew and Snay*, 1988]. With DYNAP we are able to make single epoch adjustments to search for any observational errors during the individual surveys, and we are able to evaluate the effect of making reduction corrections to the distance and direction observations.

We first performed separate network adjustments for 1962 and 1982. A particular solution was determined by holding the minimum number of free parameters fixed. For the two-dimensional adjustment of 1962 triangulation data, these free parameters are two components of translation, a network rotation, and scale. For the two-dimensional adjustment of the 1982 trilateration data, scale is not a free parameter. Examination of the largest standardized residuals (given by the difference between observed and calculated values divided by the standard deviation of the observation) indicates that the 1962 direction observations to the

station Panoche have large residuals. This may account for the anomalously large angle changes associated with Panoche discussed earlier. Large residuals are not systematically associated with any one station in the 1982 adjustment.

From the analysis utilizing the Prescott method we obtained the result that the angle changes associated with the stations Bitter and Hepsedam were consistent with right-lateral slip at the approximate orientation of the Paicines fault. To test this result we solved for strain parameters and horizontal coordinates for a small subnetwork consisting of Bitter, Hepsedam, Smoker, and Ley (Figure 2). The rate of shear strain was estimated to be 0.53 ± 0.35 μrad/yr with $\psi = N40°W \pm 19°$, similar to the orientation of the San Andreas and Paicines faults.

The shear strain rate parameters $\dot{\gamma}_1$ and $\dot{\gamma}_2$ were estimated by the DYNAP method using data from the central portion of the network (excluding measurements to Panoche, Bitter and Hepsedam). Without taking into account corrections the rate of shear strain $\dot{\gamma} = 0.15 \pm 0.09$ μrad/yr and $\beta = N17°E \pm 16°$, similar to the result obtained utilizing Prescott's method. The rate of shear strain determined using the corrected data, denoted by $\dot{\gamma}_C$ is 0.19 ± 0.09 μrad/yr, with $\beta = N16°E \pm 13°$ (Figure 4).

As shown in Figure 4, at the 95% confidence level $\dot{\gamma}$ is not significantly greater than zero and β is not significantly different from the orientation predicted for shear strain associated with slip on the San Andreas fault (N4°E). The orientation of β, however, is similar to the direction of maximum compressive strain indicated by the orientation of major fold structures in this region. If we assume that the strain represents uniform horizontal contraction across a 30-km-wide region in the direction N16°E and that there is no extension in the orthogonal direction, this average strain rate corresponds to 5.7 ± 2.7 mm/yr of shortening.

The error in the estimate of shear strain rate determined in this study is dominated by the less accurate triangulation survey (see Appendix). It is instructive to estimate the accuracy that could be achieved with an additional trilateration survey of this network. An additional survey of all the stations in the San Benito network in 1992, for instance, would provide ~0.02 μstrain/yr accuracy in the principal strains, and all of the horizontal components of the tensor rate of strain ($\dot{\varepsilon}_{ij}$) could be estimated. At this level of accuracy we could better constrain the rate of crustal deformation across the Diablo Range as well as discern spatial variations in the deformation field.

Coalinga Trilateration Network

We have employed short and intermediate-length lines from the Coalinga trilateration network (Figure 2) to update previous estimates [*Lisowski and Prescott*, 1981] of the slip rates on the Calaveras and Paicines faults. Since 1972 trilateration measurements have been made periodically by the USGS in central California on a regional scale spanning a 20-km-wide zone centered on the San Andreas fault and including several distinct faults, as well as on smaller (1-2 km) aperture networks that span a single fault (Pionne, Dry Lake and Tully nets). The estimated accuracy in the line lengths determined from the short-range measurements is 4 mm [*Lisowski and Prescott*, 1981]. The estimates of line-length change made by *Lisowski and Prescott* [1981] also included

earlier data collected by the California Division of Mines and Geology, but we have utilized only the more homogeneous set of USGS data.

For the region within 10 km to the east of the San Andreas fault we assume that the predominant mode of crustal deformation is right-lateral fault slip on the Calaveras-Paicines fault system. This is equivalent to the assumption that the measured deformation in this region is due neither to elastic strain accumulation that will be released episodically in earthquakes on the adjacent San Andreas fault nor to crustal shortening normal to the San Andreas fault. Several lines of reasoning support this assumption. As discussed above, on the segment of the San Andreas fault adjacent to the San Benito network, fault slip occurs primarily by steady creep, and we expect little right-lateral shear strain accumulation associated with the San Andreas fault to be measured on off-fault geodetic lines. In addition, elastic strain accumulation associated with the San Andreas fault would be measurable geodetically on both sides of the fault, yet to the west of the San Andreas fault the maximum right-lateral shear strain within the Salinian block, estimated from triangulation data measured during the time interval 1944-1963, is poorly resolved and is not oriented parallel to the San Andreas fault [*Thatcher*, 1979a]. An alternative mode of deformation adjacent to the San Andreas is compression across structures such as the Paicines syncline (Figure 3). Strike-slip motion across this region would shorten north-south lines and extend east-west lines, whereas contraction would shorten northeast-southwest lines. Line length changes in the Pionne short-range network and the lines from Bitter to Hepsedam and Browns to Cross are consistent with the hypothesis of right-lateral slip on the Calaveras-Paicines fault system. As discussed above, results from the San Benito geodetic subnetwork that includes measurements to Bitter and Hepsedam are most consistent with right-lateral shear at the orientation of the San Andreas and Paicines fault.

If the deformation in this region occurs as rigid block motion along the Calaveras-Paicines fault system, the observed length changes can be converted into a fault-parallel displacement rate from the slope of the least-squares linear fit to the interstation length data [*Prescott and Lisowski*, 1983]. The slip rates determined from lines crossing the fault at a low angle are given in Table 2 for the Calaveras-Paicines region just south of Hollister and for the Paicines fault zone between Bitter and Coalinga. The sum of the slip rate determined from the station pairs that cross only the San Andreas fault (Cross-Chalone and Chalone-Bitter lines) and the slip rate from pairs that are completely east of the San Andreas fault (Browns-Cross and Bitter-Hepsedam) are approximately equal to the slip rate from station pairs that span both fault zones (Browns-Chalone and Chalone-Hepsedam lines). The line length changes across the Calaveras-Paicines fault zone are consistent with ~10 mm/yr of right-lateral slip. The rate of slip estimated for the Paicines fault south of the city of San Benito is 4 ± 1 mm/yr.

The Bitter to Hepsedam line showed a significant change in slope beginning in mid-1978. This change corresponded to an increase in the rate of slip on the Calaveras-Paicines system and a decrease in slip rate on the San Andreas fault. A similar change after 1979 in the slip rates for the Calaveras and San Andreas faults has been inferred from geodetic measurements of the USGS Hollister trilateration network [G. Gu and J. C. Savage, personal communication, 1986; *Matsu'ura et al.*, 1986]. The increase in slip on the Calaveras-Paicines fault coincided approximately

with the occurrence of the 1979 Coyote Lake earthquake (M_L=5.7) on the northern Calaveras fault. The rate of line length change, L, between Bitter and Hepsedam for the 1973-1978 time period was 1 ± 1 mm/yr [*Lisowski and Prescott*, 1981]. The higher rate of slip given in Table 2 thus is largely due to the increased rate during 1978-1984.

The average fault slip indicated by the three short-range networks (Figure 2), again assuming simple block motion, is given in Table 3. The rate of slip on the Pionne net, 12 ± 2 mm/yr, is similar to the rate estimated from the line between Cross and Browns which crosses the Calaveras-Paicines fault zone (10 ± 1 mm/yr). Between the Dry Lake and Tully networks the rate of creep on the San Andreas fault increases from 27 ± 2 to 32 ± 1 mm/yr. South of the Tully network the rate of slip determined from near-fault data on the San Andreas fault is the same as the rate estimated from the Chalone to Hepsedam line [*Prescott and Lisowski*, 1981].

The short and intermediate-range trilateration measurements document a transfer of slip associated with the Calaveras-Paicines fault zone to the San Andreas fault. The narrowing of the region that accommodates the ~32 mm/yr slip rate also corresponds to a transition from a complex multi-stranded portion of the fault system with locked segments that break in periodic moderate-to-large earthquakes to a geometrically simpler segment that accommodates slip through creep.

Comparison with Other Geodetic and Geologic Observations

As noted above, the strain rate parameters estimated on the basis of angle changes in the central portion of the San Benito network are $\dot{\gamma}_c$ = 0.19 ± 0.09 μrad/yr and β = N16°E ± 13°, or ψ = N29°W ± 13°. Interpreted in terms of uniform horizontal contraction in the direction given by the angle β, the rate of shortening is 5.7 ± 2.7 mm/yr. Although there is no significant strain at the 95% confidence limit, the orientation of the principal strain directions are consistent with the geological structures of the region (Figure 3). The azimuth of the least compressive strain (N74°W ± 13°) is close to the trend of the major fold structures of the region (N65°W). The direction of maximum rate of right-lateral shear is also close to the trend of the major strike-slip faults of the region.

From a geological reconstruction of the structures between the Great Valley and the San Andreas fault at the approximate latitude of Coalinga, *Namson and Davis* [1987] inferred that 11 km of late Cenozoic shortening has occurred perpendicular to the San Andreas fault. If active folding commenced 5 m.y. ago, the average rate of shortening has been 2.2 mm/yr. If folding began as recently as 2 m.y. ago an average rate of shortening of 5.5 mm/yr is implied. These figures are comparable to the geodetically inferred rate.

The rate of slip obtained in this study for the Calaveras-Paicines fault zone south of Hollister is 10 ± 1 mm/yr (Browns to Cross, Table 2) and 12 ± 2 mm/yr (Pionne net, Table 3). These slip rates may be compared to other estimates of slip rate derived from geological and geodetic observations. *Harms et al.* [1987] inferred a late Quaternary slip rate on the Paicines fault of 3.5-13 mm/yr from an offset terrace riser and an offset hill ~10 km south of Hollister. Between 1973 and 1986 the average rate of slip obtained from offset of the USGS Thomas Road alinement array, which spans the Paicines fault near its intersection with

the Browns-Cross line, is approximately 6 mm/yr [*Harsh and Pavoni*, 1978; S. Burford, personal communication, 1988]. From trilateration measurements made between the stations Browns and Cross during an interval earlier than but overlapping that of our study (69.8-78.4), *Prescott and Lisowski* [1981] determined a slip rate of 8 ± 1 mm/yr. *Prescott and Lisowski* [1981] also calculated the rate of the slip from short-range trilateration measurements of the Pionne net to be 10 ± 3 mm/yr for approximately the same period. These estimates are not significantly different from the results reported here. Utilizing data from the (USGS) Hollister trilateration network, located north of our study region, *Matsu'ura et al.* [1986] inverted for fault displacement rate versus depth on the San Andreas, Calaveras, and Sargent faults. They estimated the rate of slip on the Calaveras-Paicines fault between 1971 and 1983 and between latitudes 36.70° and 36.87°N to be 18 ± 4 mm/yr, with no significant surface creep. This result is higher than the rate of surface slip documented from the Thomas Road alinement array as well as with that obtained in this study. The inconsistency of the *Matsu'ura et al.* [1986] rate with other results from the region may be due to the fact that the Hollister network does not span the southern portion of the Calaveras fault; in particular, the 18 mm/yr value may reflect an average rate over a region where slip on the Calaveras fault is decreasing to the southeast.

The rate of slip obtained in this study for the Paicines fault south of the city of San Benito is 4 ± 1 mm/yr (Bitter to Hepsedam, Table 2). While geological mapping indicates that recent right-lateral slip has occurred on the Paicines fault as far south as the city of San Benito, no active fault trace has been mapped further south (J. Perkins, personal communication, 1988). Sedimentation rates are high in this region, however, so a low rate of slip on the fault may be masked by alluvium. From a study of earthquake focal mechanisms and seismicity of this region, *Ellsworth* [1975] suggested that slip on the San Andreas fault is transferred to the faults northeast of the San Andreas between Bitter and Cross (Figure 2). The rate of slip estimated from the change in the Bitter-to-Hepsedam line length, 3-4 mm/yr, however, suggests that some slip may be occurring on an extension of the Paicines fault south of San Benito. As discussed above, the slip rate inferred for this line is higher than the rate of slip of 1 ± 1 mm/yr estimated by *Lisowski and Prescott* [1981] for an earlier period and may indicate a temporal variation in the rate of deformation in this region.

Principal Directions of Strain and Stress

The principal directions determined geodetically for rate of strain within the San Benito network may be compared with the orientation of the maximum principal stress (σ_1) estimated from wellbore breakouts and the azimuths of P axes determined from earthquake focal mechanisms for the region east of the San Andreas fault. As noted earlier, the orientations of principal stress directions determined from breakout orientations, earthquake fault plane solutions, and the azimuths of major fold structures in central California have been used to distinguish between models relating the formation of fold structures in the southern Coast Ranges to motion along the San Andreas fault and to infer the state of stress on and near the San Andreas fault [*Zoback et al.*, 1987; *Mount and Suppe*, 1987; *Namson and Davis*, 1988].

Due to extensive drilling for oil to the east of the San Andreas fault, a large number of wells have been available for measurement of stress-induced wellbore breakout orientations. Borehole breakouts are caused by unequal stress concentrations around a borehole wall and create elongations of the hole in directions perpendicular to the orientation of the maximum horizontal stress [*Springer*, 1987]. Breakouts are generally oriented northwest-southeast, indicating a northeast-southwest orientation for the greatest compressive stress, a direction perpendicular to the axes of major folds near the Great Valley and at a 70°-90° angle to the San Andreas fault [*Springer*, 1987; *Zoback et al.*, 1987; *Mount and Suppe*, 1987]. To the east of the San Andreas fault the majority of breakout measurements have been made in wells near the western edge of the Great Valley (Figure 5); comparatively few wellbore breakout orientations have been obtained closer to the San Andreas fault within the area of the geodetic measurements reported in this paper.

The orientation of maximum principal stress may also be inferred from well-determined fault plane mechanisms, notably from the 1982 Idria, the 1983 Coalinga, and the 1985 North Kettleman Hills earthquakes (Figure 5). For the Coalinga and the North Kettleman Hills events the P-axis orientation is ~N37°E [*Eaton*, 1985; J.P. Eaton, personal communication, 1987], similar to the directions of σ_1 inferred from breakout orientations in the same region. The azimuth of the P axis for the Idria event is N12°E [*Eaton*, 1985].

As may be seen in Figure 5, the breakout orientations and the P-axis directions are very similar to the orientation of maximum compressive strain implied by the trend of local fold structures and by the inferred direction of horizontal shortening across the San Benito network. Along the western edge of the Great Valley and near Coalinga, the direction of σ_1 inferred from the breakout orientations and two earthquake focal mechanisms and the orientation of maximum compressive strain inferred from the fold trends is N30-50°E. To the northwest of Coalinga, including the region spanned by the San Benito network, the direction of maximum compressive strain predicted from the azimuth of the local fold structures, the σ_1 direction inferred from one wellbore breakout orientation, and the P-axis orientation of the Idria earthquake are N12-35°E. While *Mount and Suppe* [1987] have suggested that the folds in this area have been inactive since the Miocene, the rate of deformation determined for the region spanned by the San Benito network suggests that ongoing compressive strain is being accommodated across these folds. The recency of folding in this region is further supported by the geological observation that the folds deform Quaternary deposits [*Namson and Davis*, 1988].

As summarized by *Mount and Suppe* [1987] and *Namson and Davis* [1988] the occurrence of folding in the Coast Ranges has been variously attributed to distributed right-lateral shear associated with the San Andreas fault or to oblique displacement across the region. On the basis of experimental simulations of simple shear and field studies of wrench faulting, en echelon fold structures are predicted to occur adjacent to a strike-slip fault due to distributed shear [*Wilcox et al.*, 1973]. Fold axes are expected to be oriented perpendicular to σ_1 in the early stages of wrench faulting; the folds may subsequently rotate into parallelism with the strike-slip fault through distributed shear [*Mount and Suppe*, 1987]. In central California, the axes of early-forming en echelon folds would be

at an angle of 30° ± 15° to the trend of the San Andreas fault (~N41°W) in a counterclockwise direction, or N71°W ± 15° (β = N19°E ± 15°).

In an alternative model deformation is due to oblique displacement, sometimes termed "transpression"[*Harland*, 1971], across the southern Coast Ranges. This deformation is thought to be decoupled into a low-shear-stress, strike-slip component and a high-deviatoric-stress, thrust component [*Mount and Suppe*, 1987; *Zoback et al.*, 1987]. In this model the strike-slip component is accommodated within a narrow (< 3-10 km wide) zone and the compressive component is accommodated over a wider zone (10-100 km). The compression is held to be at least partly the result of a small (~ 6°) difference between the orientation of the San Andreas fault in central California and the local direction of Pacific-North American relative plate motion [*DeMets et al.*, 1987]. The precise orientation of σ_1 adjacent to the San Andreas fault, according to this model, depends on the relative strength of the fault zone and the surrounding lithosphere [*Mount and Suppe*, 1987; *Zoback et al.*, 1987]; for a substantially weaker fault zone σ_1 may be nearly normal to the fault zone (β ~ N49°E).

The direction of maximum compressive strain indicated by orientations of the local fold structures in the San Benito region is N25°E, close to the orientation of maximum incremental compressive strain estimated from the geodetic data (β = N16°E ± 13°). These orientations are in apparent agreement with the wrench faulting model. The significant difference between the trend of the fold axes in the San Benito region and in the San Emigdo Mountains [*Davis*, 1986] and the strike of the San Andreas fault is in contrast, however, to the situation throughout most of the Coast Ranges in central California where fold axes have orientations approximately parallel to the San Andreas [*Mount and Suppe*, 1987]. In these two regions the fold orientations are thought to be controlled by reactivation of older structures (T.L. Davis, personal communication, 1988); in the San Benito region these older structures may be related to a late Miocene deformation event [*Namson and Davis*, 1988]. Given such structural control, the geodetic data reported here are also consistent with the oblique displacement, or transpression, model for deformation of the Coast Ranges.

As discussed earlier there are two observations which argue against models in which right-lateral shear strain is distributed across a zone significantly greater than 10 km in width. Because slip on the adjacent San Andreas fault occurs primarily by steady creep, little of the right-lateral shear strain accumulation associated with fault should be measurable on off-fault geodetic lines. Additionally, distributed shear strain associated with the San Andreas fault would be observable on both sides of the fault, yet there is no geodetic or geologic evidence of deformation within the Salinian block [*Thatcher*, 1979a].

There are several factors which may complicate the interpretation of measurements used to distinguish between models relating the formation of fold structures in the Coast Ranges to motion along the San Andreas fault. First, there may be processes that act on different length scales which might explain the change in the σ_1 direction and the trend of fold structures at different distances from the San Andreas fault. Within a narrow zone centered on the San Andreas fault, local geological structures and focal mechanisms may be the result of geometrical complexities in the fault trace [*Segall and Pollard*, 1980] or the rheological structure of the fault zone [*Horns et al.*, 1985]. Between the San Andreas fault and the

Paicines fault, for example, the focal mechanisms determined by *Ellsworth* [1975] may be due to interaction between the two faults. As seen in the San Benito region, fold orientations may also vary due to reactivation of older structures or material heterogeneity. Finally, as will be discussed in the next section, there is the additional complexity that deformation in the southern Coast Ranges is related, in a kinematic sense, to the overall deformation across the Pacific-North American plate boundary.

Relation of Deformation East of the San Andreas Fault to the Accommodation of Plate Motion

The results of the geodetic measurements presented in this paper are relevant to deformation in other subregions of the Coast Ranges and to the question of how Pacific-North American plate motion is accommodated across California.

Global plate motion models, which yield the relative motion between the North American and Pacific plates, have been used as kinematic boundary conditions on the integrated deformation across the plate boundary zone in the western United States [*Minster and Jordan*, 1984, 1987; *Bird and Rosenstock*, 1984; *Weldon and Humphreys*, 1986]. If the San Andreas fault functioned as a simple boundary that accommodated the full motion between two rigid plates, the rate of slip in central California predicted by the NUVEL-1 global plate motion model would be about 49 mm/yr at N35°W [*DeMets et al.*, 1987]. Deformation across the Pacific-North American boundary is instead thought to be distributed across a broad zone between the continental escarpment and the eastern front of the Basin and Range province. As summarized above, the rate of slip on the San Andreas fault in central California oriented at N41°W ± 2° is constrained from Holocene geological data and ground-based geodetic measurements to be 34 ± 3 mm/yr. The vector difference between the plate motion and the San Andreas rate is about 16 mm/yr in the direction N21°W. The integrated rate of extensional deformation to the east of the San Andreas fault across the Basin and Range has been estimated from geological observations averaged over the Holocene and from very long baseline interferometry (VLBI) to be 9.7 ± 2.1 mm/yr at N56°W ± 10° [*Minster and Jordan*, 1987]. The vector difference derived using the above rates of motion for the San Andreas fault and Basin and Range, referred to as the discrepancy vector by *Minster and Jordan* [1987], is about 10 mm/yr in the direction N14°E, or 5 mm/yr of slip parallel to the San Andreas fault and 8 mm/yr of convergence normal to the fault. On the basis of the estimates of *Minster and Jordan* [1987], the uncertainties in the discrepancy vector are approximately ± 5 mm/yr for the rate of slip and ± 15° for the direction. Although some minor internal deformation within the Sierra Nevada block [*Lockwood and Moore*, 1979] or across the Great Valley syncline may occur, most of the deformation represented by the discrepancy vector is thought to occur within the Coast Ranges. *Weldon and Humphreys* [1987] and *Saucier and Humphreys* [1988] have constructed a self-consistent description of deformation in southern and central California from geodetic data and Quaternary geologic slip rates. From their model they predict that the Pacific-North American relative plate motion vector is 9° more westerly than that given by NUVEL-1. They estimate ~ 5 mm/yr of convergence normal to the San Andreas fault in central California.

A compilation of estimated and measured rates of deformation in the Coast Ranges, separated into right-lateral strike-slip motion on specific faults and distributed compression, is given in Table 4. In general the geological data are most useful for indicating long-term modes of deformation and for placing upper and lower bounds on rates. The large range in most geologically determined rates is due to uncertainties in dating rock units and in the timing of geological reconstructions.

A comparison of incremental strain rates determined over a geologically short interval to long-term slip rates is meaningful only if the deformation process accumulates strain in a temporally uniform manner. On short-time scales (1-100 yrs) there are a number of mechanisms associated with temporal variations in strain rate. An increase in the rate of shear strain has been documented to occur after large earthquakes in a region adjacent to the rupture zone [*Thatcher*, 1986]. There is no evidence, however, for a change in the rate of slip on the San Andreas fault in central California for the time interval that spans the occurrence of the great 1906 earthquake on the northern locked segment of the San Andreas fault [*Thatcher*, 1979a]. As discussed above, there is a suggestion that the rate of slip on the Paicines and Calaveras faults changed at about the time of the 1979 Coyote Lake earthquake.

Within a fold-and-thrust belt such as the southern Coast Ranges the short-term temporal variations in the rate of deformation are poorly constrained. The pattern of moderate size earthquakes ($M_L > 5.0$) between 1932-1982 in the southern Coast Ranges [*Engdahl and Rinehart*, 1989] is similar to the seismicity pattern given in Figure 1; there is some additional seismicity in the region between the Rinconada fault and the continental escarpment (Figure 1). This result suggests that over the past ~50 years the pattern of release of stress and strain by earthquakes has been approximately time-stationary. Comparison with geological data is further complicated by the observation that the plate boundary zone undergoes evolution on geological times scales. Field geological evidence from the Coalinga region indicates that the most recent episode of uplift began only 2-3 m.y. ago, well after slip commenced on the San Andreas fault [*Namson and Davis*, 1988]. A fold-and-thrust belt typically undergoes an evolution such that the locus of deformation changes. In the initial stages of deformation the locus of activity is controlled by such factors as the nature and position of the driving and resisting forces, pre-existing zones of weakness, and rock properties such as the elastic moduli, effective viscosity, and stratification of the deforming medium [*Biot*, 1961; *Harland*, 1971]. At some point beyond this initial stage less work may be required to break new faults or build new folds, and the folding and faulting may commence elsewhere.

To explore the implications of the constraints provided by the San Andreas discrepancy vector we compare the predicted rate of ~5 mm/yr of fault-parallel and ~8 mm/yr of fault-normal deformation to the values given in Table 4. The rates of right-lateral slip on the Rinconada and San Gregorio faults estimated from geological observations are 0-2 and 6-9 mm/yr, respectively [*Clark et al.*, 1984]. These values compare with geodetically measured rates of 2 ± 1 mm/yr (Table 4) and 0 ± 8 mm/yr [*Prescott and Yu*, 1986], respectively. These results for the rate of slip on the San Gregorio fault are significantly smaller than some earlier estimates [*Minster and Jordan*, 1984; *Weldon and Humphreys*, 1986] but are more consistent with recent kinematic models [e.g., Model D, *Minster and Jordan*, 1987].

Geological and seismicity data suggest that northeast-southwest compression across the southern Coast Ranges may be localized to two regions, the 30-km-wide zone spanned by the San Benito network and a second zone to the west of the Rinconada fault [*Eaton*, 1984; *Dehlinger and Bolt*, 1987]. If shortening across the Coast Ranges is divided equally between these two regions, approximately 4 mm/yr of shortening should be occurring within the Diablo Range. If in contrast, the predicted 8 mm/yr [*Minster and Jordan*, 1987] is distributed uniformly across the 170-km-wide zone between the continental escarpment and the Great Valley, the shortening across the region spanned by the San Benito network would be approximately 1.4 mm/yr. The rate of deformation estimated from the San Benito study is most consistent with the first hypothesis, but the uncertainties in our calculated values do not allow the latter possibility to be ruled out.

Results from ongoing geodetic studies with stations in central California should provide additional constraints on the rate and distribution of slip within the Coast Ranges. The rate of slip estimated from VLBI measurements made at Vandenberg, Fort Ord, Presidio, and Point Reyes (Figure 6) could potentially be used to constrain the rate of deformation across the Coast Ranges. To distinguish between different models will require that uncertainties in the rate of slip, relative to a fixed reference, be 2-3 mm/yr or less. Our preliminary analysis of VLBI data, based on measurements between October 1982 and March 1987, indicate that only the rate of slip at the station Vandenberg meets this requirement [*Sauber et al.*, 1987; see also *Clark et al.*, 1987]. Additional measurements at all of the VLBI stations in central California have been made within the last year, and an analysis of these measurements will be the subject of a later paper. The rate of deformation estimated from measurements to the Farallon Islands (Figure 6) will be updated on the basis a trilateration survey of the network by the USGS in 1988; such information should provide a better constraint on the rate of slip on the San Gregorio fault.

Summary

Triangulation and trilateration data from two geodetic networks located between the San Andreas fault and the Great Valley have been used to calculate shear strain rates in the Diablo Range and to estimate the slip rate along the Calaveras and Paicines faults in central California. The shear strain rates, $\dot{\gamma}_1$ and $\dot{\gamma}_2$, were estimated independently from angle changes using Prescott's method and from the simultaneous reduction for station position and strain parameters using the DYNAP method. On the basis of Prescott method, the average shear strain rate for the time period between 1962 and 1982 is 0.15 ± 0.08 μrad/yr, with the orientation of the most compressive strain (β) at N16°E ± 14°. Utilizing the DYNAP method with corrections for the deflection of the vertical and the geoid - reference ellipsoid separation computed on the basis of local gravity observations, $\dot{\gamma} = 0.19 \pm 0.09$ μrad/yr and β = N16°E ± 13°. At the 95% confidence level $\dot{\gamma}$ is not significantly greater than zero. The orientation of β, however, is similar to the orientation of maximum compressive strain indicated by the orientations of major fold structures in the region (N25°E). We infer that the measured strain is due to compression across the folds of this area; the average shear straining corresponds to a relative shortening rate of 5.7 ± 2.7 mm/yr.

The orientations of maximum principal stress inferred from wellbore breakouts and the azimuths of P axes determined from earthquake focal mechanisms within the Diablo Range and near the western edge of the Great Valley are similar to the orientation of maximum compressive strain implied by the trend of local fold structures. In contrast to the situation throughout most of the Coast Ranges in central California where fold axes have orientations approximately parallel to the San Andreas fault, within the Diablo Ranges between Hollister and Coalinga the trends of the fold axes are different and are thought to be controlled by reactivation of older structures. Given such structural control, the geodetic data reported here are consistent with transpression across the Coast Ranges.

For a zone within 10 km of the San Andreas fault, trilateration measurements on off-fault lines east of the San Andreas fault as well as lines that cross the San Andreas fault have been used to estimate the rate of slip along the Calaveras-Paicines fault and to document the gradual southward transition in the width of the zone accommodating right-lateral fault slip. South of Hollister the inferred rate of slip on the Calaveras-Paicines fault was found to be 10-12 mm/yr. The rate of slip on the Paicines fault near Bitter is ~4 mm/yr. Further to the south all of the right-lateral slip (at least across the 20-km-wide zone of measurements) occurs on the San Andreas fault.

To distinguish between different models that describe the distribution of strike-slip and compressive displacements within the Coast Ranges we examined data from regional geologic and geodetic studies and global plate models. Geological and seismicity data [*Eaton*, 1984; *Dehlinger and Bolt*, 1987], as well as our geodetic results, suggest that northeast-southwest compression across the southern Coast Regions may be localized to two regions, although uniform compression across the 170-km-wide zone between the continental escarpment and the Great Valley cannot be ruled out.

Appendix. Details of Data Reduction for the San Benito Network

Accuracy of the Triangulation and Trilateration Measurements

Triangulation is a measurement system consisting of joined or overlapping triangles of angular observations. During a single session observations of direction are made from a particular mark to several other marks that are located within a few tens of kilometers from the mark occupied. An angle observation is determined by differencing two direction measurements. Seventy of the 72 directions utilized in this study were second-order observations, with a priori uncertainty estimated to be σ_d = 3.4 μrad [*Federal Geodetic Control Committee*, 1984], and two were third-order observations (σ_d =5.8 μrad). The expected uncertainty in a second-order angle measurement (σ_a) is $\sqrt{2}\,\sigma_d$, or about 4.8 μrad. The order of the triangulation denotes the measurement precision, which is determined by survey procedures and is reflected in the degree to which internal checks of the data are satisfied [*Thatcher*, 1979b]. The principal internal check is the triangle closure requirement that the angles within each triangle sum to 180° plus the known excess due to the Earth's sphericity. Triangle closures for these data indicate that the standard deviation of a single angle is approximately 5.3 μrad, very close to the expected value.

As practiced by the USGS, trilateration consists of distance measurements among a network of stations. The distances between geodetic monuments were measured in this study with a Geodolite, a precise electro-optical distance-measuring instrument. Regional trilateration measurements made by the USGS on line lengths of 10-40 km have a precision of approximately 0.2-0.3 ppm [*Savage and Prescott*, 1973]. After corrections for refractivity and instrument and reflector height, a line length corresponds to the distance between two geodetic monuments.

Assumptions Made in the Estimation of Horizontal Shear Parameters

The full three-dimensional strain tensor includes horizontal and vertical shear components, dilatation, and vector rotation. Since height changes were not directly measured in either the 1962 or 1982 survey, we can estimate only the horizontal components of the strain tensor. Here we assume that vertical changes in station height are negligible. Since no large earthquakes occurred within the region spanned by the San Benito network between 1932-1982 [*Engdahl and Rinehart*, 1989], the estimated rate of uplift on the folds of the Diablo Range is only 1-3 mm/yr [*Zepeda et al.*, 1987], or 2-6 cm over the 20-year time period of this study. A 6-cm change in the height of Tum (Figure 2) between 1962 and 1982, for example, will cause a 0.1 ppm change in the 20-km-length line between Tum and Bonito (calculated from equation 1.72 of *Bomford* [1980]). Because of ground-water-induced subsidence, larger vertical changes may have occurred at the stations Stubble, located in the Great Valley, and Panoche, located in Panoche Valley. Further, astronomic azimuth measurements are made only at Hepsedam. Without a reliable external or conventionally adopted internal reference direction, we cannot estimate rotation of the network about a vertical axis. Additionally, since length measurements were made only in the 1982 survey, surface dilatation can not be estimated. We are thus able to estimate only the rate of change of horizontal shear components $\dot{\gamma}_1$ and $\dot{\gamma}_2$. If the fold structures of the region are deforming as the result of simple uniaxial compression, block rotation is not expected and dilatation is assumed to be uniform.

The two modes of deformation suggested from the geological structures of the region (see text) can be used to interpret the values of $\dot{\gamma}_1$ and $\dot{\gamma}_2$. Right-lateral strike-slip motion at the orientation of the San Andreas fault (N41°W) would be seen primarily as $\dot{\gamma}_1 > 0$. North-south compression is also consistent with $\dot{\gamma}_1 > 0$. If the orientation of compressional strain is northeast-southwest, as is predicted from the orientation of the folds within the southern Coast Ranges, then $\dot{\gamma}_2 < 0$.

Prescott's Method

Angle changes are the observations used to estimate $\dot{\gamma}_1$ and $\dot{\gamma}_2$ in the extended version of Frank's method [*Prescott*, 1976]. The fundamental equation of the technique,

$$\Delta\Phi_i = (t_i - t_o)\left(A_i^1 \dot{\gamma}_1 + A_i^2 \dot{\gamma}_2\right) \qquad (A.1)$$

where

$$A_i^1 = [(\sin\theta_{i2} - \sin\theta_{i1})\dot{\gamma}_1] / 2$$

$$A_i^2 = [(\cos\theta_{i2} - \cos\theta_{i1})\dot{\gamma}_2] / 2$$

relates an observed angular change $\Delta\Phi_i$ for the time interval $t_i - t_o$ to the parameters $\dot{\gamma}_1$ and $\dot{\gamma}_2$. Here θ_{i1} and θ_{i2} represent the azimuths (clockwise from north) of the initial and terminal sides of the angle. To derive angles the 1982 data were used to adjust for station position. Rather than making an adjustment on a three-dimensional surface, the distances were projected onto the Clark 1866 reference ellipsoid (NAD27 geodetic system, *Defense Mapping Agency* [1987] and an adjustment was made employing a variation of coordinates method [*Anderson*, 1969]. Azimuths for each station-to-station pair were then determined for comparison to the 1962 observations. In this approach we are comparing angles measured on the Earth's surface to angles determined from a network adjustment on the reference ellipsoid. The classical solution to the adjustment of geodetic data derived from different measurement techniques has involved making corrections to the direction and distance observations such that the measurements are then given on a common reference ellipsoid [*Bomford*, 1980; *Vanicek and Krakiwsky*, 1986]. In employing the DYNAP method an alternative approach is used.

DYNAP Method

In the DYNAP (DYNamic Adjustment Program) technique the directions measured in 1962 and the distances measured in 1982 are used simultaneously to solve for both crustal motion parameters and positional coordinates of the geodetic marks for a specified reference time via weighted least squares [*Snay*, 1986; *Drew and Snay*, 1988]. A two-dimensional adjustment was carried out by holding the station elevations fixed. In this approach the direction observations are corrected for the deflection of the vertical, and the separation of the geoid and a reference ellipsoid are used to correct the distance observations. This technique is based on the assumption that the velocity field is linear in space and constant over the time interval of interest. The time dependent station positions can be written as

$$x(t_i) = x(t_o) + (t_i - t_o)\,\mathbf{L}\,x\,(t_o) \qquad (A.2)$$

where $x(t_i)$ are the two dimensional station coordinates at time t_i and t_o is the reference time. The four components of the 2 x 2 tensor **L** parameterize the velocity field v by its gradient [*Malvern*, 1969]:

$$L_{ij} = \frac{\delta v_i}{\delta x_j} \qquad (A.3)$$

In equation (A.2) the origin is arbitrary. In practice one station is chosen as an origin and is held fixed for all epochs. **L** can be decomposed into a

sum of a symmetric tensor **D**, called the rate of deformation tensor, and a skew-symmetric tensor **W**, called the spin tensor [*Malvern*, 1969]

$$\mathbf{L} = \mathbf{D} + \mathbf{W} \tag{A.4}$$

For the case where all of the components of rate of deformation are zero, the instantaneous motion is then a rigid-body rotation. When displacements and displacement gradients are small **D** is approximately equal to $\dot{\varepsilon}_{ij}$.

Corrections to Reduce the Observations to a Common Reference System

When a direction measurement is made the theodolite is leveled; thus the measurement is made normal to the geoid, not normal to a reference surface. A correction for the deflection of the vertical is therefore required [*Bomford*, 1980; *Vanicek and Krakiwsky*, 1986]. The deflection of the vertical is the spatial angle between the vector normal to the geoid and the vector normal to an ellipsoidal surface. The correction $\Delta\alpha_{ij}$ to a direction of azimuth α_{ij} and elevation angle ν_{ij} [*Bomford*, 1980] is

$$\Delta\alpha_{ij} = -[\xi_i \sin \alpha_{ij} - \eta_i \cos \alpha_{ij}] \tan \nu_{ij} \tag{A.5}$$

where ξ_i and η_i are the meridian and prime vertical components of the deflection of the vertical at the observing, or *i*th, station. Deflections of the vertical are usually estimated from astronomical azimuth observations or from computed values based on local gravity observations [*Coleman and Lambeck*, 1983]. Alternatively, the deflections can be computed from the long-wavelength part of the geopotential together with necessary transformation parameters between the geoid and the ellipsoid reference system.

In this study the initial latitude and longitude of the station are positions given in the NAD83 reference system [*Defense Mapping Agency*, 1987]. The initial heights are orthometric heights, the height above the geoid estimated primarily from spirit leveling. For the station coordinates to be in a common reference frame, the heights need to be converted to heights above the GRS 80 reference ellipsoid [*Defense Mapping Agency*, 1987]. To make this calculation the separation of the geoid and the reference ellipsoid needs to be estimated. Since astronomical azimuths are not available, the deflection of the vertical and the geoid - ellipsoid separation are initially estimated from the long-wavelength part of the geopotential.

The global gravity field representation given by the WGS 84 Earth Gravitational Model (EGM) [*Defense Mapping Agency*, 1987] was used to calculate the deflection of the vertical and geoid height at each station using the Defense Mapping Agency program CLENQUENT [*Gleason*, 1985]. The form of the WGS 84 EGM is a spherical harmonic expansion of the gravitational potential; we used an expansion to degree and order 360. The gravitational coefficients are from *Rapp and Cruz* [1986] and R. Rapp (personal communication, 1988). The reference ellipsoid used to calculate the deflections of the vertical and the geoid - ellipsoid height separation was GRS 80 [*Defense Mapping Agency*, 1987], which is used in both the WGS 84 and NAD 83 reference systems. The deflections of the vertical vary in the network from 1.14"S to 0.14"N for ξ and from 1.40"E to 3.60"E for η. Utilizing the geoid - reference ellipsoid height

separation and deflections of the vertical calculated from the long-wavelength part of the geopotential, the strain rate parameters were estimated using the DYNAP method; yielding $\dot{\gamma} = 0.12 \pm 0.09$ μstrain/yr and $\beta = N17°E \pm 21°$ and an increase in the rms misfit by 2%. The strain rate results are similar to those obtained without corrections. The surface topography as well as the density distribution within the crust of the San Benito region is irregular, so the geoid representation used represents poorly the higher order features of the gravity field.

Because we expect significant short wavelength variations in the geoid, we have obtained from the Defense Mapping Agency geoid - reference ellipsoid separations and deflections of the vertical computed for network station positions from local gravity observations. The deflections of the vertical vary in the network from 6.00"S to 7.38"N for ξ and from 12.47"E to 6.38"W for η. The strain rate parameters utilizing these corrections are $\dot{\gamma} = 0.19 \pm 0.09$ μstrain/yr and $\beta = N16°E \pm 13°$. The rms misfit decreases by 8%. This decrease is due to a lower misfit for the direction observations; the corrections do not change the rms misfit for distance observations. These results suggest that while it is desirable to correct for deflection of the vertical and for the separation between the geoid and the reference ellipsoid, these corrections are valuable only when based on local observations.

Acknowledgements. We thank Wayne Thatcher, Will Prescott, Jerry Eaton, and Jim Savage for assistance while JS was in Menlo Park; Richard Snay for the triangulation direction lists; Alice Drew, Kurt Feigl, and Bob King for their help in the use of DYNAP; and L. Decker and H. White of the Defense Mapping Agency for providing values for the deflection of the vertical and the geoid - reference ellipsoid separation. We also thank Tom Jordan for his constructive suggestions. Trilateration surveys were performed by the USGS Crustal Strain Project under the direction of Will Prescott. Support for part of this research was provided by the U.S. Geological Survey while JS was in Menlo Park. The portion of this research conducted at the Massachusetts Institute of Technology was supported by the National Aeronautics and Space Administration through a Graduate Student Research Fellowship (NGT-50103) to JS and through the Crustal Dynamics Project under grant NAG 5-814.

References

Anderson, W.L., Weighted triangulation adjustment, *U.S. Geol. Surv. Open File Rep.*, Computer Contribution Number 1, 52 pp., U.S. Geol. Surv. Computer Center Div., Washington, D.C., 1969.

Biot, M.A., Theory of folding of stratified viscoelastic media and its implications in tectonics and orogenesis, *Geol. Soc. Am. Bull., 72*, 1592-1620, 1961.

Bird, P., and R.W. Rosenstock, Kinematics of present crust and mantle flow in southern California, *Geol. Soc. Am. Bull., 95*, 946-957, 1984.

Bomford, G., *Geodesy*, 855 pp., Clarendon Press, Oxford, 1980.

Burford, R.O., Strain analysis across the San Andreas fault and Coast Ranges of California, Ph.D. thesis, 74 pp., Stanford University, Stanford, California, 1967.

Burford, R.O., and P.W. Harsh, Slip on the San Andreas fault in central California from alinement array surveys, *Bull. Seismol. Soc. Am., 70*, 1233-1261, 1980.

Clark, M.M., K. Harms, J. Lienkaemper, D. Harwood, K. Lajoie, J. Matti, J. Perkins, M. Rymer, A. Sarna-Wojcicki, R. Sharp, J. Sims, J. Tinsley, and J. Ziony, Preliminary slip-rate table and map of late Quaternary faults of California, *U.S. Geol. Surv. Open File Rep.*, 84-106, 12 pp., 1984.

Clark, T.A., D. Gordon, W.E. Himwich, C. Ma, A. Mallama, and J.W. Ryan, Determination of relative site motions in the western United States using Mark III very long baseline interferometry, *J. Geophys. Res., 92*, 12,741-12,750, 1987.

Coleman, R., and K. Lambeck, Crustal motion in southeastern Australia: Is there geodetic evidence for it?, *Aust. J. Geod. Photo. Surv., 39*, 1-26, 1983.

Crouch, J.K., S.B. Bachman, and J.T. Shay, Post-Miocene compressional tectonics along the central California margin, in *Tectonics and Sedimentation along the California Margin*, edited by J.K. Crouch and S.B. Bachman, Pac. Sect. Soc. Econ. Paleontol. Mineral., *38*, 37-54, 1984.

Davis, T.L., A structural outline of the San Emigdo Mountains, in *Geologic Transect Across the Western Transverse Ranges*, edited by T.L. Davis and J. Namson, Pac. Sect. Soc. Econ. Paleontol. Mineral. Guidebook, pp. 23-32, 1986.

Defense Mapping Agency, Department of Defense World Geodetic System 1984: Its definition and relationships with local geodetic systems, *DMA Tech. Rep.*, 8350.2, 120 pp., 1987.

Dehlinger, P., and B.A. Bolt, Earthquakes and associated tectonics in a part of coastal central California, *Bull. Seismol. Soc. Am, 77*, 2056-2073, 1987.

DeMets, C., R.G. Gordon, S. Stein, and D.F. Argus, A revised estimate of Pacific-North American motion and implications for western North America plate boundary zone tectonics, *Geophys. Res. Lett., 14*, 911-914, 1987.

Dibblee, T.W., Regional geology of the central Diablo Range between Hollister and New Idria, in *Field Trip Guidebook for the Geological Society of America Cordilleran Section Meeting*, edited by T.H. Nilsen and T.W. Dibblee, pp. 6-16, Geol. Soc. Am., Boulder, Colo., 1979.

Drew, A., and R. Snay, DYNAP: Software for estimating crustal deformation from geodetic data (abstract), *Eos Trans. AGU, 69*, 325, 1988.

Eaton, J.P., Focal mechanisms of near-shore earthquakes between Santa Barbara and Monterey, California, *U.S. Geol. Surv. Open File Rep.*, 84-477, 13 pp., 1984.

Eaton, J.P., Regional seismic background of the May 2, 1983 Coalinga earthquake, in *Proceedings of Workshop XXVII, Mechanics of the May 2, 1983 Coalinga Earthquake*, edited by M.J. Rymer and W.L. Ellsworth, *U.S. Geol. Surv. Open File Rep.*, 85-44, pp. 44-60, 1985.

Ellsworth, W.L., Bear Valley, California, earthquake sequence of February-March 1972, *Bull. Seismol. Soc. Am., 65*, 483-506, 1975.

Engdahl, E.R., and W.A. Rinehart, Seismicity map of North America, in *Neotectonics of North America*, edited by D.B. Slemmons, Geol. Soc. Amer., Boulder, Colo., in press, 1989.

Federal Geodetic Control Committee, Standards and Specifications for Geodetic Control Networks, Nat. Ocean. Atmos. Admin., U.S. Dept. Commerce, Rockville, Md., 1984.

Frank, F.C., Deduction of earth strains from survey data, *Bull. Seismol. Soc. Am., 56*, 35-42, 1966.

Gawthrop, W.J., Seismicity and tectonics of the central California coastal region, M.S. thesis, University of Colorado, Boulder, 76 pp., 1977.

Gleason, D.M., Partial sum of Legendre series via Clenshaw summation, *Manuscripta Geodetica, 10*, 115-130, 1985.

Hamilton, D.H., Characterization of the San Gregorio-Hosgri fault system, coastal central California (abstract), *Geol. Soc. Am. Abstr. Programs, 19*, 385, 1987.

Harding, T.P., Tectonic significance and hydrocarbon trapping consequences of sequential folding synchronous with San Andreas faulting, San Joaquin Valley, California, *Am. Assoc. Petro. Geol. Bull., 60*, 356-378, 1976.

Harland, W.B., Tectonic transpression in Caledonian Spitsbergen, *Geol. Mag., 108*, 27-42, 1971.

Harms, K.K., J.W. Harden, and M.M. Clark, Use of quantified soil development to determine slip rates on the Paicines fault, northern California (abstract), *Geol. Soc. Am. Abstr. Programs, 19*, 387, 1987.

Harris, R.A., and P. Segall, Detection of a locked zone at depth on the Parkfield, California, segment of the San Andreas fault, *J. Geophys. Res., 92*, 7945-7962, 1987.

Harsh, P.W., and N. Pavoni, Slip on the Paicines fault, *Bull. Seismol. Soc. Am., 68*, 1191-1193, 1978.

Hart, E.W., W.A. Bryant, M.W. Manson, and J.E. Kahle, Summary report: Fault evaluation program 1984-1985, south Coast Ranges region and other areas, *Calif. Div. Mines Geol. Open File Rep.*, 86-3SF, 1986.

Heiskanen, W.A., and H. Moritz, *Physical Geology*, 364 pp., Freeman, San Francisco, 1967.

Horns, D.M., C.Y. Wang, and Y. Shi, Investigation of the uplift along the San Andreas fault zone (abstract), *Eos Trans. AGU, 66*, 1093, 1985.

Jennings, C.W., Fault map of California, *Calif. Geol. Data Map Ser.*, map 1, Calif. Div. of Mines and Geol., Sacramento, 1975.

Lisowski, M., and W.H. Prescott, Short-range distance measurements along the San Andreas fault system in central California, 1975 to 1979, *Bull. Seismol. Soc. Am., 71*, 1607-1624, 1981.

Lockwood, J.P., and J.G. Moore, Regional deformation of the Sierra Nevada, California, on conjugate microfault sets, *J. Geophys. Res., 92*, 2747-2766, 1987.

Malvern, L.E., *Introduction to the Mechanics of a Continuous Medium*, 713 pp., Prentice-Hall, Englewood Cliffs, N.J., 1969.

Matsu'ura, M., D.D. Jackson, and A. Cheng, Dislocation model for aseismic crustal deformation at Hollister, California, *J. Geophys. Res., 91*, 12,661-12,674, 1986.

Minster, J.B., and T.H. Jordan, Vector constraints on Quaternary deformation of the western United States east and west of the San Andreas fault, in *Tectonics and Sedimentation along the California Margin*, edited by J.K. Crouch and S.B. Bachman, Pac. Sect. Soc. Econ. Paleontol. Mineral., *38*, 1-16, 1984.

Minster, J.B., and T.H. Jordan, Vector constraints on western U.S. deformation from space geodesy, neotectonics, and plate motions, *J. Geophys. Res.*, 92, 4798-4804, 1987.

Mount, V.S., and J. Suppe, State of stress near the San Andreas fault: Implications for wrench tectonics, *Geology, 15*, 1143-1146, 1987.

Namson, J.S., and T.L. Davis, Seismically active fold and thrust belt in the San Joaquin Valley, central California, *Geol. Soc. Am. Bull., 100*, 257-273, 1988.

Page, B.M., The southern Coast Ranges, in *The Geotectonic Development of California*, edited by W. G. Ernst, pp. 329-417, Prentice Hall, Englewood Cliffs, N.J., 1981.

Page, B.M., Geologic background of the Coalinga earthquake of May 2, 1983, in *Proceedings of Workshop XXVII, Mechanics of the May 2, 1983 Coalinga Earthquake*, edited by M.J. Rymer and W.L. Ellsworth, *U.S. Geol. Surv. Open File Rep.*, 85-44, pp. 4-9, 1985.

Page, B.M., and D.C. Engebretson, Correlation between the geologic record and computed plate motions for central California, *Tectonics, 3*, 133-155, 1984.

Prescott, W.H., An extension of Frank's method for obtaining crustal shear strains from survey data, *Bull. Seismol. Soc. Am., 66*, 1847-1853, 1976.

Prescott, W.H., and M. Lisowski, Strain accumulation along the San Andreas fault system east of San Francisco Bay, California, *Tectonophysics, 97*, 41-56, 1983.

Prescott, W.H., and S.Yu, Geodetic measurement of horizontal deformation in the northern San Francisco Bay region, California, *J. Geophys. Res., 91*, 7475-7484, 1986.

Rapp, R.H., and J.Y. Cruz, The representation of the Earth's gravitational potential in a spherical harmonic expansion to degree 250, *Air Force Geophys. Lab. Tech. Rep.*, 86-0191, 64 pp., 1986.

Raymond, L.A., Tesla-Ortigalita fault, Coast Range thrust fault, and Franciscan metamorphism, northeastern Diablo Range, California, *Geol. Soc. Am. Bull., 84*, 3547-3562, 1973.

Sauber, J., T.H. Jordan, G.C. Beroza, T.A. Clark, and M. Lisowski, Constraints on North American-Pacific plate boundary deformation in central California from VLBI and ground-based geodetic data (abstract), in *Programs and Abstracts, The Impact of VLBI on Astrophysics and Geophysics*, Inter. Astron. Un. Symp. No. 129, p. 7.1, 1987.

Saucier, F., and E. Humphreys, Finite element kinematic model of southern California (abstract), *Eos Trans. AGU, 69*, 331, 1988.

Savage, J.C., Strain accumulation in western United States, *Ann. Rev. Earth Planet. Sci., 11*, 11-43, 1983.

Savage, J.C., and R.O. Burford, Geodetic determination of relative plate motion in central California, *J. Geophys. Res., 78*, 832-845, 1973.

Savage, J.C., and W.H. Prescott, Precision of Geodolite distance measurements for determining fault movements, *J. Geophys. Res., 78*, 6001-6008, 1973.

Segall, P., and R. Harris, Slip deficit on the San Andreas fault at Parkfield, California, as revealed by inversion of geodetic data, *Science, 233*, 1409-1413, 1986.

Segall, P., and D.D. Pollard, The mechanics of discontinuous faults, *J. Geophys. Res., 85*, 4337-4350, 1980.

Sieh, K.E., and R.H. Jahns, Holocene activity of the San Andreas fault at Wallace Creek, California, *Geol. Soc. Am. Bull., 95*, 883-896, 1984.

Slemmons, D.B., Capable faults and tectonically active folds of the California central Coast Ranges (abstract), *Geol. Soc. Am. Abstr. Programs, 19*, 452, 1987.

Snay, R.A., Horizontal deformation in New York and Connecticut: Examining contradictory results from the geodetic evidence, *J. Geophys. Res., 91*, 12695-12702, 1986.

Springer, J.E., Stress orientations from wellbore breakouts in the Coalinga region, *Tectonics, 6*, 667-676, 1987.

Stein, R.S., Evidence for surface folding and subsurface fault slip from geodetic elevation changes associated with 1983 Coalinga, California earthquake, in *Proceedings of Workshop XXVII, Mechanics of the May 2, 1983 Coalinga Earthquake*, edited by M.J. Rymer and W.L. Ellsworth, *U.S. Geol. Surv. Open File Rep.*, 85-44, pp. 225-253, 1985.

Stein, R.S., and G.C.P. King, Seismic potential revealed by surface folding: 1983 Coalinga, California, earthquake, *Science, 224*, 869-872, 1984.

Thatcher, W., Systematic inversion of geodetic data in central California, *J. Geophys. Res.*, 84, 2283-2295, 1979a.

Thatcher, W., Horizontal crustal deformation from historic geodetic measurements in southern California, *J. Geophys. Res., 84*, 2351-2370, 1979b.

Thatcher, W., Geodetic measurement of active-tectonic processes, in *Active Tectonics*, pp. 155-163, National Academy Press, Washington, D.C., 1986.

Vanicek, P., and E. Krakiwsky, *Geodesy: The Concepts*, 697 pp., Elsevier, New York, 1986.

Weldon, R., and E. Humphreys, A kinematic model of southern California, *Tectonics, 5*, 33-48, 1986.

Weldon, R. and E. Humphreys, Plate model constraints on the deformation of coastal southern California north of the Transverse Ranges (abstract), *Geol. Soc. Am. Abstr. Programs, 19*, 462, 1987.

Zepeda, R.L., E.A. Keller, and T.K. Rockwell, Soil chronosequence at Wheeler Ridge, southern San Joaquin Valley, California (abstract), *Geol. Soc. Am. Abstr. Programs, 19*, 466, 1987.

Zoback, M.D., M.L. Zoback, V.S. Mount, J. Suppe, J.P. Eaton, J.H. Healy, D. Oppenheimer, P. Reasenberg, L. Jones, C.B. Raleigh, I.G.

Wong, O. Scotti, and C. Wentworth, New evidence on the state of stress of the San Andreas fault sytem, *Science*, *238*, 1105-1111, 1987.

Figure Captions

Figure 1. Epicenters of earthquakes ($M_L \geq 4.0$) in the Coast Ranges during 1962 - 1982 [*Engdahl and Rinehart*, 1989]. The locations of three earthquakes with well-determined focal mechanisms, the 1982 Idria, the 1983 Coalinga, and the 1985 North Kettleman Hills events, are indicated by stars. Fault traces are simplified from *Jennings* [1975]: HF = Hosgri fault, RF = Rinconada fault, SAF = San Andreas fault, SGF = San Gregorio fault, WTR =Western Transverse Ranges. An outline of the San Benito triangulation/trilateration network is given for reference. MB = Monterey Bay.

Figure 2. Location of stations in the San Benito triangulation - trilateration network (solid circles), the Coalinga trilateration network (open circles), and small aperture trilateration networks (triangles). Half-filled circles denote stations that were part of both the San Benito and Coalinga networks. Surface traces of Quaternary faults are indicated by solid lines where well located, by dashed lines where approximately located or inferred, and by dotted lines where concealed by younger rocks or by lakes or bays [*Jennings*, 1975]: CFZ= Calaveras fault zone, OFZ= Ortigalita fault zone, PF=Paicines fault, RF=Rinconada fault, SAF=San Andreas fault. Stations discussed in the text include BIT = Bitter, BON = Bonito, BRN = Browns, CHL = Chalone, CRS = Cross, HEP = Hepsedam, LEY = Ley, PAN = Panoche, SMO = Smoker and TUM = Tum. Also shown are the locations of Coalinga (C), Hollister (H), and San Benito (SB).

Figure 3. Major structural features of the Diablo Range between Hollister (H) and Coalinga (C), modified from *Dibblee* [1979]. The locations of stations in the San Benito triangulation/trilateration network are shown as circles for reference. Structures shown include: CA = Coalinga anticline, CFZ = Calaveras fault zone, NI = New Idria diapir, OFZ = Ortigalita fault zone, PF = Paicines fault, PS = Paicines syncline, and VS = Vallecitos syncline. Inward pointing double arrows indicate a syncline, outward pointing double arrows an anticline. Single arrows indicate the direction of plunge of a fold axis.

Figure 4. Strain rate inferred for the San Benito network by use of the DYNAP method including corrections for deflection of the vertical and separation of the geoid and reference spheroid. (a) The orientation (β) of the axis of maximum compressive strain. The uncertainty in azimuth, at 95% confidence, is shown by an arc. (b) The shear strain rate parameters $\dot{\gamma}_1$ and $\dot{\gamma}_2$ together with a 95% confidence ellipse.

Figure 5. Fold structures and measured stress orientations in the region east of the San Andreas fault in central California [modified from *Mount and Suppe*, 1987]. Synclines are indicated by dashed lines, anticlines by dotted lines. Single arrows indicate the direction of plunge of a fold axis. Wellbore breakout measurements are given by a solid line with inward pointing arrows perpendicular to the direction of σ_1. The direction of σ_1 inferred from the azimuth of the P axes for three earthquakes are labeled by number: 1 = 1982 New Idria earthquake, 2 = 1983 Coalinga earthquake, and 3 = 1985 North Kettleman Hills earthquake. The axis of maximum

compressive strain (β) determined from triangulation and trilateration data from the San Benito network is given along with its standard deviation.

Figure 6. Reference figure for the geodetic and geological studies cited in Table 4. Brush (B) and Mulligan (M) are two stations in the USGS Pajaro trilateration network. At sites f and g, rates of fault slip were estimated geologically [*Clark et al.*, 1984] for the San Gregorio and Hosgri faults. The line A-A' is that for which *Namson and Davis* [1988] constructed their geological cross section (see Table 4). Fault traces are as given in Figure 1. Geodetic networks include FIN = Farallon Islands network, SBN = San Benito network, and SLN = San Luis network. VLBI stations include FORT = Fort Ord, PRES = Presidio, PT. R = Point Reyes, and VNDN = Vandenberg.

TABLE 1. Strain Rate Parameters for Spatial Subsets of the San Benito Network

Subnet	Number of Angles	$\dot{\gamma}_1$, μrad/yr	$\dot{\gamma}_2$, μrad/yr	$\dot{\gamma}$, μrad/yr	β	ψ
East	14	0.18 ± 0.11	0.01 ± 0.12	0.18 ± 0.10	N 1°W ± 20°	N46°W ± 20°
West	9	0.07 ± 0.14	-0.18 ± 0.13	0.19 ± 0.13	N34°E ± 22°	N11°W ± 22°
North	13	0.04 ± 0.10	-0.12 ± 0.10	0.16 ± 0.11	N37°E ± 20°	N 8°W ± 20°
South	7	0.22 ± 0.16	-0.13 ± 0.22	0.25 ± 0.20	N10°E ± 20°	N35°W ± 20°
All stations except BIT, HEP, and PAN	25	0.13 ± 0.08	-0.08 ± 0.08	0.15 ± 0.08*	N16°E ± 14°*	N29°W ± 14°*

* These strain parameters have been scaled by the a posteriori variance factor [*Vanicek and Krakiwsky*, 1986].

TABLE 2. Fault-Slip Rates Inferred from Length Changes on Fault-Crossing Lines

Calaveras - Paicines Fault Zone

Station 1	Station 2	No. of Obs.	Period	$\dot{L}$, mm/yr	Azimuth, deg	Slip Rate, mm/yr
BRN	CRS	7	72.7-83.9	-8.7 ± 0.8	168	9.9 ± 0.9
CRS	CHL	9	72.1-83.9	-18.5 ± 0.4	181	24.9 ± 0.5
BRN	CHL	8	72.1-83.9	27.4 ± 0.4	175	33.8 ± 0.5

Paicines Fault Adjacent to the Central Creeping Portion of the San Andreas Fault

Station 1	Station 2	No. of Obs.	Period	$\dot{L}$, mm/yr	Azimuth, deg	Slip Rate, mm/yr
BIT	HEP	6	73.1-83.9	3.7 ± 0.5	129	3.8 ± 0.5
CHL	BIT	8	72.1-83.9	19.8 ± 0.7	280	25.8 ± 0.9
CHL	HEP	7	72.7-83.9	27.4 ± 0.6	113	30.7 ± 0.6

The quantity $\dot{L}$ is the rate of change of line length determined by least-squares, shown together with one standard deviation. Azimuth is measured clockwise from north. The slip rate is that appropriate to the strike-slip fault crossed by the indicated line. The time intervals of observations are given in decimal fractions of years.

TABLE 3. Fault Slip Rates Indicated by Short-Range Trilateration Networks

Network	No. of Observations	Period	Slip Rate, mm/yr
Pionne	8	75.2-87.3	12 ± 2
Dry Lake	4	79.0-87.3	27 ± 2
Tully	8	74.9-87.3	32 ± 1

See Table 2 for explanation of notation.

TABLE 4. Summary of Deformation Rates within the Central Coast Ranges

Fault	Orientation	Geological Slip Rate, mm/yr	Geodetic Slip Rate, mm/yr
Right-lateral strike-slip faults			
Ortigalita	N35°W	0-2[a]	
San Andreas	N41°W	31-37[b]	32 ± 3[c]
Rinconada	N35°W	0-2[d]	2 ± 1[e]
San Simeon	N34°W	6-9[f]	
San Gregorio	N20°W	7-11[g]	0 ± 8[h]
Compression in the Coast Ranges			
East of San Andreas		2.2-5.5[i]	5.7 ± 2.7[j]
West of San Andreas		4.4-11[i]	6.1 ± 1.7[k,l]

[a] *Hart et al.* [1986].

[b] *Sieh and Jahns* [1984].

[c] *Savage and Burford* [1973]; *Thatcher* [1979a]; *Burford and Harsh* [1980]; *Lisowski and Prescott* [1981]; this study.

[d] *Hart et al.* [1986]; D. B. Slemmons, personal communication, 1987; E. W. Hart, personal communication, 1988.

[e] The line between Brush and Mulligan of the USGS Pajaro trilateration network has been measured five times between May 1978 and April 1983. If it is assumed that the average line length change is due to right-lateral slip on the King City fault, a northern extension of the Rinconada fault, then a slip rate of 2 ± 1 mm/yr is indicated.

[f] Rate of right-vertical oblique slip inferred from the offset of an ancient marine shoreline; a preferred slip rate of 6 mm/yr is given by *Clark et al.* [1984].

[g] Rate of right-lateral slip inferred from the offset of an ancient marine shoreline; a preferred slip rate of 7 mm/yr is given by *Clark et al.* [1984].

[h] From trilateration measurements made to the Farallon Islands between mid-1979 and late 1985 [*Prescott and Yu*, 1986].

[i] *Namson and Davis* [1988] estimated that 11 km of late Cenozoic shortening has occurred between the San Andreas fault and the Great Valley. The 22 km of shortening to the west of the San Andreas fault was computed by *Namson and Davis* [1988] from a solution that satisfies the observed structural relief. The range in rate estimates was obtained by assuming that shortening commenced between 5 and 2 m.y. ago.

[j] This study. The direction of maximum contraction is N16°E ± 13°.

[k] *Segall and Harris* [1986]; *Harris and Segall* [1987]. Average rates of change of line length from the San Luis trilateration network were used to invert for slip rate at depth on the San Andreas fault. In order to fit the trilateration measurements from this network, it was necessary to include a component of contraction normal to the trend of the San Andreas fault. The inversion results suggest a spatially uniform normal strain of -0.06 μstrain/yr. The net shortening rate across the network is 6.1 ± 1.7 mm/yr. This estimated compression, however, may be due to a systematic bias in the older trilateration data [J.C. Savage, personal communication, 1987] .

[l] Two additional geodetic studies using historical triangulation data have been made west of the San Andreas fault. *Burford* [1967] analyzed triangulation data measured between 1930 and 1951 from two networks. One extends from Monterey Bay to the region where the San Andreas and Calaveras faults diverge (Figure 1), and one extends from Kettleman Hills near Parkfield west to San Luis Obisbo. Outside a zone close to the San Andreas fault, the direction of maximum shortening was estimated to be approximately N35°E. As part of a general study of the deformation in central California, *Thatcher* [1979a] examined triangulation data measured during the time interval 1944-1963 from the Salinias Valley network. Most of this network lies within the Salinian block located between the San Andreas and Rinconada faults. Examination of subregions suggest that the strains are poorly resolved, with the orientation of the inferred strain field not correlated with any known faults or tectonic trends. Because of the uncertainties in the results, neither of these studies were used for rate determinations.

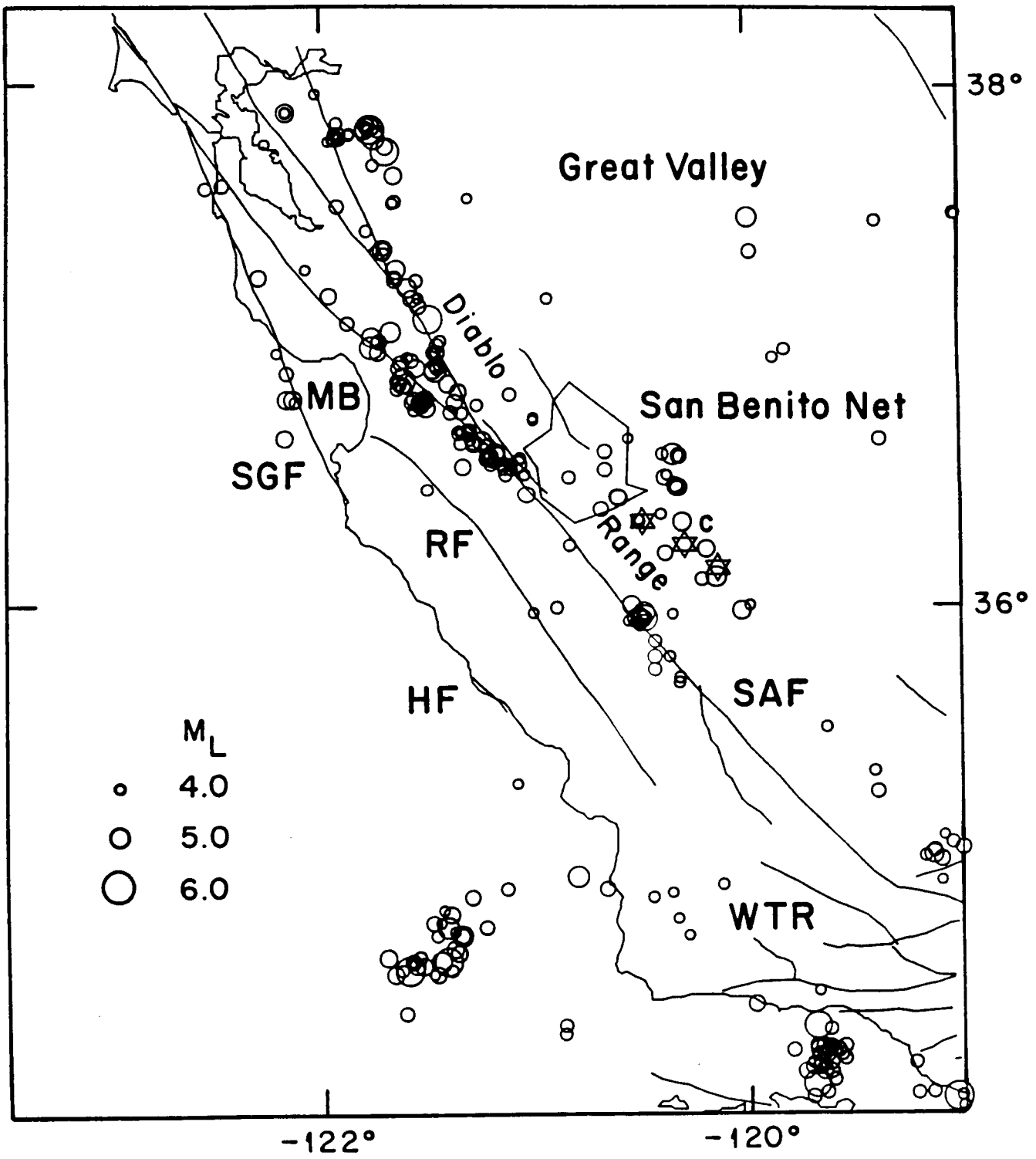
38°
Great Valley
Diablo
MB
San Benito Net
SGF
RF
Range
36°
HF
SAF
M_L
4.0
5.0
6.0
WTR
-122°
-120°

Figure 1

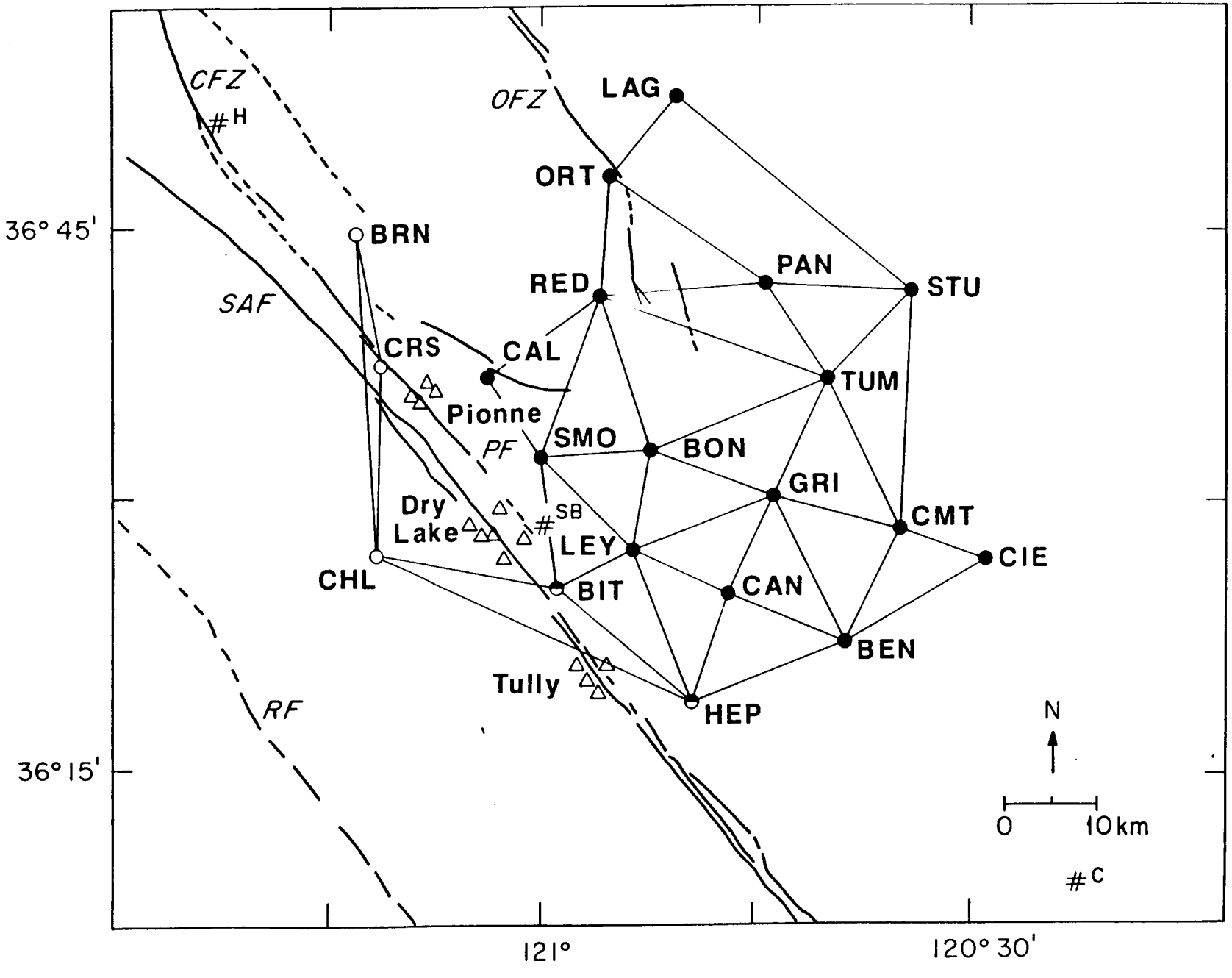
CFZ
#H
OFZ
LAG
ORT
36° 45'
BRN
PAN
STU
RED
SAF
CRS
CAL
TUM
Pionne
SMO
BON
PF
GRI
Dry
Lake
#SB
CMT
LEY
CIE
CHL
BIT
CAN
BEN
Tully
HEP
RF
N
36° 15'
0
10km
#C
121°
120° 30'

Figure 2

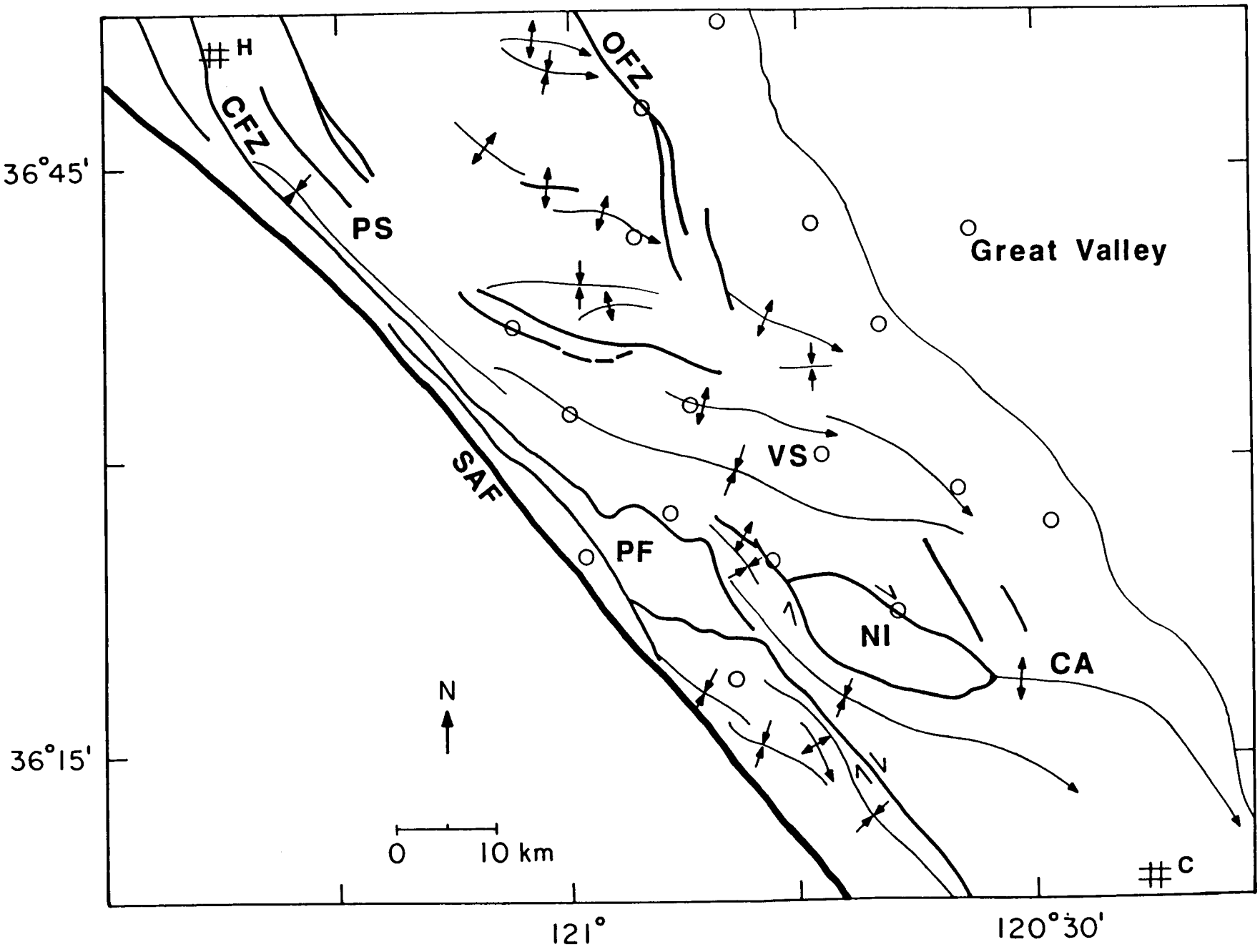
#H
CFZ
OFZ
PS
Great Valley
SAF
VS
PF
NI
CA
N
0
10 km
#C
36°45'
36°15'
121°
120°30'

Figure 3

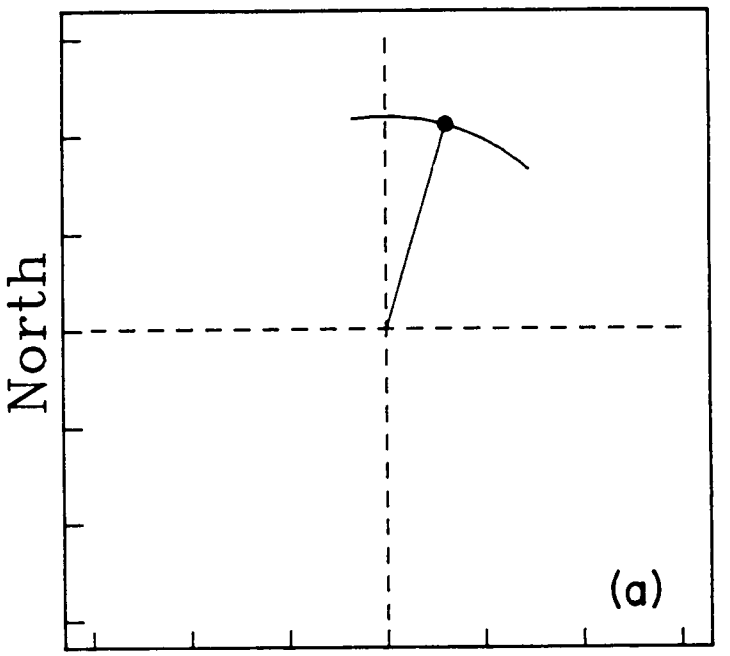

East

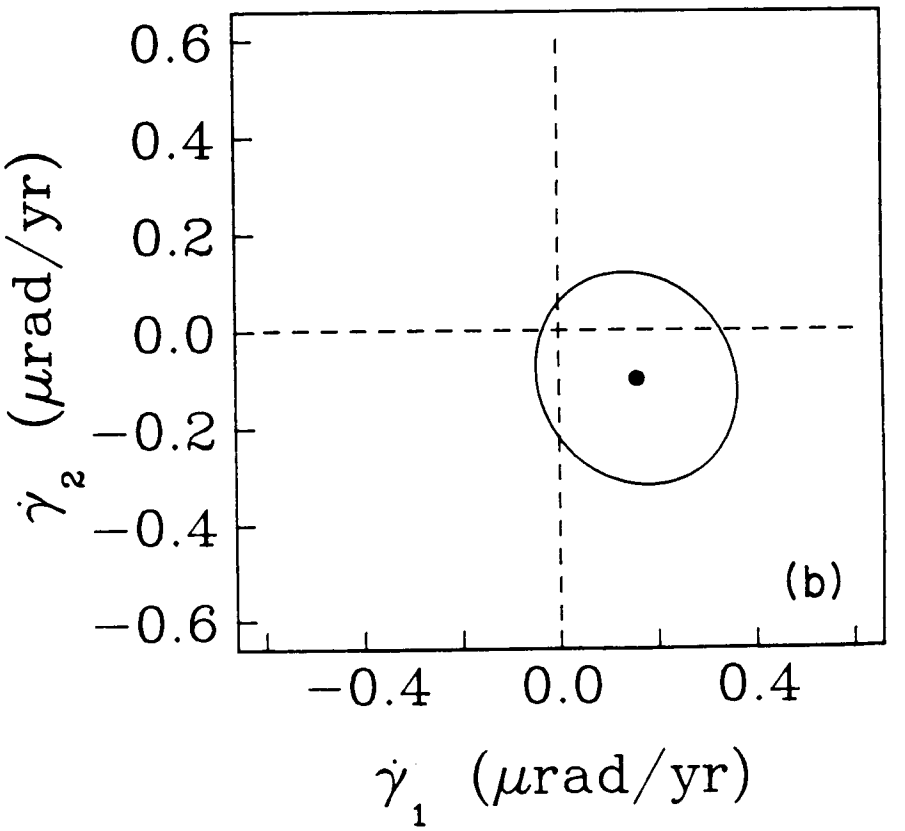

Figure 4

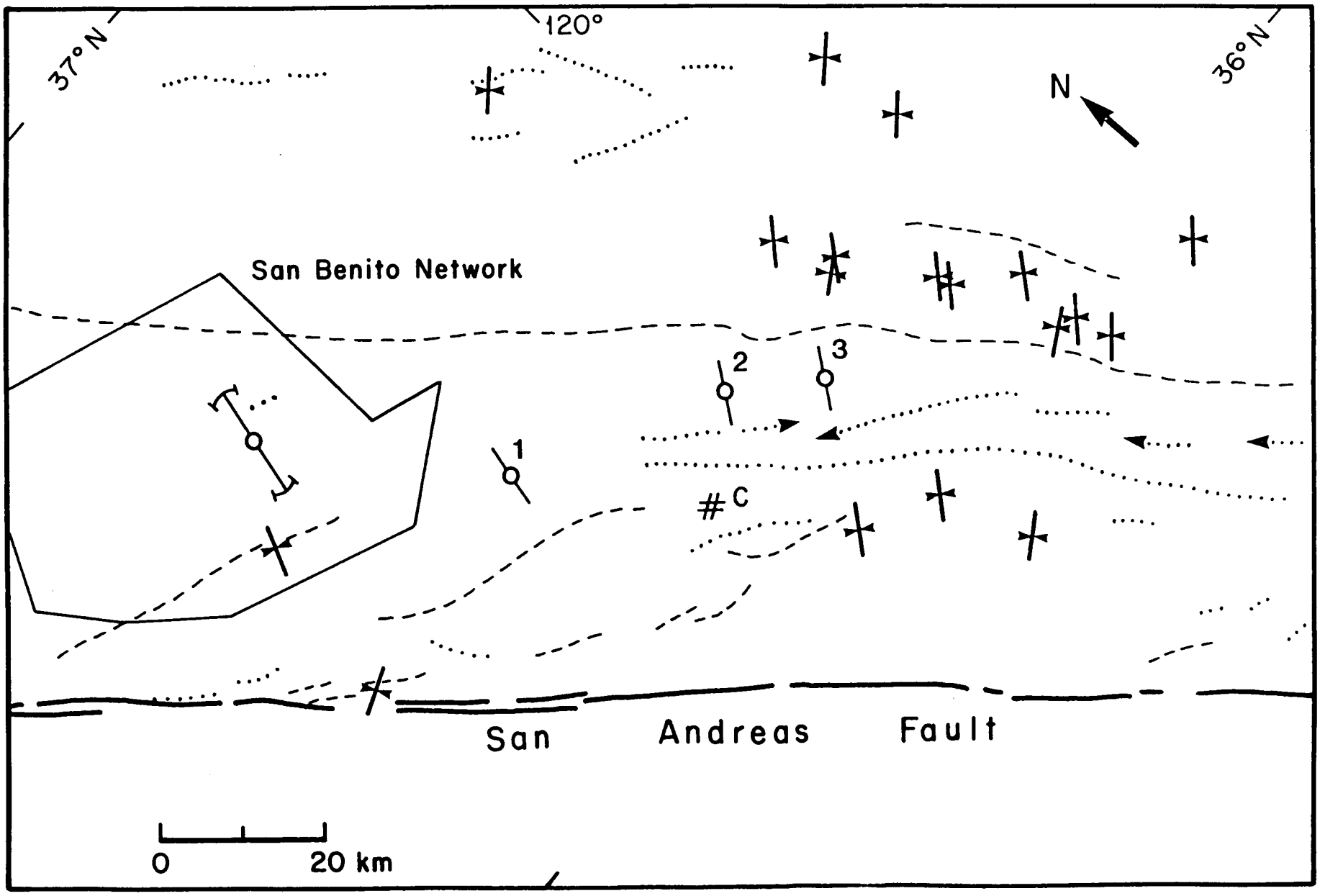
37°N
120°
36°N
N
San Benito Network
1
2
3
#C
San Andreas Fault
0
20 km

Figure 5

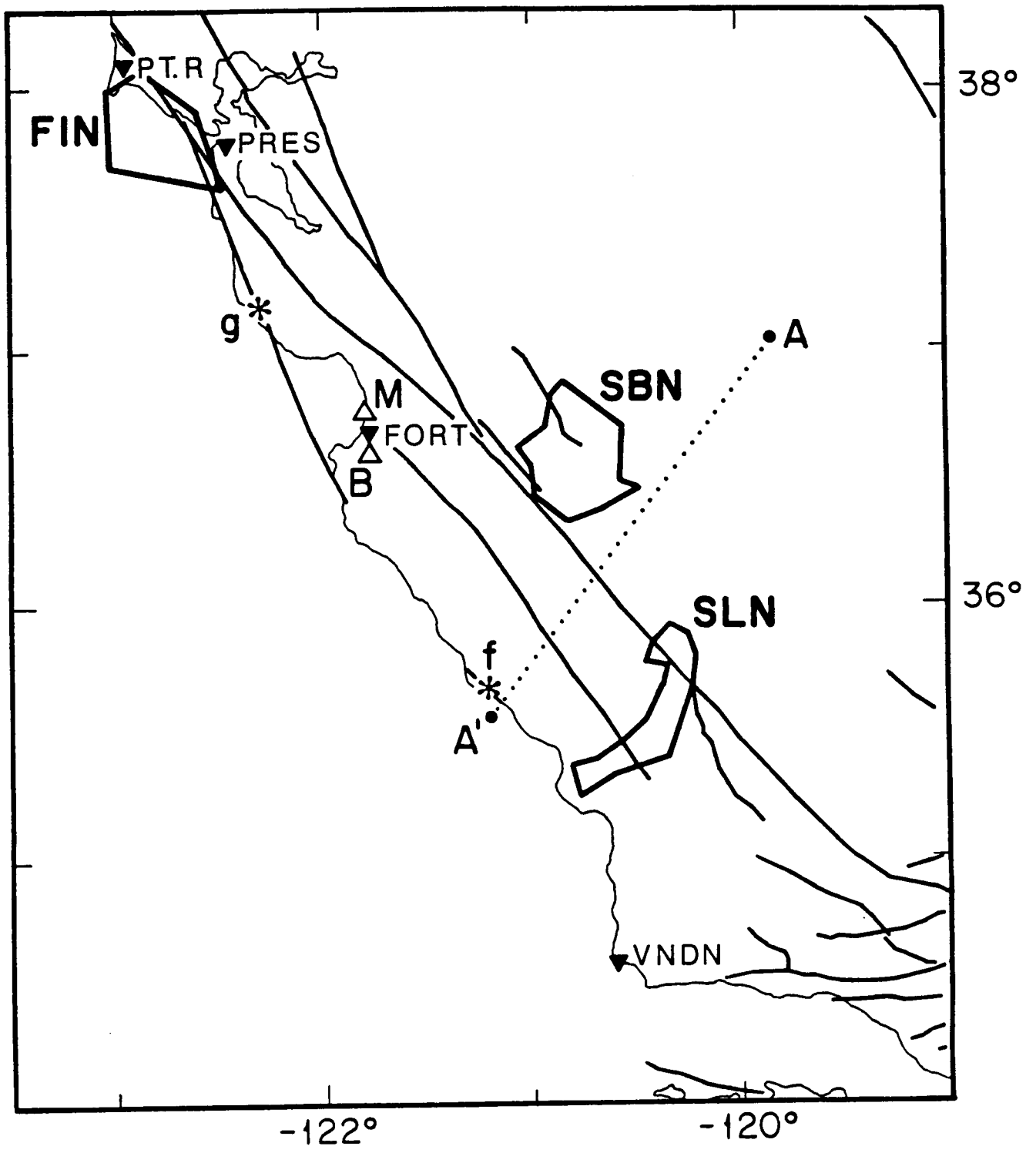

Figure 6

APPENDIX 3

Geodetic Measurement of Deformation in California

Jeanne M. Sauber

Abstract from Ph.D. thesis, 219 pp., Massachusetts Institute of Technology, Cambridge, 1988.

GEODETIC MEASUREMENT OF DEFORMATION IN CALIFORNIA

by

Jeanne M.Sauber

Submitted to the Department of Earth, Atmospheric, and Planetary Sciences on November 22, 1988, in partial fulfillment of the requirements for the Degree of Doctor of Philosophy in Geophysics

Abstract

The very long baseline interferometry (VLBI) measurements made in the western U.S. since 1979 as part of the National Aeronautics and Space Administration Crustal Dynamics Project provide discrete samples of the temporal and spatial deformation field. The interpretation of the VLBI-derived rates of deformation requires an examination of geologic information and more densely sampled ground-based geodetic data. In the first two of three related studies embodying this thesis I process triangulation and trilateration data measured on two regional networks, one in the central Mojave Desert and one in the Coast Ranges east of the San Andreas fault. At the spatial scales spanned by these local geodetic networks, auxilliary geologic and geophysical data have been utilized to examine the relation between measured incremental strain and the accommodation of strain seen in local geological structures, strain release in earthquakes, and principal stress directions inferred from *in situ* measurements. In the third study I process VLBI data from stations distributed across the Pacific - North American plate boundary zone in the western United States. The VLBI data have been used to constrain the integrated rate of deformation across portions of the continental plate boundary in California and to provide a tectonic framework to interpret regional geodetic and geologic studies.

Shear strain rates in the central Mojave Desert of California have been calculated with data from triangulation and trilateration surveys made during 1934-1982. For the region between the Helendale and Camp Rock faults the shear strain rate was determined to be 0.16 ± 0.03 μrad/yr, with maximum right-lateral shear straining occurring on a plane oriented N41°W ± 5°. If we assume that this deformation is due to right-lateral motion across the northwest trending local faults, the average shear straining corresponds to a relative displacement of 6.7 ± 1.3 mm/yr across this portion of the network. From the Camp Rock fault eastward across the network there is a transition from significant to very low strain rates. Examination of nine focal mechanisms and their relation to the local geology and the strain data suggests that most of the long-term displacement occurs on the major northwest trending faults oriented nearly along the direction of relation motion between the North American and Pacific plates. Secondary faulting, controlled by a Coulomb-Anderson failure mechanism or by slip on preexisting faults, can account for the occurrence of earthquakes on faults of other orientations.

Triangulation and trilateration data from two geodetic networks located between the San Andreas fault and the Great Valley have been used to calculate the shear strain rates in the Diablo Range and to estimate the slip rate along the Calaveras and Paicines faults in central California. The shear strain rates, $\dot{\gamma}_1$ and $\dot{\gamma}_2$, have been estimated independently from angle changes using Prescott's method and from the simultaneous reduction for station position and strain parameters using the DYNAP method with corrections to reduce the triangulation and trilateration data to a common reference surface. On the basis of Prescott's method, the average shear strain rate across the Diablo Range for the time period between 1962 and 1982 is 0.15 ± 0.08 μrad/yr, with the orientation of the most compressive strain (β) at N16°E ± 14°. With corrections for the deflection of the vertical

and the geoid - reference ellipsoid separation computed on the basis of local gravity observations, the average shear strain estimated using the DYNAP method is 0.19 ± 0.09 μrad/yr, and $\beta = N16°E \pm 13°$. Although $\dot{\gamma}$ is not significantly greater than zero at the 95% confidence level, the orientation β is similar to the direction of maximum compressive strain indicated by the orientation of major fold structures in the region (N25°E). We infer that the measured strain is due to compression across the folds of this area; the average shear straining corresponds to a relative shortening rate of 5.7 ± 2.7 mm/yr. In contrast to the situation throughout most of the Coast Ranges, where fold axes have orientations approximately parallel to the San Andreas fault, within the Diablo Range between Hollister and Coalinga the trends of the fold axes are different and are thought to be controlled by reactivation of older structures. From trilateration measurements made between 1972 and 1987 on lines that are within 10 km of the San Andreas fault, a slip rate of 10-12 mm/yr has been calculated for the Calaveras-Paicines fault south of Hollister. The slip rate on the Paicines fault decreases to 4 mm/yr near Bitter.

To distinguish between different models that describe the distribution of strike-slip and compressive displacements within the southern Coast Ranges we compared the findings of regional geologic and geodetic studies with predictions from kinematic plate models. Such comparisons support the view that the fault-parallel component of the San Andreas "discrepancy vector" may be accommodated by strike-slip motion on the Rinconada as well as the San Gregorio fault. Geological and seismicity data, as well as our geodetic results, suggest that northeast-southwest compression in the Coast Ranges of central California may be localized to two regions, the 30-km-wide zone spanned by the triangulation and trilateration network of this study and a second zone to the west of the Rinconada fault. The inferred shortening to the east of the San Andreas fault may represent a significant component of the fault-normal compression predicted by the discrepancy vector.

The geocentric position vectors from a set of 77 VLBI experiments beginning in October 1982 have been used to estimate the tangential rate of change of station positions in the western U.S. in a North-America-fixed reference frame. These data have been processed with a procedure that removes from apparent tectonic motion the contamination due to errors in Earth-orientation parameters and non-uniform station geometry; this procedure accounts fully for the position covariance between stations. For three regions, across southern California just north of the Imperial fault, in the "big-bend" region, and in central California, the rates of deformation derived from VLBI and ground-based geodetic data have been compared, and the relationship between the rates of deformation determined from geological data and those estimated from the geodetic data have been examined.

Deformation across southernmost California is fairly well described by simple right-lateral shear on the San Andreas, San Jacinto, Elsinore, and possibly the offshore faults of the California borderlands. An estimate of the integrated rate of deformation across the southern region of the Basin and Range province given by the station Yuma (3.4 ± 2.7 mm/yr at $N84°W \pm 16°$) is consistent with the low rate of deformation inferred from geologic data. A large earthquake has not occurred on the southern segment of the San Andreas fault within the last ~400 years, and strain accumulation is observed over a broad region. If the vector velocity given by the Monument Peak - Yuma difference vector (37.6 ± 3.4 mm/yr at $N40°W \pm 8°$) is approximately equal to the accumulated rate of long-term slip across the San Andreas, San Jacinto, and Elsinore faults, additional deformation is predicted to occur on faults offshore in the California borderlands. The velocity difference vector between Vandenberg and Monument Peak (5.9 ± 2.9 mm/yr at $N23°W \pm 4°$) further supports the hypothesis that additional deformation occurs on such offshore faults.

In the big-bend region of the San Andreas fault recent deformation has been measured across the right-lateral strike-slip faults of the central Mojave, along the San Andreas fault, and as northeast-southwest compression across the western Transverse Ranges and the offshore faults in the Channel Islands. The result for the VLBI station Mojave (7.1 ± 0.9 mm/yr at N50°W ± 1°), along with ground-based geodetic and geologic data from the Mojave Desert, the Garlock fault, and the Basin and Range, suggest that the estimated rate of deformation on the northwest-striking faults of the central Mojave may be kinematically related to deformation north of the Garlock. The station Mojave as well as the western Garlock fault are then within a deforming region connecting slip in the central Mojave to deformation north of the Garlock. The alternative hypothesis that the Mojave VLBI and central Mojave trilateration-triangulation results are due to elastic strain accumulation which will be relieved in the next large earthquake on the San Andreas fault is rejected on the basis of several arguments, the most convincing of which is that recent slip has been documented along the faults of the central Mojave. Over the broad region between Mojave and JPL the rate of deformation given by the differenced velocity vector is 26.9 ± 2.6 mm/yr at N43°W ± 5° and suggests that the long term rate of slip on this segment of the San Andreas fault may be ~25 mm/yr. The velocity difference vector for Vandenberg - Santa Paula suggest 15.2 ± 6.7 mm/yr of northeast-southwest compression (N15°E ± 7°) between the two sites.

In central California slip along the San Andreas fault is thought to occur primarily through surface creep. As noted above, recent deformation has also been measured on tectonic elements east and west of the San Andreas and include extension across the Basin and Range, right-lateral strike-slip motion on the Rinconada and San Gregorio faults and northeast-southwest compression within the Coast Ranges. The vector rate of change of the station position for OVRO (Owens Valley Radio Observatory), 10.3 ± 2.7 mm/yr at N37°W ± 4.5°, is closer to the local orientation of the Owens Valley fault than the assumed direction of extension in the Basin and Range (N60°W). The difference velocity vector between Fort Ord and OVRO, 37.1 ± 2.8 mm/yr at N37°W ± 5°, is similar to the integrated rate of deformation estimated from ground-based geodetic networks and from geological data.

Thesis Supervisors: Sean C. Solomon, Professor of Geophysics
Thomas H. Jordan, Professor of Geophysics

APPENDIX 4

On the State of Stress Near Oceanic Transforms and Fracture Zones

Sean C. Solomon, Eric A. Bergman,
William S. D. Wilcock and G. M. Purdy

To appear in *Eos Trans. Amer. Geophys. Un.*, *70*, in press, 1989.

On the State of Stress Near Oceanic Transforms and Fracture Zones

Sean C. Solomon, Eric A. Bergman (both at Dept. of Earth, Atmospheric, and Planetary Sciences, MIT, Cambridge, MA 02139), William S. D. Wilcock (MIT-WHOI Joint Program in Oceanography, Cambridge, MA 02139), and G. M. Purdy (Dept. of Geology and Geophysics, WHOI, Woods Hole, MA 02543).

Recent studies of the state of stress near the San Andreas fault in central California have demonstrated that the axis of greatest compressive stress (σ_1) tends to be oriented nearly perpendicular to the fault zone, a result attributed to a small component of plate convergence across the fault and to a fault zone substantially weaker than the adjacent lithosphere. Several lines of evidence support the conclusion that oceanic transform faults also act as zones of reduced strength. During a recent microearthquake experiment in the Kane transform, most of the activity occurred to the north or south of the principal transform displacement zone, and well-constrained mechanisms displayed predominantly normal faulting mechanisms with the axis of least compressive stress (σ_3) oriented approximately perpendicular to the transform valley. That this is not an isolated occurrence is suggested by the numerous inward-facing normal faults that have been observed by side-scan sonar imaging and deep-towed camera systems in several large-offset transforms. Further, mechanical models for the orthogonal pattern of ridge crests and transforms generally require that the transform faults act as zones of relative weakness. In contrast to the situation on active transforms, neither the locations nor the mechanisms of oceanic intraplate earthquakes support the hypothesis that non-transform portions of fracture zones act as lithospheric weak zones. In particular, from the mechanisms of thrust and normal faulting earthquakes located within 50 km of a major inactive fracture zone the distribution of the angles between, respectively, σ_1 and σ_3 and the local fracture zone strike cannot be distinguished from a random distribution. One possible explanation for these results is that transforms are weak because of processes, such as fracturing or hydrothermal alteration, which can be reversed by thermal annealing when the material in the transform valley passes by the adjacent ridge-axis intersection prior to becoming part of the inactive fracture zone structure. A second possibility is that the state of stress across the transform zone is time-dependent and the relative weakness is only apparent, with σ_3 perpendicular to the transform only after a major earthquake has released shear stress along a significant length of the fault. The fracture zone material, by this second view, is indistinguishable from normal oceanic lithosphere once removed from the active transform zone. We discuss how these two alternative hypotheses may be distinguished by future experiment.

APPENDIX 5

1988 Global Positioning System (GPS)

Crustal Deformation Measurements in Turkey

Robert Reilinger, M. N. Toksöz, A. Barka,

E. Kasapoglu, P. Wilson, H. Seeger,

J. Stowell, and B. Stephens

To appear in *Eos Trans. Amer. Geophys. Un., 70*, in press, 1989.

1988 Global Positioning System (GPS) Crustal Deformation Measurements in Turkey

R. Reilinger, M. N. Toksöz, A. Barka (Earth Resources Laboratory, M.I.T., Cambridge, MA 02139), E. Kasapoglu (Dept. of Geological Engineering, Hacettepe Univ., Ankara, Turkey), P. Wilson , H. Seeger, J. Stowell (IFAG, Frankfurt, Fed. Rep. Germany), B. Stephens (UNAVCO, Univ. of Colorado, Boulder, CO)

A multi-institutional experiment involving scientist sfrom the United States, Germany, England, Turkey, Greece, and Italy was begun in September-October 1988 to directly monitor present-day deformation throughout the eastern Mediterranean region. The September observations included establishing a network of 18 GPS sites in Turkey, 4 of which were observed previously by Satellite Laser Ranging (SLR) under the WEGENER/MEDLAS Project. Continuous GPS observations were maintained at 3 SLR sites in Greece (Dionysos, Askites, Rhodes), 1 in southern Italy (Matera), and 3 in northern Europe (Wettzell, Onsala, Tromso) throughout the Turkey Campaign.

The 18 sites established in Turkey were observed during a 23 day period using 4 TI-4100 dual frequency receivers provided by the University Navstar Consortium (UNAVCO). The GPS site at Ankara (Hacettepe University) was monitored continuously throughout the Turkey Campaign, while most other sites in Turkey were observed a minimum of 3 days each. Sites in Turkey were located to monitor broad scale plate tectonic movements and intraplate deformations, deformations along the western and central parts of the North Anatolian fault (including strain accumulation, fault creep near Karabuk, and the distribution of strain where the fault bifurcates in northwest Turkey), and lithospheric extension in the Aegean Trough region of Southwest Anatolia. The GPS network will be extended into eastern Turkey during the Fall of 1989 to begin monitoring deformation associated with collision of the Arabian Plate with Eurasia. Selected baselines will be reobserved yearly, with a complete reoccupation every 2 years.

APPENDIX 6

Preliminary Report on 1989 GPS

Imperial Valley/Salton Trough experiment

Robert Reilinger

PRELIMINARY REPORT ON 1989 GPS IMPERIAL VALLEY/SALTON TROUGH EXPERIMENT

30 March 1989

This is a brief report on our recent GPS field campaign in the Imperial Valley-Salton Trough region of southern California.

OBJECTIVES

(1) Reobserve a dense network of GPS sites established in the Imperial Valley in 1986/1988 by NGS and MIT in order to continue developing a history of the spatial and temporal distribution of strain in this critical area.

(2) Establish direct GPS ties to "new" sites located along the southern San Andreas fault between Palm Springs and Bombay Beach.

(3) Reobserve sites in the vicinity of the 1987 Superstition Hills earthquake to monitor post-earthquake deformation for the period February 1988 to March 1989 (approximately a 1 year period beginning 3 months after the earthquake).

(4) Conduct repeat GPS observations at 4 L-DGO tide gauge stations in the Salton Sea.

(5) Establish GPS sites near the "Extra fault", which may trigger a large earthquake on the southern San Andreas fault (Hudnut, Phd. Thesis).

(6) Make GPS observations at 4 regional VLBI sites (Pinyon Flat, Black Butt, Monument Peak, Ocotillo) for intercomparison, and to densify VLBI spatial coverage.

(7) Strengthen ties between the Imperial Valley-Salton Trough GPS network and a GPS network established by the Riverside Flood Control District/ Riverside Survey in March 1988.

(8) Undertake a high precision Kinematic GPS survey using Trimble 4000SD receivers in order to demonstrate the applicability of this technique to future geodynamic GPS surveys.

PARTICIPANTS

(1) Carlos Aiken (U.T. Dallas)
(2) John Benson (L-DGO)
(3) Mike Bevis (N.C. State)
(4) Douglas Charley (ORSTOM)
(5) Bob Cicerone (MIT)
(6) Roger DeCourt (ORSTOM)
(7) Mauricio de la Fuente (U. of Mexico)
(8) Lewis Gilbert (L-DGO)
(9) Ken Hudnut (L-DGO/Caltech)
(10) Michael Jackson (UNAVCO)
(11) Shawn Larsen (Caltech)
(12) Rob Reilinger (MIT)
(13) Bruce Stephens (UNAVCO)

(14) James Stowell (UNAVCO)

A number of individuals, not listed above, assisted us in the field campaign. Most notably, Bill Young, Bob Jackson, and others from Riverside County Flood Control District, with support from Riverside County Survey, set 5 3-D first order bench marks specifically for this experiment. Three of these new marks were at L-DGO tide gauge stations, and 2 were along the Coachella segment of the San Andreas fault. Bob Estes of the Imperial County Survey provided detailed information on bench marks in Imperial County. This was particularly critical for recovering an alternate mark at Calexico (the original mark was destroyed since our 1988 observations). Brian Westfall and Ralph Smith of Trimble provided technical advice on the Trimble receivers and generously arranged overnight delivery of an additional receiver at one point in the experiment.

LOGISTICS

Duncan Agnew arranged space at UCSD, La Jolla for preparing the instruments for field deployment and for conducting a 3 day training session. Instrument preparation and operator training was directed by James Stowell, Bruce Stephens, and Michael Jackson. All participants in the Imperial Valley-Salton Trough Campaign attended the full training session. In addition, a number of individuals from UCLA, UCSD, and Caltech, who were to participate in the S. California Regional GPS Experiment, attended parts of this training session (some participants from this group visited us in the field to gain additional experience).

UNAVCO arranged for seven receivers to carry out this field campaign. This included the 3 UNAVCO TI RAM units, 1 TI ROM unit with a Grid computer to record data and simulate the GEASAR software (unit provided by NRL), and 3 Trimble 4000SD duel frequency receivers. The Trimble receivers were provided by the manufacturer.

The specific observation schedules for each session are shown in the accompanying Figures. During the first 6 observation sessions (5-10 March) we operated out of 2 bases - El Centro in the south and Indio in the north. Mike Bevis and Bruce Stephens directed 4 teams in Indio and Michael Jackson and I directed 3 teams in El Centro and coordinated activities between the north and south. Instrument teams during the first week were as follows:

UN01 (TI 4100) - Larsen
UN02 (TI 4100) - Gilbert/DeCourt
UN03 (TI 4100) - Benson/Stephens/Hudnut
UN04 (TI 4100) - Cicerone/Jackson
TB07 (Trimble 4000SD) - Bevis/Missegue/Charley
TB08 (Trimble 4000SD) - de la Fuente/Aiken
TB09 (Trimble 4000SD) - Reilinger

For sessions 6 through 12 (12-17 March) all 7 teams operated from a single base in El Centro. A number of participants had to leave during the second week, leaving the following instrument teams:

UN01 - Larsen
UN02 - Gilbert/DeCourt
UN03 - Benson
UN04 - Cicerone
TB07 - Missegue/Charley
TB08 - Stephens
TB09 - Reilinger

On March 11 and 12 Michael Jackson of UNAVCO directed a kinematic GPS survey using the Trimble receivers. The primary reference receiver was maintained at station TAMA and the roving receiver visited stations COLL, ORIE, HAMA, and ACUT. A second reference receiver was operated at station L589 on 11 March, and at station GLOC on 12 March (see maps for sessions 6B and 7). Lize Nel (Boulder, CO) came specifically to participate in the Kinematic field tests. Other participants included Bruce Stephens, Ken Hudnut, and Rob Reilinger.

The equipment was cleaned and inventoried by our observing teams under the direction of Bruce Stephens on 18 March and delivered to UCSD, La Jolla by mid-afternoon of that same day.

DATA QUALITY

The Imperial Valley-Salton Trough experiment was clearly impacted by the intense solar activity and associated ionospheric disturbances which began on March 5-6. The extent to which the data were degraded can not be ascertained until a complete reduction is attempted. A major effort is underway at UNAVCO to reduce the Trimble data, and Shawn Larsen is currently processing at least some of the TI measurements. This "quick look" should be completed within a few weeks (hopefully prior to the NASA CDP Meeting at JPL on April 10). From our preliminary field analysis (i.e., notes taken by the observers regarding maintaining lock on satellite transmissions and signal to noise ratios), it appears that the TI receivers maintained lock on both L1 and L2, while the Trimble receivers had more difficulty tracking L2. We emphasize that this almost certainly results from the fact that the Trimble is a codeless receiver, and that all codeless receivers will likely be subject to similar difficulties. In any case, we are confident that the ionospheric corrections can be obtained from the TI data and applied retroactively to the Trimble data with very little, if any, loss in precision.

Distribution

Padovani
Thatcher
Flinn
Frey
Mayhew
Strange
Ware

MARCH 1989 IMPERIAL VALLEY GPS STATIONS

Station Name	Notes	4 letter I.D.	4 number I.D.	Lat (N)	Long (W)	Elev (M)
Pinyon Flats	VLBI	PINY	5487	33.61(37')	116.45(26')	1245
Black Butte	VLBI	BLAC	5445	33.66(40')	115.72(42')	518
Monument Peak	VLBI	MONU	5401	32.9(54')	116.4(24')	1870
Ocotillo NCMN	VLBI	OCOT	5477	32.79(47')	115.8(48')	−7
FTJS reset	TIDE	ROBO	5402	33.44(26')	116.05(02')	−52
Coach 2		COAC	5452	33.2(12')	115.41(24')	23
SSSP reset	TIDE	VARN	5403	33.5(30')	115.88(53')	−67
Sand Point	TIDE	SAN1	5404	33.19(12')	115.83(50')	−68
Thermal reset	RCFCD	VORO	5405	33.63(38')	116.16(10')	−39
Frink 1934		FRIN	5458	33.36(22')	115.65(40')	−52
BOB1 reset	TIDE	TRAN	5406	33.40(25')	115.82(50')	−50
GLO Corners		GLOC	5460	32.84(50')	115.25(15')	18
Alamo 1934		ALAM	5444	33.2(12')	115.61(37')	−38
L589 1967		L589	5471	32.96(58')	115.76(45')	47
Kane 1939		KANE	5469	33.06(04')	115.82(49')	44
Hamar 2 1967		HAMA	5462	33.04(02')	115.5(30')	−46
Offset 217		0217	5480	32.7(42')	115.3(18')	17
Calexico reset 89		BORD	5449	32.66(40')	115.51(30')	0
Orient 1939		ORIE	5484	32.92(55')	115.41(24')	−28
Ocotillo 1934		OCTI	5478	32.73(44')	116(00')	145
Tamarisk 1967		TAMA	5493	32.9(54')	115.5(30')	−34
College 1967		COLL	5453	32.8(48')	115.5(30')	−22
Junction		JUNC	5467	32.71(42')	115.06(04')	43
Dune Port	RCFCD	DUNP	5408	33.75(45')	116.28(14')	18
Painted Canyon		PAIN	5409	33.56(34')	116.13(02')	125
Extra		EXTR	5410	33.18(11')	115.86(51')	−15
Siphon 20	RCFCD	SIPH	0061	33.43(26')	115.68(41')	24
Coach MWD		COCH	5411	33.74(45')	116.16(10')	66
Acute 1934		ACUT	5443	33.03(02')	115.61(37')	−47
Calipatria 2		CALI	5450	33.17(10')	115.51(30')	−55

MARCH 1989 OBSERVATION SCHEDULE

Session 1

PINY	TB
BLAC	TI
ROBO (FTJS)	TI
COAC	TB
MONU	TI
OCOT	TI
EXTR	TB

Session 2

PINY	TB
BLAC	TI
ROBO	TI
COAC	TB
MONU	TI
OCOT	TI
EXTR	TB

Session 3

PINY	TB
BLAC	TI
VARN (SSSP)	TI
SAN1	TB
MONU	TI
OCOT	TI
PAIN	TB

Session 4

TRAN(BOB1)	TB
COCH	TI
VARN	TI
SAN1	TB
FRIN	TI
OCOT	TI
PAIN	TB

Session 5

TRAN	TB
DUNP	TI
COCH	TI
GLOC	TB
FRIN	TI
OCOT	TI
VORO	TB

Session 6

TRAN	TB
ROBO	TI
DUNP	TI
GLOC	TB
ALAM	TI
OCOT	TI
VORO	TB

Session 7

L589	TI
KANE	TI
(KinTAMA	TB)
GLOC	TB
ALAM	TI
OCOT	TI
KINEM (COLL, ACUT	
HAMA, ORIE)	

Session 8

L589	TI
KANE	TI
0217	TB
TAMA	TB
OCOT	TI
ACUT	TB

Session 9

SIPH	TI
ORIE	TI
OCTI	TB
0217	TB
BORD	TI
OCOT	TI
ACUT	TB

Session 10

SIPH	TI
ORIE	TI
OCTI	TB
CALI	TI
OCOT	TI
BORD	TB
TAMA	TB

Session 11

SIPH	TI
JUNC	TI
HAMA	TB
OCOT	TI
COLL	TB
SAN1	TI
TAMA	TB

Session 12

JUNC	TI
COLL	TI
ORIE	TB
SAN1	TI
GLOC	TB
OCTI	TI
TAMA	TB

TI = TI 4100
TB = Trimble 4000 SD

FIGURE 1. Map of the Imperial Valley-Salton Trough area showing major faults (including orthogonal, cross faults in the critical transition zone between the Imperial and San Andreas faults). Solid dots show GPS stations observed by our group during the March 1989 campaign. Small open circles are GPS stations observed in 1986 and 1988 which were not occupied this year. NGS will most likely observe these stations this summer. Large open circles are GPS stations established by Riverside County Flood Control District in March 1988. We established strong ties to this network and are cooperating with RCFCD on reduction of their 1988 observations (made with dual frequency TI receivers). Triangles show mobile VLBI sites we occupied with GPS during the 1989 campaign.

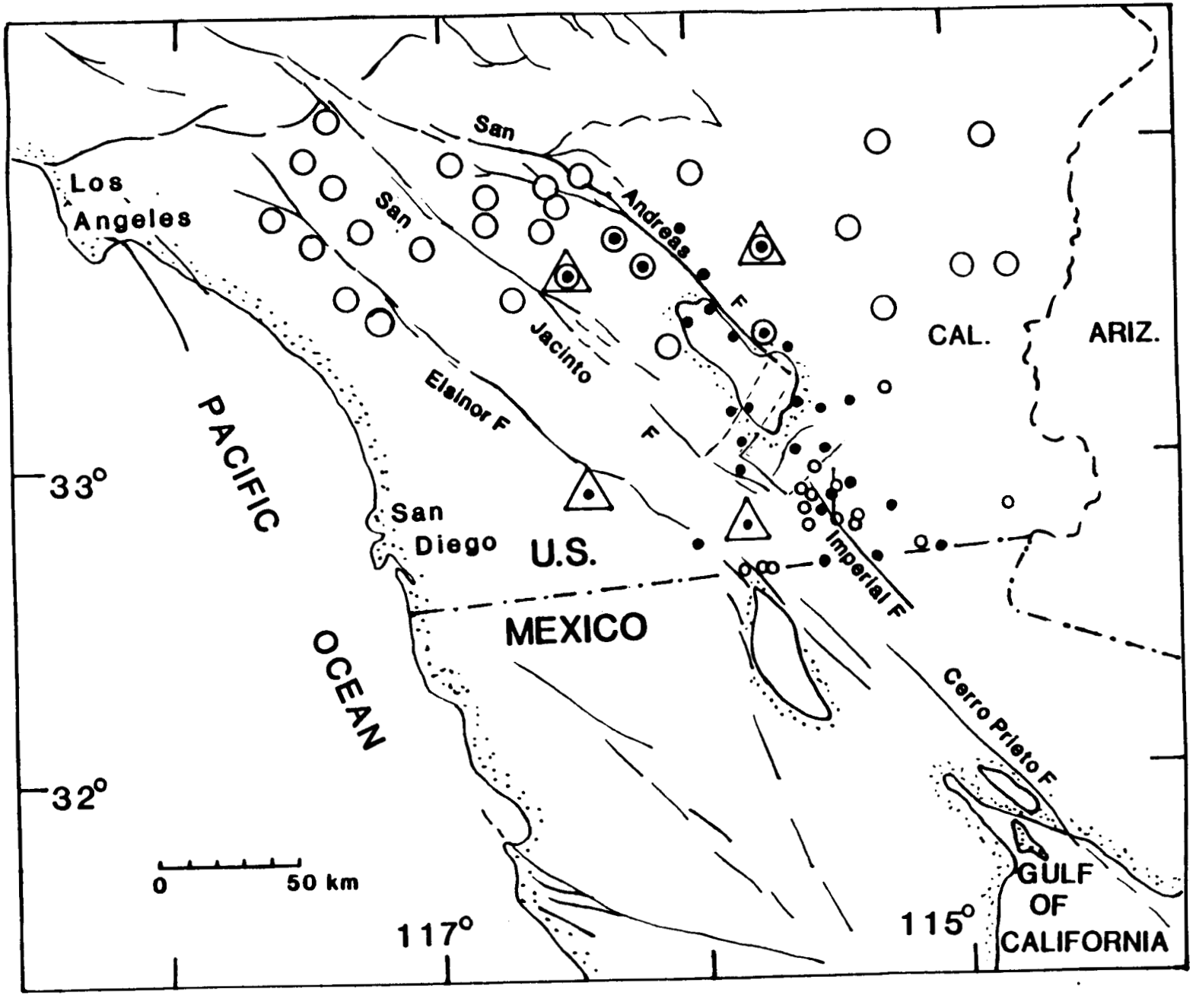
San
Andreas
F
San
Jacinto
F
Elsinor F
Los
Angeles
CAL.
ARIZ.
PACIFIC
OCEAN
33°
San
Diego
U.S.
MEXICO
Imperial F
Cerro Prieto F
32°
0
50 km
117°
115°
GULF
OF
CALIFORNIA

FIGURE 1.

FIGURE 2. Station names (4 character I.D.) for sites occupied by our group during March 1989 campaign. See Table 1 for details on bench marks.

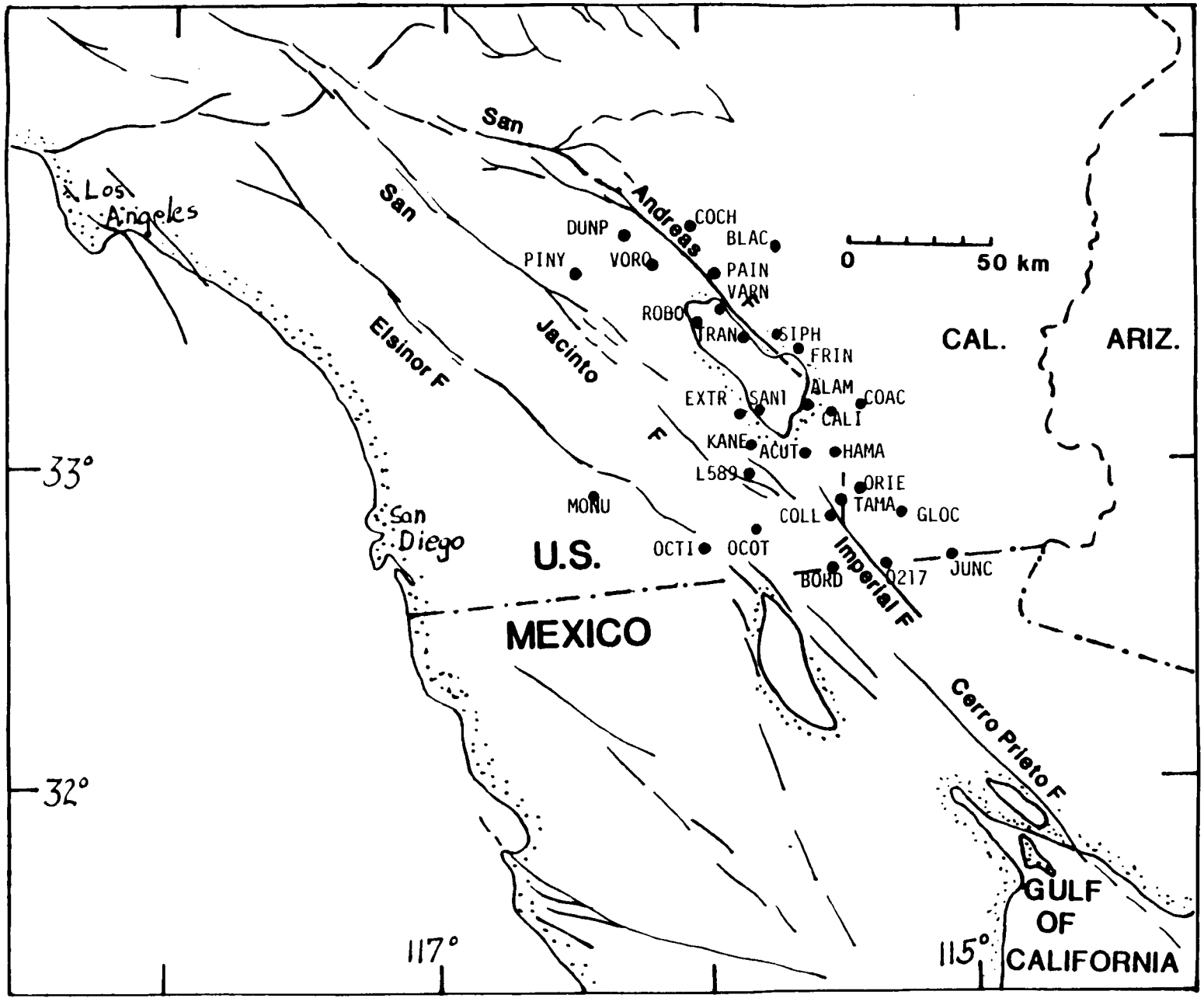
San
Andreas
San
Jacinto
F
Elsinor F
Los
Angeles
COCH
DUNP
BLAC
PINY
VORO
PAIN
VARN
ROBO
TRAN
SIPH
FRIN
ALAM
COAC
EXTR
SANI
CALI
KANE
ACUT
HAMA
L589
ORIE
TAMA
GLOC
COLL
MONU
OCTI
OCOT
BORD
0217
JUNC
Imperial F
Cerro Prieto F
0
50 km
CAL.
ARIZ.
33°
32°
117°
115°
San
Diego
U.S.
MEXICO
GULF
OF
CALIFORNIA

FIGURE 2.

FIGURE 3. Map showing stations occupied during each observing session. Triangles represent TI 4100 and squares Trimble 400 SD receivers.

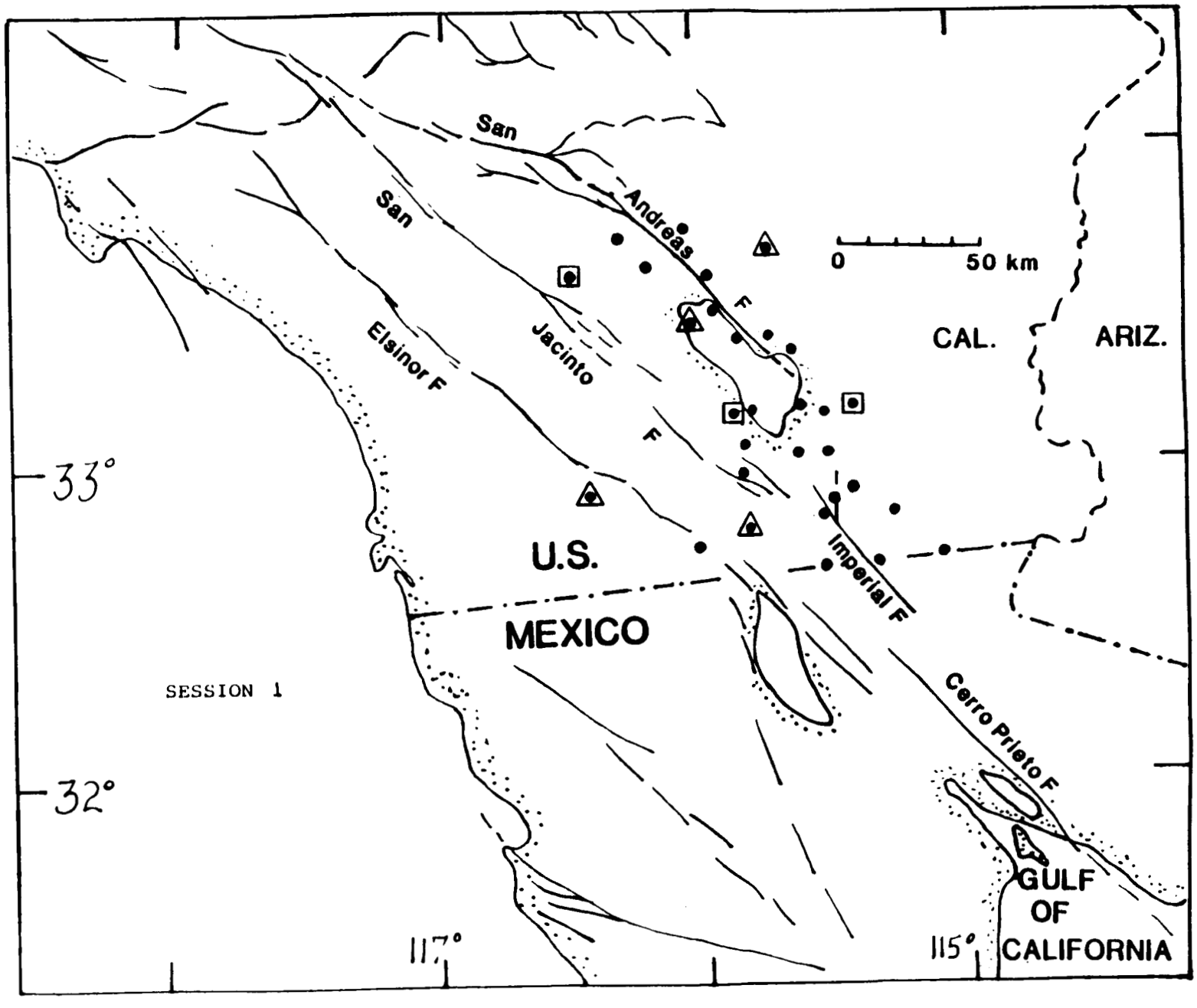
San
Andreas
F
San
Jacinto
F
Elsinor F
0
50 km
CAL.
ARIZ.
33°
U.S.
MEXICO
Imperial F
Cerro Prieto F
SESSION 1
32°
117°
115°
GULF
OF
CALIFORNIA

FIGURE 3.

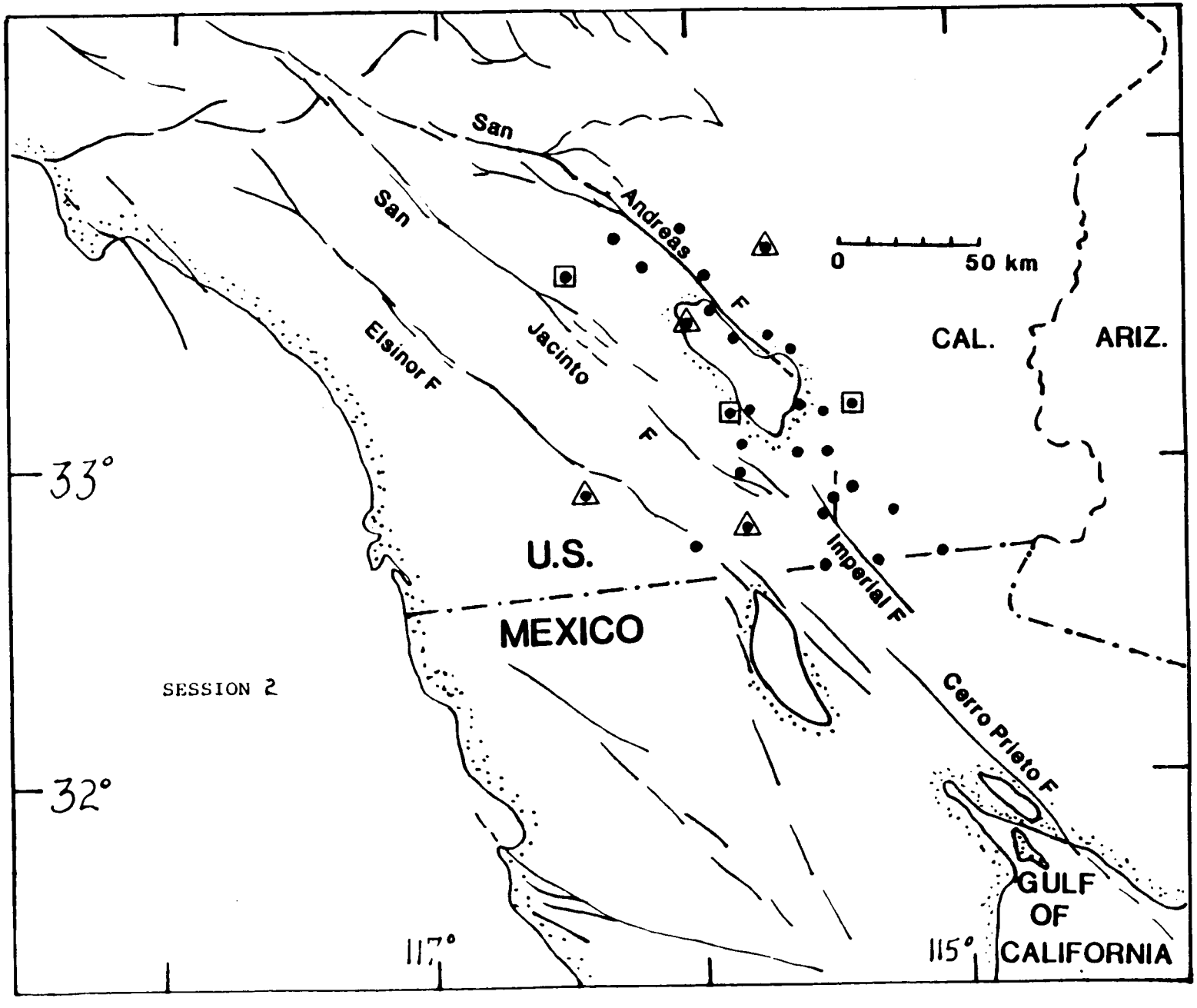
San
Andreas
F
San
Jacinto
F
Elsinor F
0
50 km
CAL.
ARIZ.
33°
U.S.
MEXICO
Imperial F
Cerro Prieto F
SESSION 2
32°
GULF
OF
CALIFORNIA
117°
115°

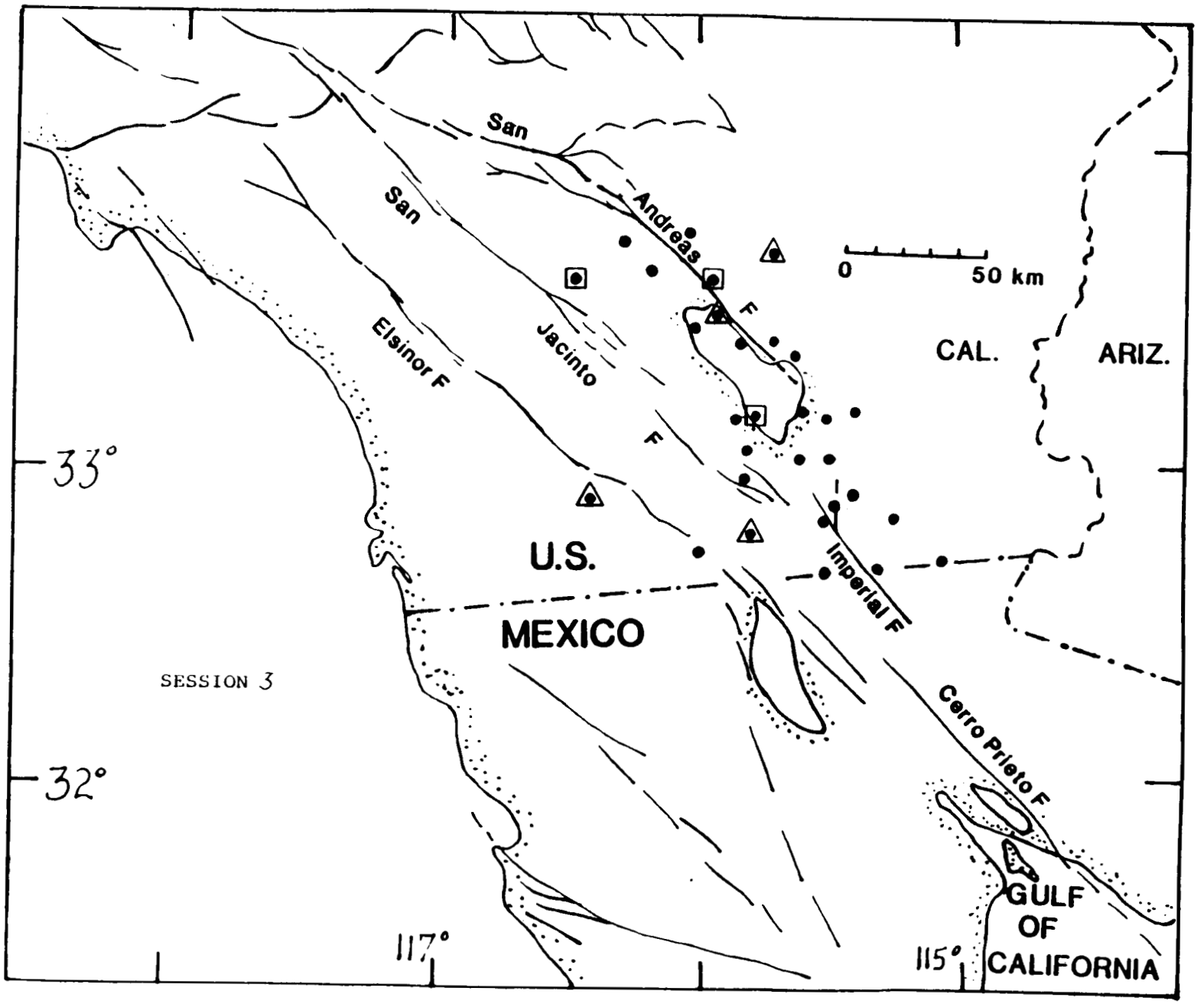
San
Andreas
F
San
Jacinto
F
Elsinor F
0
50 km
CAL.
ARIZ.
33°
U.S.
MEXICO
Imperial F
SESSION 3
Cerro Prieto F
32°
GULF
OF
CALIFORNIA
117°
115°

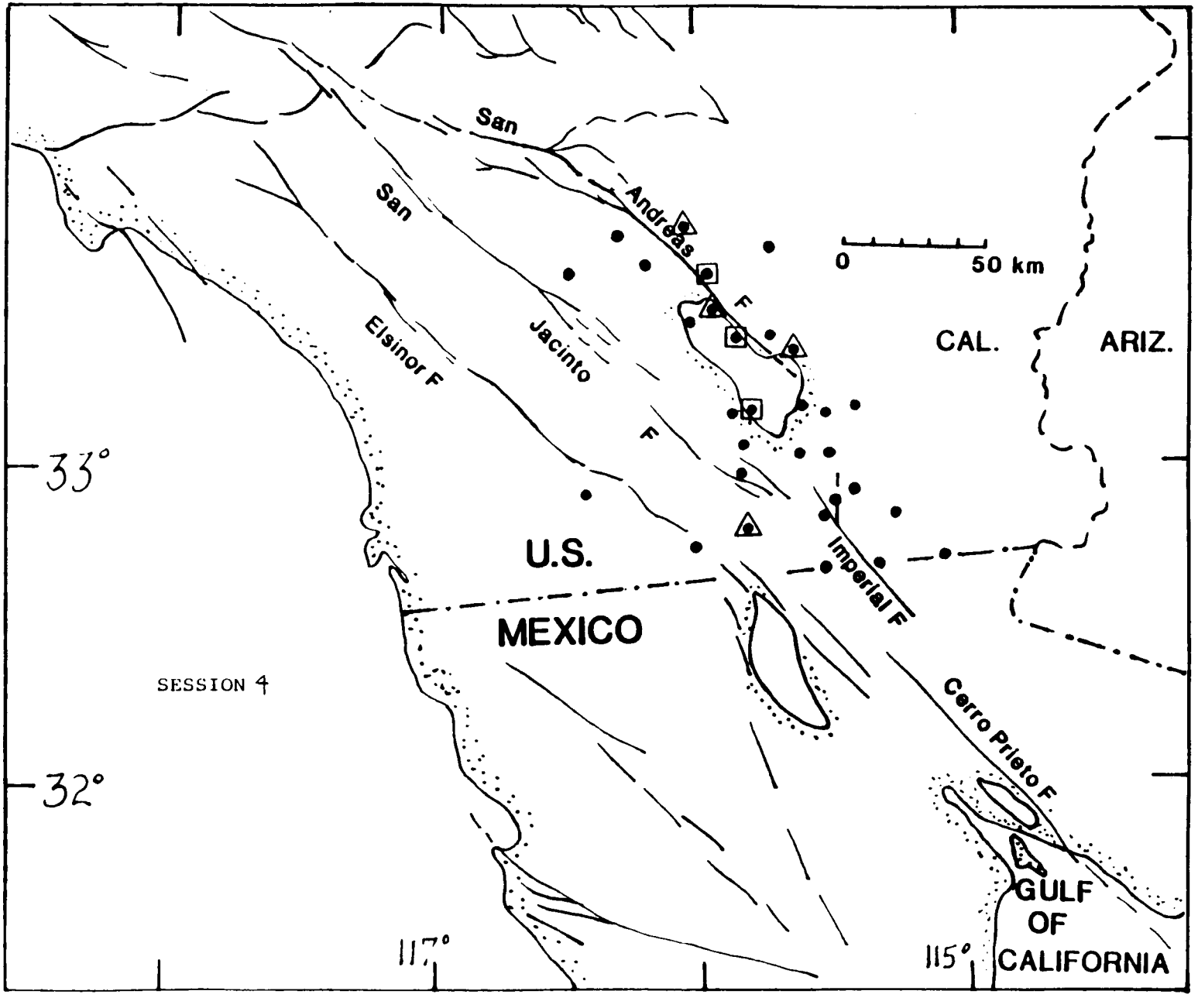
San
Andreas
F
San
Jacinto
F
Elsinor F
0
50 km
CAL.
ARIZ.
33°
U.S.
MEXICO
Imperial F
Cerro Prieto F
SESSION 4
32°
117°
115°
GULF
OF
CALIFORNIA

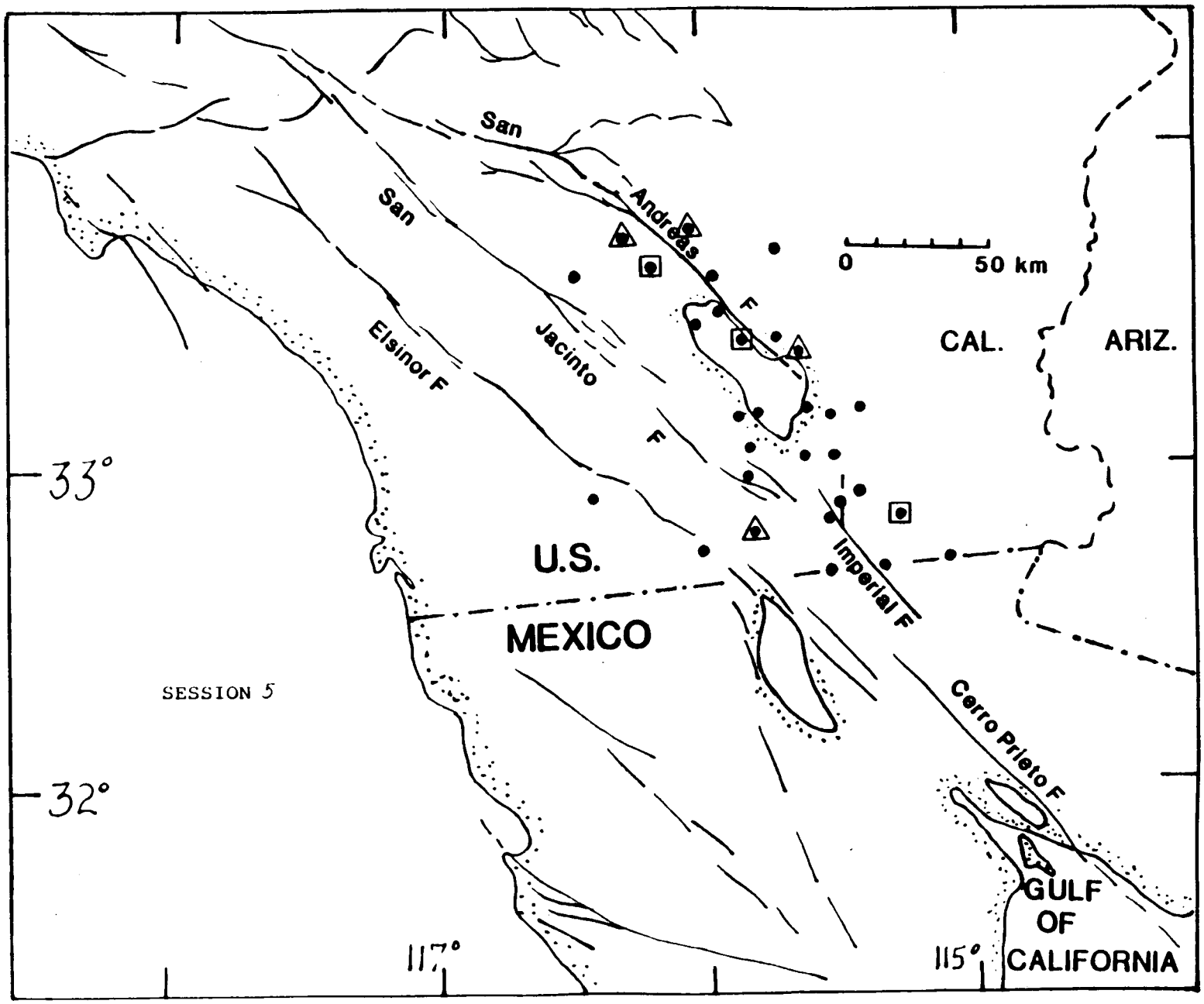
San
Andreas
F
San
Jacinto
F
Elsinor F
0
50 km
CAL.
ARIZ.
33°
U.S.
MEXICO
Imperial F
Cerro Prieto F
SESSION 5
32°
117°
115°
GULF
OF
CALIFORNIA

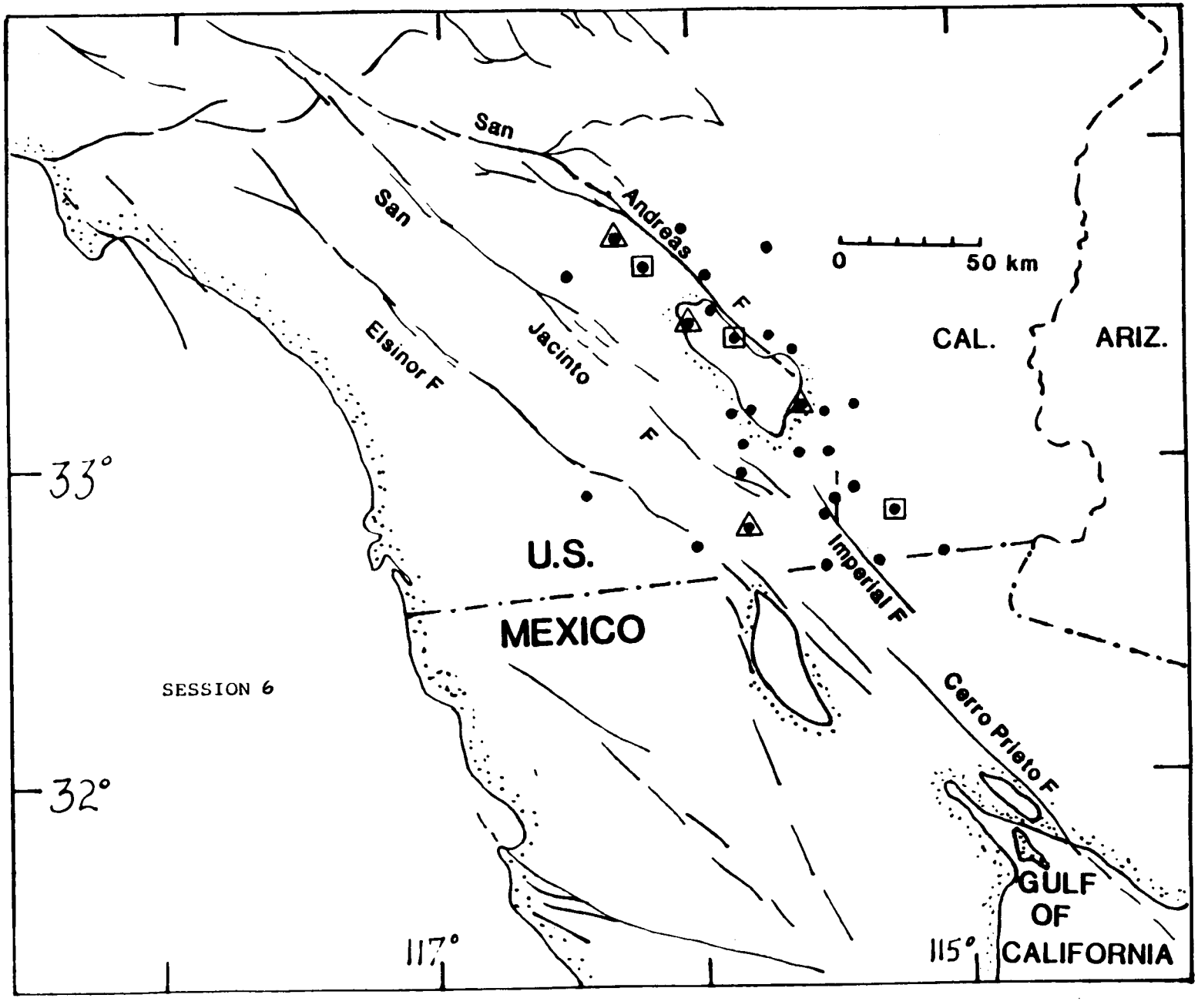
San
Andreas F
San
Jacinto
F
Elsinor F
0
50 km
CAL.
ARIZ.
33°
U.S.
MEXICO
Imperial F
Cerro Prieto F
SESSION 6
32°
117°
115°
GULF
OF
CALIFORNIA

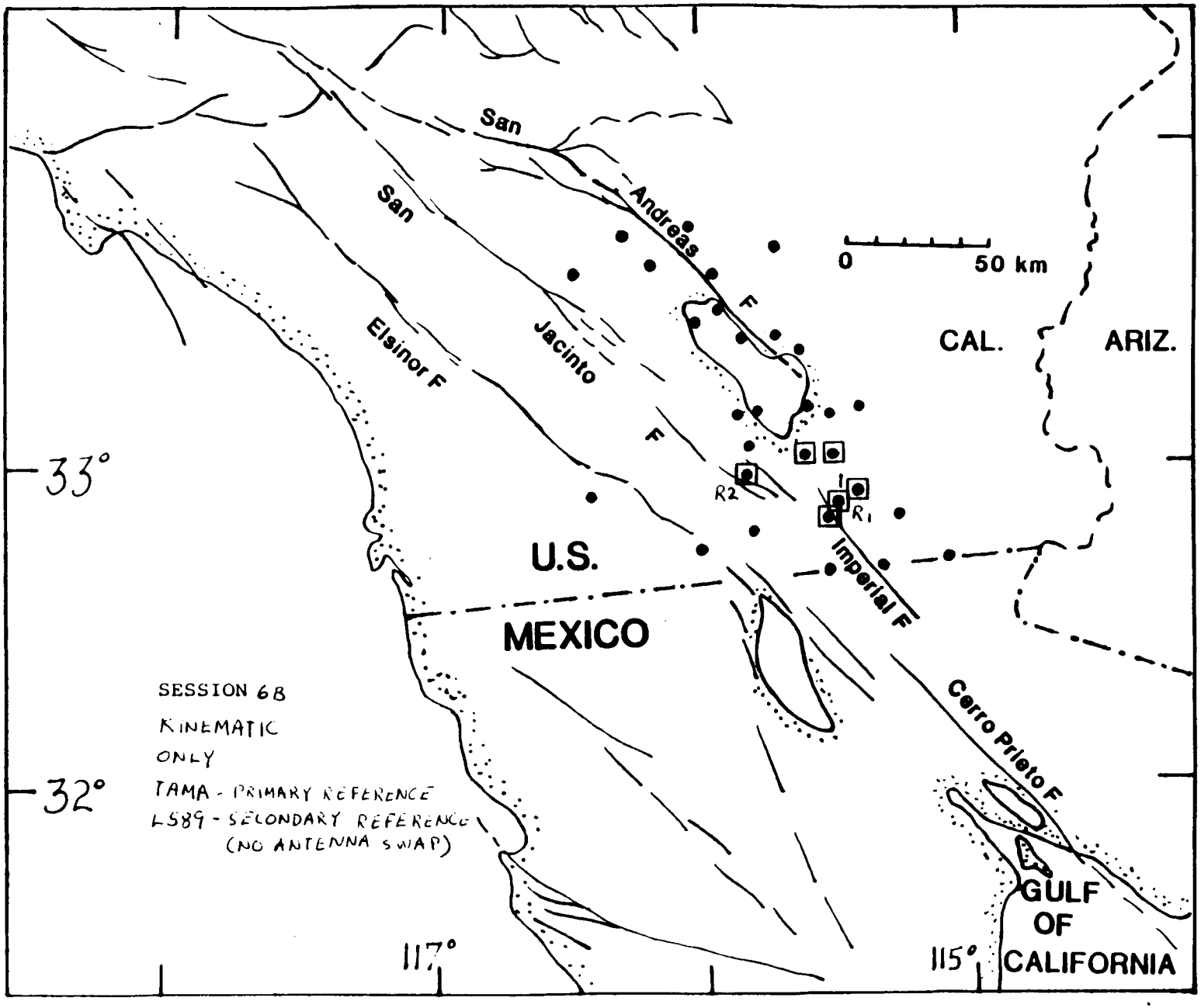
San
Andreas
F
San
Jacinto
F
Elsinor F
0
50 km
CAL.
ARIZ.
33°
R2
R1
U.S.
MEXICO
Imperial F
Cerro Prieto F
SESSION 6B
KINEMATIC
ONLY
TAMA - PRIMARY REFERENCE
L589 - SECONDARY REFERENCE
(NO ANTENNA SWAP)
32°
117°
115°
GULF
OF
CALIFORNIA

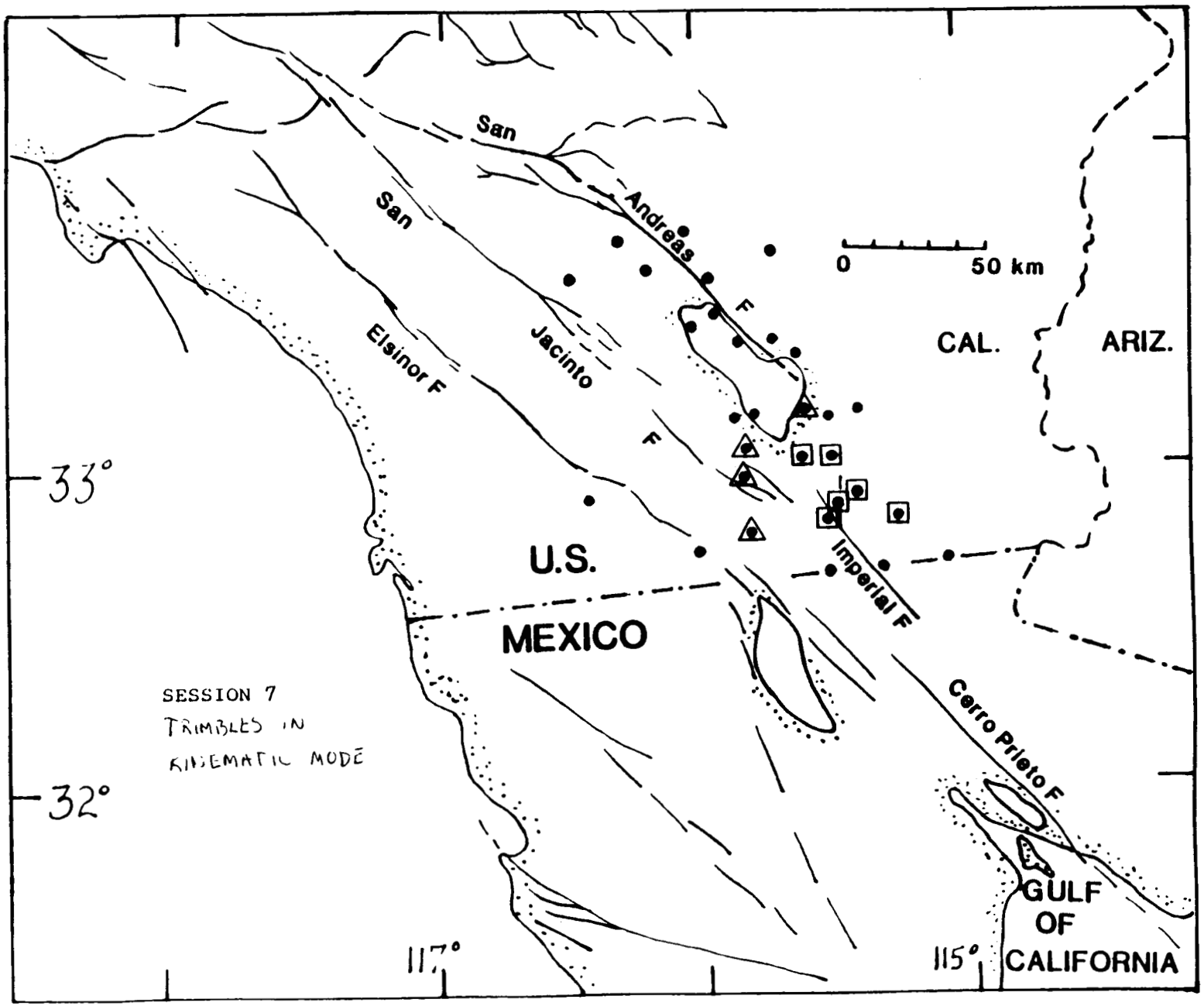
San
Andreas
F
San
Jacinto
F
Elsinor F
0
50 km
CAL.
ARIZ.
33°
U.S.
MEXICO
Imperial F
Cerro Prieto F
SESSION 7
TRIMBLES IN
KINEMATIC MODE
32°
117°
115°
GULF
OF
CALIFORNIA

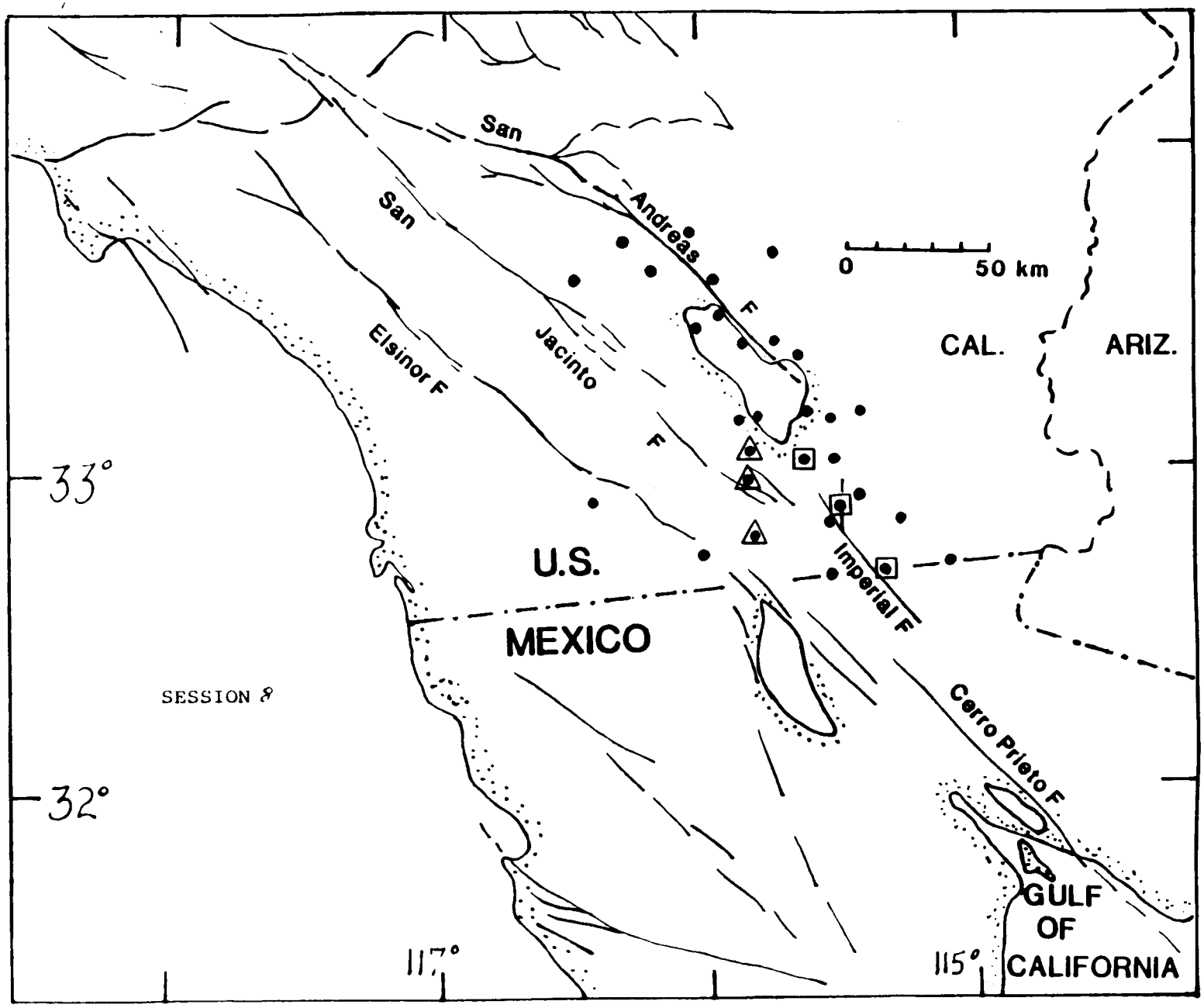
San
Andreas
F
San
Jacinto
F
Elsinor F
0
50 km
CAL.
ARIZ.
33°
U.S.
MEXICO
Imperial F
Cerro Prieto F
SESSION 8
32°
117°
115°
GULF
OF
CALIFORNIA

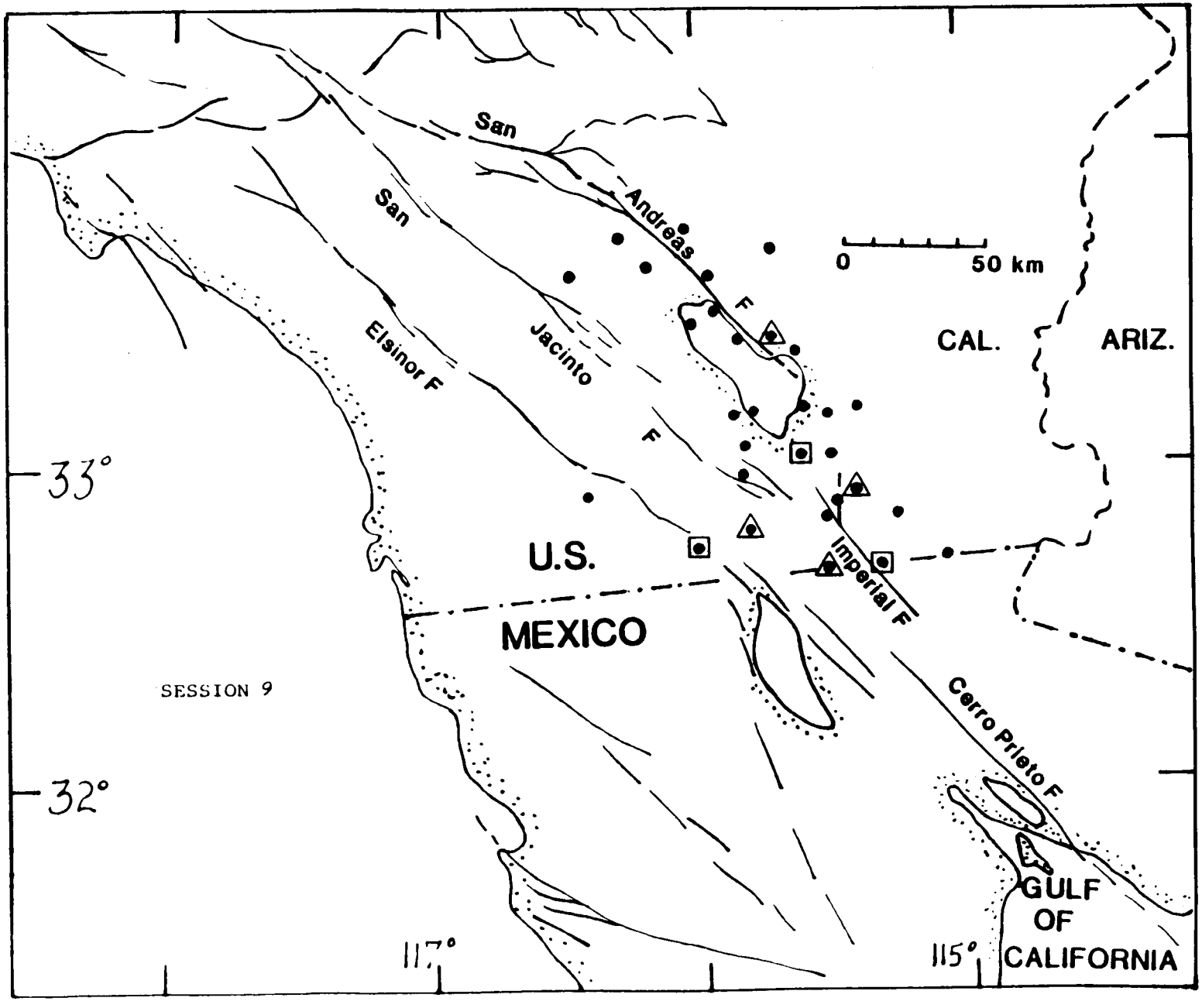
San
Andreas
F
San
Jacinto
F
Elsinor F
0
50 km
CAL.
ARIZ.
33°
U.S.
MEXICO
Imperial F
Cerro Prieto F
32°
117°
115°
GULF
OF
CALIFORNIA

SESSION 9

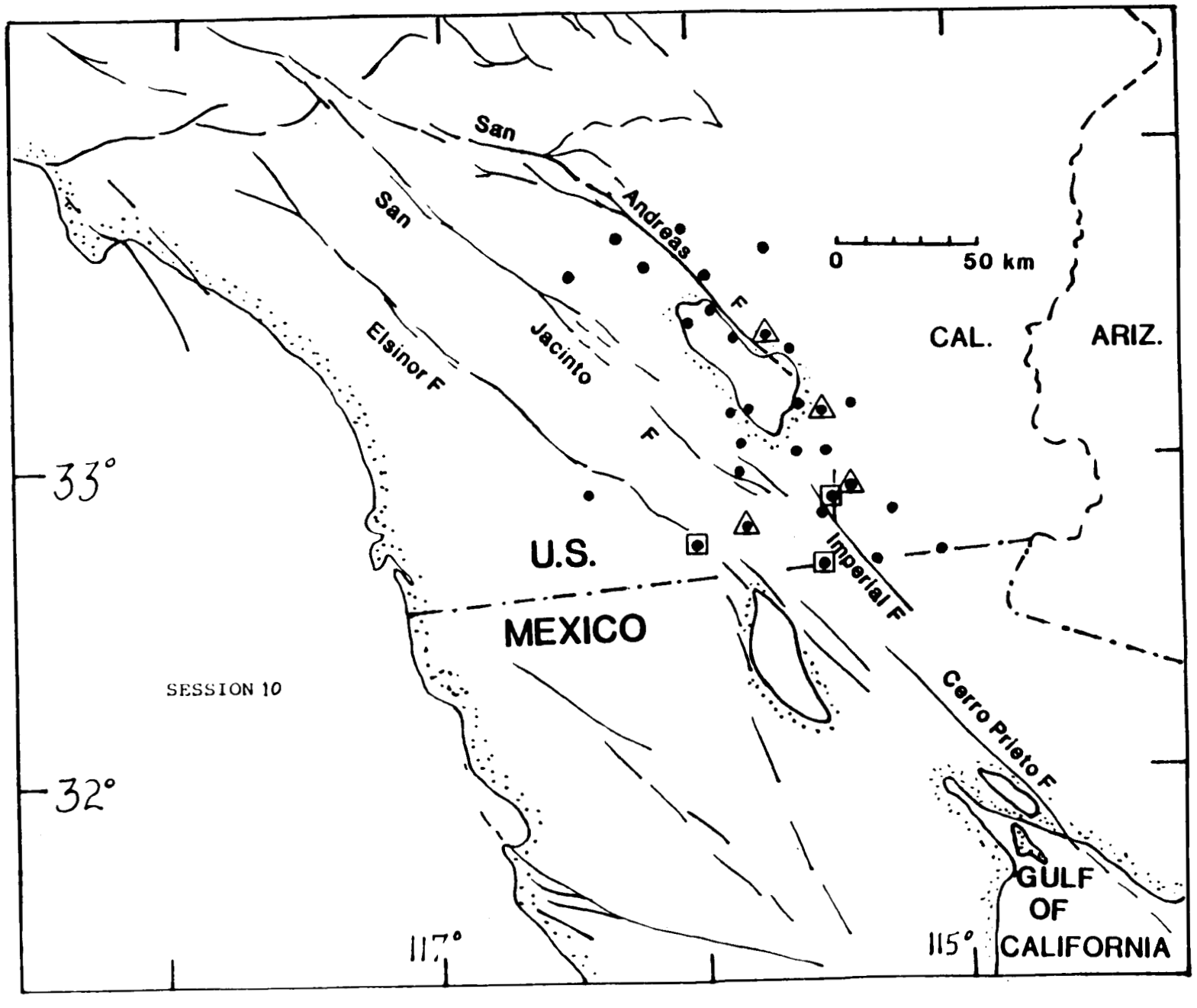
San
Andreas
F
San
Jacinto
F
Elsinor F
0
50 km
CAL.
ARIZ.
33°
U.S.
MEXICO
Imperial F
Cerro Prieto F
SESSION 10
32°
117°
115°
GULF
OF
CALIFORNIA

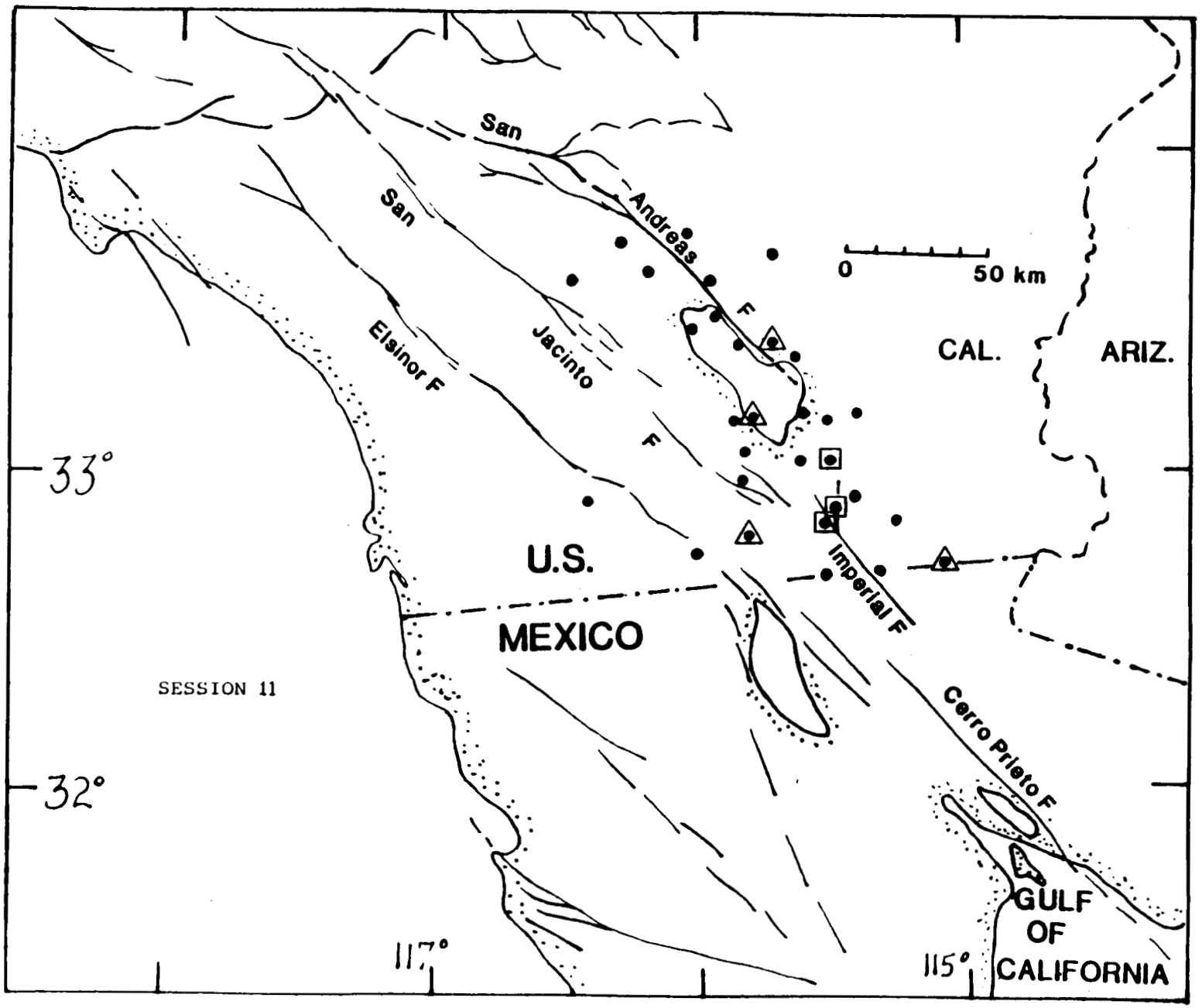
San
Andreas
F
San
Jacinto
F
Elsinor F
0
50 km
CAL.
ARIZ.
33°
U.S.
MEXICO
Imperial F
Cerro Prieto F
SESSION 11
32°
117°
115°
GULF
OF
CALIFORNIA

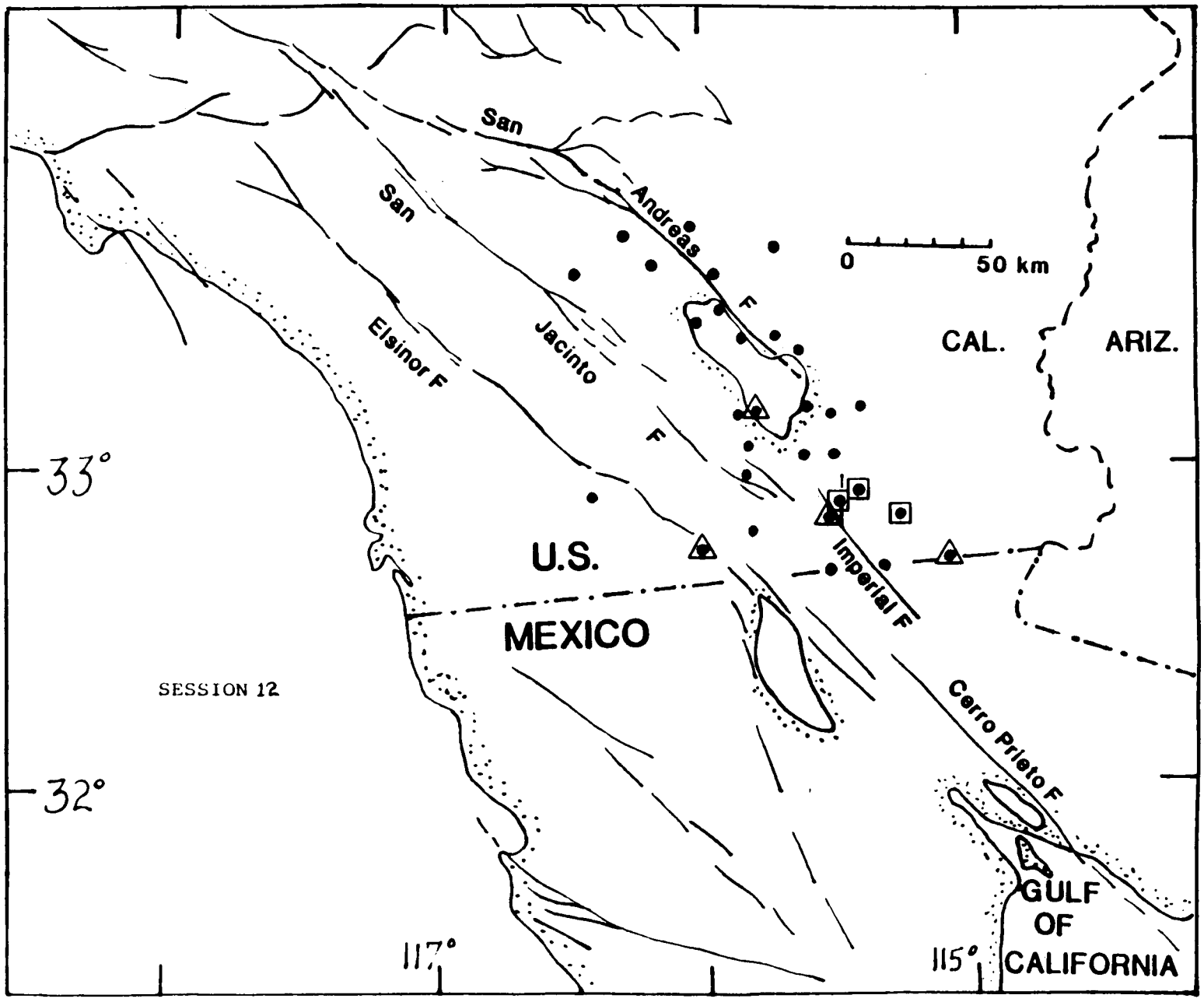
San
Andreas F
San
Jacinto
F
Elsinor F
0
50 km
CAL.
ARIZ.
33°
U.S.
MEXICO
Imperial F
Cerro Prieto F
SESSION 12
32°
117°
115°
GULF
OF
CALIFORNIA